# Feedback Control Of Vibrations In Surface Rotary Blasthole Drilling

Claude E. Aboujaoude, B.Eng. (A.U.B), M.Eng. (McGill)

Department of Mining and Metallurgical Engineering
McGill University, Montreal, Canada.

April 1997

A thesis submitted to the Faculty of Graduate Studies and Research
in partial fulfillment of the requirements for the degree of
Philosophy Doctorate

April 1997

0-612-29867-1

To my parents,
my family,
and in memory of
my brother

## Abstract

Most blasthole drills currently used in the mining industry are manually controlled. The drilling control systems which do exist are based mainly on ladder programming logic techniques. This thesis presents a comprehensive strategy for the automatic control of blasthole drills, based on closed loop feedback control approach.

A detailed model for the controlled process consisting of the drill rig's mechanical actuators, machine structure, and the drilling process at the bit-rock interface is presented. The model equations are refined and validated by experimental (field) testing. The instrumentation of an Ingersoll-Rand DM-45E drill rig and the subsequent drilling tests in a limestone quarry are described, with an in-depth discussion of the field tests results. Analysis of the field tests data establishes the dependencies between the drilling variables and ground conditions during actual drilling. The transfer functions of the mechanical actuators of the machine are also identified.

A strategy for automatic control of feed pressure and rotary speed is proposed. The controller is tested and tuned by interfacing it to a software simulator of the controlled process which implements the relationships identified from field testing. Simulation results are presented and analysed.

Results of implementing the controller on a Gardner-Denver GD-120 electric drill, and an Ingersoll-Rand DM-H hydraulic drill at two surface coal mines in British Columbia, Canada, are also presented. These results validate the drilling controller design and tuning.

The thesis concludes with suggestions for future research and refinement of the control strategy.

# RESUME

Le nombre de modèles de foreuses rotatives de très grande puissance utilisées pour les trous de pré-clivage et dynamitage dans les mines à ciel ouvert présentement dotées d'un système à commande automatique demeure réduit. Cependant, les systèmes qui existent sont basés sur les techniques de programmation étagée (Ladder Programming). Cette thèse traite l'étude d'un nouveau système de commande qui utilise le principe de boucle à rétroaction fermée.

Un modèle mathématique du circuit composé des actionneurs mécaniques et du procédé de forage au niveau de l'interface foret-roche a été déduit des résultats de recherches antérieures dans ce domaine. Dans le but d'améliorer les équations décrites, une foreuse DM45E de la compagnie Ingersoll-Rand a été instrumentée et testée dans une mine de charbon à ciel ouvert. Les résultats de ces tests sont analysés en profondeur à l'aide de graphes qui montrent les différentes relations entre les variables concernées et la nature de la roche. Les fonctions de transfer des actionneurs mécaniques ont été également identifiées.

Une stratégie de commande automatique pour la force de pression et de la vitesse de rotation du foret est présentée. Le système de commande a été réglé en l'enchainant a un logiciel de simulation du circuit qui incorpore le modèle amélioré, défini d'après les résultats des tests réels. Les résultats des simulations ont prouvé la viabilité de la stratégie proposée.

Le système de commande a été par la suite testé sur deux foreuses de conception différente, l'une d'elles basée sur des actionneurs éléctriques, tandis que la deuxième utilise des actionneurs hydrauliques. Les résultats des tests ont démontré que la stratégie de controle telle que proposée est fonctionelle.

La thèse est conclue par des suggestions de recherches pour l'amélioration du système de commande proposé.

# ACKNOWLEDGEMENTS

I wish to express my deepest gratitude and appreciation to Dr. Laeeque K. Daneshmend and Dr. Jonathan Peck for supervision, guidance and encouragement during the course of this research work.

I am also indebted to Dr. Jonathan P. Peck whose hard work, devotion and dedication made field testing possible under severe time restrictions and budget limitations. His contribution to the success of this research is invaluable and greatly appreciated.

I wish to thank Ingersoll-Rand Rotary Drills Division, Dallas, U.S.A., for providing financial and technical support during the initial phase of this work, under a research contract with McGill University, as well as disclosing confidential technical information. In particular, I am indebted to Mr. George Schivley, former manager of engineering, and Mr. John Stinson, product support manager, large rotary drills.

The Lafarge quarry at Alpena, Michigan, U.S.A., and Mr. Jean-Yves Roch, maintenance superintendant, must also be thanked for providing the necessary commodities for the first experimental field testing, and assistance whenever needed.

In particular, I am grateful to Aquila Mining Systems Ltd., under whose auspices the implementation and field testing of the controller was made possible. The code implemented under QNX was the work of Aquila's highly skilled software engineers.

I also wish to thank the Quintette Operating Corporation (Mr. Robert Taylor, Maintenance Superintendant), and the Bullmoose Operating Corporation (Mr. Bill Flemming, Mine Manager), B.C., Canada, for their faith in drilling automation, and for providing the necessary support for implementing and testing the proposed control strategy.

At McGill university, I thank the students, staff, and the faculty of Mining Engineering, as well as the Canadian Centre for Automation and Robotics in Mining (CCARM), for providing an excellent working environment and computing facilities.

Finally I wish to thank my parents, my wife and my son, whose endless support helped me throughout the hard times during this work, and all the friends and persons who directly and indirectly contributed to this project but are not mentioned here.

# Note on the Units of Measurements used

Throughout this thesis, both S.I. and imperial units of measurements are used. Where appropriate, the S.I. metric equivalent of imperial units have been provided. The reason for adopting imperial units is justified by the following:

- This work is oriented towards technical advances in the drilling industry. The majority of the drill manufacturers are in the United States where imperial units are more commonly used.

- Large surface blasthole drilling equipment manufacturers have only recently started to adopt metric units. Most available literature is in imperial units.

- Pressure gauges on the operator panel of the monitored drill at the Lafarge quarry and the drills on which the controller was tested, were in both imperial and metric units. However, at the Lafarge quarry, all drilling instructions were given in imperial units.

- The majority of previous publications relating to the thesis research were in imperial units.

Hence, it was decided to maintain imperial units for data presentation and calculations. The following page provides a *Table of Conversion* for imperial units to their metric equivalents.

TABLE OF CONVERSION; IMPERIAL TO METRIC

| Imperial | Multiplying factor | Metric |
|---|---|---|
| feet | 0.3048 | m |
| in | 25.4 | mm |
| ft/hr | 0.3048 | m/hr |
| psi | 0.0069 | MPa |
| lbs mass | 0.4536 | Kgs mass |
| rev/min (rpm) | 0.1047 | rd/s |
| ft-lb | 1.36 | N.M |

TABLE OF CONTENT

# Chapter 1 INTRODUCTION

## 1.1 Blasthole Drilling

The surface mining and quarrying industry uses blasthole drills for drilling holes that can be loaded with explosives to fragment rock. The fragmented material is then excavated by other mine equipment such as shovels, draglines, and front end loaders. In addition, in instances where a knowledge of bench geology is required in advance of explosive loading, the holes are used to introduce various geophysical instrumentation (e.g. gamma, sonic and neutron logging) into the rock mass towards identifying variations in lithology along the hole length [Doveton 1986].

A generic rotary drilling concept is illustrated in Fig.1.1. A bit rotating under a feed force breaks the rock and generates small cuttings called *chips* that are removed from the hole by flushing air.

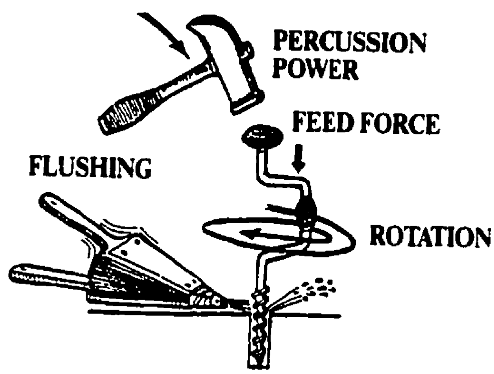


**Figure 1.1**: Elements of surface drilling (after [Tamrock 1989])

In addition, percussion power can be used to assist in the breakage process. These basic concepts are implemented in modern drills, in a broad line of models and categories designed to meet the needs of individual mining operations. For example, different machine design criteria apply to underground and open pit mines. Drills using percussion are called *percussive drills*, non percussive machines are referred to as *rotary drills*. Percussive drills are effective in drilling smaller diameter holes than rotary drills, and are generally used in underground mines.

Figure 1.2 shows a rotary drill, model DM45E from Ingersoll-Rand Co. (U.S.A.), whose design is typical of surface blasthole rigs. Rotation is generated by one (or optionally two) hydraulic motor(s) fixed onto a frame (rotary head) that can slide along the length of the mast.

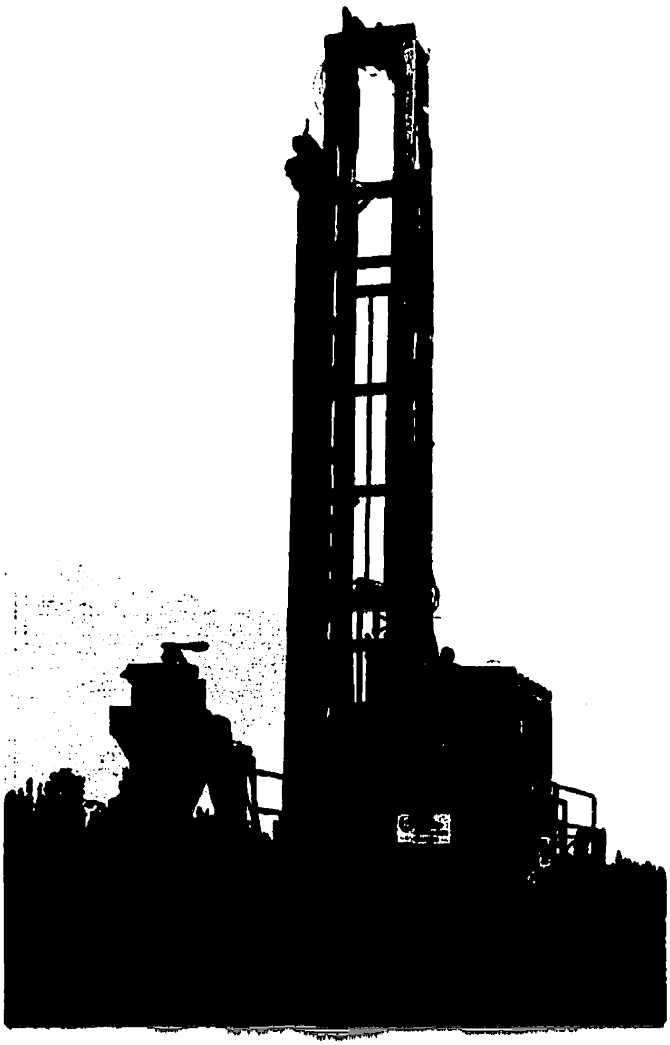

**Figure 1.2:** Ingersoll-Rand DM45E hydraulic rotary drill

The motor(s) drive a spindle sub which connects to a steel pipe via threading at one end, the other end threaded to the bit. The drill rotary head is pulled up and down by feed chains powered by two hydraulic cylinders, with pulldown force controlled by adjusting the cylinders' hydraulic (feed) pressure. The resulting force at the bit level is referred to as the weight-on-bit, and consists of the drill string and rotary head weight added to the pulldown force. Up to four additional steel pipes are stored in a carousel type pipe changer. When the first steel pipe is driven down the hole over its entire length, the drill operator detaches it from the spindle sub by rotating the motor(s) in a reverse direction. He then advances the carousel into the loading position to add another steel pipe on top of the previous one, then resumes drilling. The steel column composed of one or more steel pipes connecting the spindle sub to the bit is referred to as the *drill string.*

The *drilling cycle* consists of positioning the drill rig over the designed location of the blasthole, leveling the machine by lowering three independently controlled jacks and adjusting the mast angle. The operator then loads the first steel pipes, pulls down the rotary head until the bit reaches ground level, starts rotation slowly while exerting a moderate pulldown force until the bit reaches a depth of approximately 5 meters (15 ft.). The process of drilling slowly through the first section of the hole is called *collaring* the hole, and is essential to avoid deviation in the hole trajectory.

After collaring, the drill operator adjusts feed pressure and rotary speed to achieve maximum production footage while trying to ensure the longest possible bit life and minimizing downtime and maintenance costs. The operator's reaction to the process is based upon feedback of visual information from gauge displays of rotary speed, feed pressure, rotation pressure (which is responsible for torque generation), bailing air pressure, condition and size of flushed chips, plus his perception of noise and vibration levels.

## 1.2 Automatic Control of Rotary Drilling

### 1.2.1 Context

The mining industry is becoming increasingly competitive and machine manufacturers and users are continually exploring ways of reducing drilling costs and enhancing machine productivity. One way of achieving these objectives is through the application of automatic control.

A typical breakdown of the time needed to drill a hole is described as follows: 2-3 minutes in tramming and positioning the drill over the blasthole location, 1 minute to level the drill, about 20 to 40 minutes spent in actual drilling time (depending on ground condition), 2-3 minutes for every steel pipe addition or removal, then finally one more minute to unlevel the drill prior to propelling to the next hole location. As an example, Fig.1.3 shows the percentage of time spent on each drilling activity, by an Ingersoll-Rand DM45E drill, drilling a 200 mm (7 7/8 in.) diameter hole, to a depth of 33.5 m (110 ft.), in a limestone quarry, using five steel pipes. The total drilling cycle time per blasthole was approximately 60 minutes.

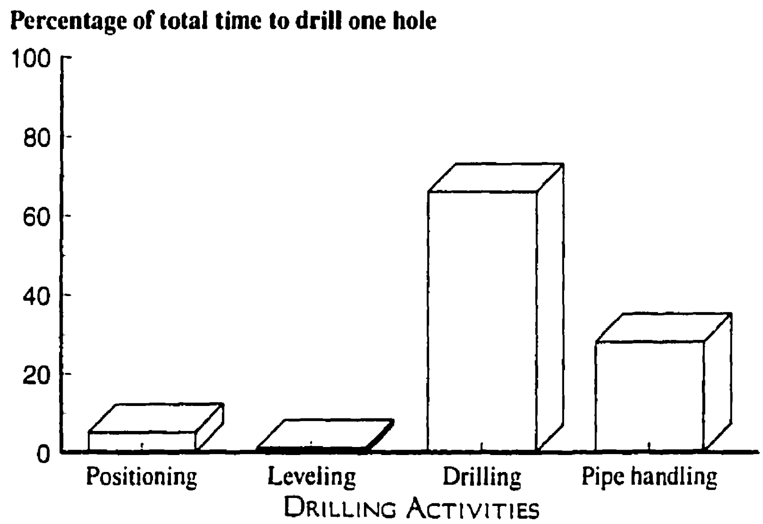


**Figure 1.3:** Example of drilling activities time slice

Based on the above, the first step towards drill automation, an initial automatic control strategy should be focused towards controlling the rotary drill during the actual drilling phase, since automating this procedure would have the largest direct impact on productivity. This goal can be fulfilled by providing automatic control of rotary speed and weight-on-bit (e.g. feed pressure) once the drill has been positioned and the hole has been collared.

### 1.2.2 Benefits of Drill Automation

The benefits of drill automation for the mining industry would be:

- More productive and energy effective drills. Power usage is minimized and rate of advance and machine life maximized, as the ideal chip is generated [Aboujaoude 1991], [Hodgins 1992].

- Reduce instances of severe vibrations by avoiding over-loading or under-loading the bit. Too much weight-on-bit increases the power consumed with little or no increase in penetration rate and causes significantly more vibration in the drill string and structure. Too little weight-on-bit results in large vibration loads when the rock is not being readily fractured and could lead to mechanical drill failure. Both instances result in reduced bit life. Reduced wear and tear of the drill lowers maintenance costs and downtime, at the same time increases the drill's availability.

- More consistent drilling per shift, mainly between the day and the night shifts.

- Less machine abuse by the operator, and therefore less downtime and higher machine availability.

- More autonomous drills, and therefore less operator fatigue, as well as releasing the operator to perform other tasks.

- The partial automation of the drilling functions presents one step towards future unmanned drilling operations.

The purchase price of the drills equipped with automation systems, however, may increase. In addition, changes may be required in maintenance skills and infrastructure, due to the introduction of the new technology.

### 1.2.3 Preceding Work

A strategy for controlling the penetration rate per revolution, by adjusting the feed cylinder's hydraulic pressure had previously been formulated, and simulated, in earlier work that formed the Master's Thesis research of the author [Aboujaoude 1991]. The simulation results indicated that the proposed control strategy was likely to be viable under actual drilling conditions. The rotary speed, however, remained under manual control of the drill operator, in that strategy.

## 1.3 Research Overview

The present Ph.D. thesis research describes the formulation and development of a strategy for the automatic control of rotary speed, during drilling, that is viable and compatible with the already proposed weight-on-bit control strategy, and, also compatible with other weight-on-bit control strategies of similar functionality.

The initial phase of the research was funded by the Ingersoll-Rand Company, a leading drill manufacturer. Experimental tests relevant to the study were conducted at the Ingersoll-Rand, Rotary Drill Division manufacturing plant, in Garland, Texas, U.S.A. (1991), and also in the field at the Lafarge Co. quarry at Alpena, Michigan, U.S.A (1992). Finally, field testing of the developed control strategy was conducted in two coal mines, at Bullmoose Operating Corporation and at Quintette Operating Corporation, both in British Columbia, Canada (1994).

## 1.4 Rotary Speed Control in Rotary Drilling: Problem Statement

The author's Master's Thesis research showed that while weight-on-bit and rotary speed affected the primary output variable of penetration rate, and the primary output constraining variables of rotary torque and bailing air pressure, the primary constraint on rotary speed was rig vibration. Under certain circumstances, very large amplitude vibrations can occur, which, if no corrective action is taken, can result in severe damage to the drill. This vibration usually takes the form of lateral and longitudinal deflection of the drill string with subsequent severe vibration of the machine itself.

The strategy for automatic control of weight-on-bit previously proposed by the author [Aboujaoude 1991] takes into consideration all the mentioned primary output constraining variables, with the exception of vibration. Therefore, the development of a strategy for automatic control of rotary speed, compatible with the author's automatic strategy for weight-on-bit, or with any other weight-on-bit control strategy with similar functionality, must address the issue of drill vibration.

The objective of controlling rotary speed becomes one of constraining drilling vibration, i.e. to dampen drilling vibrations as they occur (or, more practically, before they achieve critical levels), in the following manner:

1. As soon as vibrations start building up, the controller adjusts rotary speed until a satisfactory level of vibration is reached, without driving the drill to a full stop, and without prior knowledge of bench geology.

2. The controller automatically restores rotary speed to the level at which it was operating prior to the onset of excessive vibration, once vibrations inducing conditions have subsided.

## 1.5 Research Methodology

The methodology followed in the course of this research for developing and refining the control algorithm is summarized as follows:

The existing drilling control systems were reviewed, followed by an analysis and a review of past attempts to control drilling vibration, mainly in the oil industry. Drilling experiments in the field were conducted, which enabled the development of an approximate empirical model for drilling, and also assisted in the formulation of a control strategy. The empirical models were subsequently used to build a drilling simulator, for the purposes of simulating and testing the control strategy. Finally, the designed controller was field tested on two drills, equipped respectively with a hydraulic and electric rotary motor. Both field tests demonstrated the viability of the proposed control strategy.

## 1.6 Ph.D. Thesis Overview

The organization of the thesis is as follows:

- Chapter 2 surveys past work and achievements in drilling control, both in the mining and oil industry. It also reviews past attempts and studies to control vibration, mainly in the oil drilling industry

- Chapter 3 analyses blasthole drilling vibration. The natural modes of vibration of a blasthole rig's drill string are obtained analytically, then compared with the drilling excitation frequencies.

- Chapter 4 describes the instrumentation of a DM45E drill rig, for the purpose of conducting field experimental tests. The field testing methodology is also detailed.

- Chapter 5 validates the drilling excitation mechanisms, by conducting frequency domain analysis of the field data. Time domain steady state vibrations are also analyzed.

- Chapter 6 derives empirical models of the drilling process, including the bit rock interface. The machine feed and rotary actuators are modeled and identified, based on experimental data. The models are then embodied in a computer simulation program to enable simulation of the drilling process.

- Chapter 7 designs and simulates the controller. Simulation results of both the continuous controller and its discrete implementation are provided.

- Chapter 8 implements and tests the controller on two drills, at two coal mines in British Columbia, Canada. One drill is equipped with a hydraulic rotation mechanism, while the other relies on an electric direct current motor-generator set to control rotation speed. In both cases, the field tests indicated the viability of the proposed control strategy.

- Chapter 9 concludes the thesis, and also recommends areas of future improvements.

# Chapter 2 LITERATURE REVIEW AND STATE-OF-THE-ART SURVEY

## 2.1 Rotary Drilling

Rotary drilling technology is mainly used for drilling oil wells, water wells, as well as blastholes for the mining and quarrying industry [Tamrock 1989]. The most common bits that are used to fragment and crush the rock are tricone bits.

### 2.1.1 Tricone Bits

Tricone bits consist of three conic shaped rollers each having arrays of milled teeth, or tungsten-carbide inserts, depending on the bit model, aligned in several rows (usually four). The cones have different meshing geometry and are designed to rotate about a fixed axis. The inserts are extremely resistant to abrasive wear and breakage and give consistent performance during the bit life. The insert length is usually row and cone dependent.

These bits may have a slight shearing action in soft rock formations, but primarily operate to break the rock into chips by a crushing action through indentation of the inserts under an applied force (weight-on-bit) and rotating action. The distance between adjacent insert rows is designed to create a free surface which allows the chips to propagate and be removed without being completely ground. The bits differ from one another by geometry, diameter, shape of inserts and inserts length. Bits designed for hard rock formations have short ovoid-shaped inserts while soft formations bits have longer tooth-shaped inserts.

Figure 2.1 shows a typical carbide inserts tricone bit.


**Figure 2.1:** Smith International Soft Formation Tricone bit, model Q2J [Smith 1994]

### 2.1.2 Rock Fragmentation And Crater Formation

When a bit insert impacts rock, the rock is elastically deformed until the crushing strength of the rock is exceeded, at which time a wedge of crushed rock is formed below the insert [Hartman 1959], [Simon 1959] (see Figure 2.2).

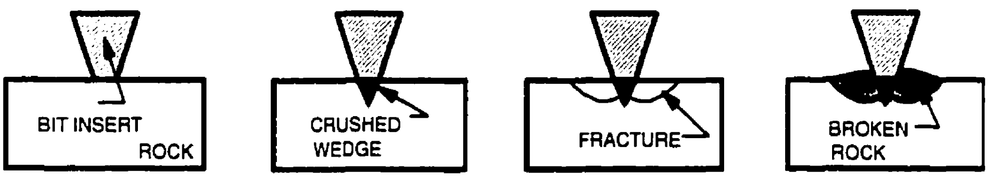


**Figure 2.2:** Crater formation mechanism (after [Maurer 1959])

As additional force is applied to the insert, the crushed material is compressed and exerts high lateral forces on the solid material surrounding the crushed wedge [Fairhurst 1956]. When these forces become sufficiently high, and exceed the compressive strength of the rock, fractures are propagated to the free surface of the rock. The trajectories of these fractures intersect the principal stresses at a constant angle [Clausing 1959], [Maurer 1959], [Simon 1959], as predicted by Mohr's and Griffith's theories of failure.

### 2.1.3 Penetration Rate Model

There have been numerous drilling models presented in the literature over the years to relate the various mechanical factors involved in the drilling process to the penetration rate. These studies were mainly developed for the petroleum industry, where very long, deep holes were considered, with water and/or mud used as flushing fluid, in contrast to compressed air used in most rotary blasthole drills, where water is generally used for dust control purposes. The model selected here was presented by Maurer [Maurer 1962] in the context of petroleum engineering. Under "perfect cleaning" conditions, i.e. all cuttings are removed from the bit-rock interface as soon as they are developed, Maurer's model, based on studies of single-insert impacts [Maurer 1959], is described by the fcllowing equation:

$$PR = K_1 \frac{N(WOB)^2}{D^2 S^2} \qquad (1)$$

where $(PR)$ is penetration rate, $N$ is rotary speed, $(WOB)$ is weight-on-bit, $D$ is bit diameter, $S$ is defined as the drillability strength of the rock and $K_l$ is a constant dependent on rock type.

According to Maurer, when a bit is drilling under imperfect cleaning conditions and the weight-on-bit or rotary speed is increased, the penetration rate still increases. However, the increase in penetration rate is accompanied by a corresponding increase in broken rock and thus in the cleaning problem. For this reason the rate of increase in the penetration rate as a function of weight-on-bit or rotary speed is smaller than that which would be expected under perfect cleaning conditions.

After conducting a series of tests, Maurer concluded that:

$$PR = K \frac{(WOB)^x N^y}{D^z} \qquad (2)$$

where $x, y, z$ and $K$ are adjustable constants dependent on drilling conditions, and should be smaller than the corresponding exponents in Eq.1.

The model has been validated for surface blasthole drilling by the author [Aboujaoude 1991], with $0.5 < x < 1$, and $0.5 < y < 1$. However, it is worth mentioning that the model has a serious handicap in that increasing weight-on-bit and rotary speed indefinitely would increase penetration rate. This response is obviously not valid. The model has its limitations because Maurer did not consider the cases of bit inserts completely buried in rock (over penetration)

### 2.1.4 Torque Model

Warren [Warren 1984] proposed a model for torque by considering a force balance concept and assuming that the torque applied to the bit is resisted largely by the bit face rolling resistance. Furthermore, for an undamaged bit, the torque that results from bearing friction inside the cone and friction along the gage surface of the bit are assumed to be negligible.

His model can be expressed as:

$$T = \left[ C_1 + C_2 \sqrt{\frac{(PR)}{ND}} \right] (WOB) \qquad (3)$$

where $(PR)$ is penetration rate, $T$ is torque, $N$ is rotary speed, $(WOB)$ is weight-on-bit, $D$ is bit diameter, $C_1$ and $C_2$ are constants.

Here again, Warren assumes that the resistance to rolling occurs at the inserts, because according to Warren, there is normally no contact between the cone shell and the rock. However, when the inserts are completely buried in the rock, the shell does contact the rock, and therefore one should expect higher resistance to rolling.

The author attempted to fit empirical data into Warren's model, however, a better fit was obtained by using a variation in the original model, as expressed below [Aboujaoude 1991]:

$$T = \alpha (WOB)^n$$

where $0.65 < n < 1$ and $\alpha$ is a constant.

## 2.2 Drilling Vibration

### 2.2.1 Review of Structural Resonance

Machines and structural systems vibrate freely about their static-equilibrium positions when displaced from those positions and then released. The frequencies at which they vibrate are known as natural frequencies, and depend primarily upon the mass and elasticity of the system. All physical systems contain some inherent type of mechanism that dissipates energy, and this energy dissipation is referred to as damping.

When a structural system is harmonically excited with a forcing frequency near the natural frequency of the structure, it will start to vibrate, with an amplitude equal to the harmonic excitation's amplitude magnified by a factor that depends on the structure's damping factor. This condition, known as *resonance*, could be potentially dangerous to both machines and structures. For steel structures, the magnification factor can be as high as 50 [James 1989].

### 2.2.2 Earlier Work In Modeling Drilling Vibration

Earlier work in modeling drilling vibrations was conducted in the context of petroleum drilling, where Bottom-Hole Assembly (BHA) failures were frequent, and the economic incentives to avoid them was substantial. Many authors have studied the BHA response by developing static and dynamic models, both 2-dimensional and 3-dimensional [Williamson 1986], [Jogi 1986], [Bradley 1975], [Millheim 1981], [Cheatham 1981], where the models attempted to predict the inclination tendencies of Bottom Hole assemblies by calculating the resultant bit forces. A few authors have concentrated on predicting dynamic instabilities that cause these failures. Deily et al [Deily 1968] set up linear lumped parameter vibration models, Pasley et al [Pasley 1964] studied drill string dynamic stability under lateral constraints.

### 2.2.3 Bottom-Hole Assembly Vibration

Bottom-Hole Assembly vibrations are similar to machinery and structural vibrations. During rotation, physical phenomena such as imbalance, misalignment, bent pipe, drill string contact with the side walls, or other geometrical phenomena create excitations that oscillate at frequencies equal to, or multiples of the rotational frequency. When the excitation frequencies match one of the BHA natural frequencies, a resonance condition is generated.

The rotary speeds at which resonant conditions occur are called critical speeds. In order to avoid BHA resonance, several authors suggested avoiding critical speeds, by defining safe rotary speed operating ranges [Dareing 1983]. Others suggested designing Bottom Hole Assemblies with configurations that shift critical speeds outside the actual drilling rotary speed range [Besaisow 1986].

For a practical implementation of either proposed approach, the critical drilling speeds needed to be predicted. Predicting critical speeds requires:

1. an accurate knowledge of the excitation mechanisms of the Bottom Hole Assembly, and,

2. an accurate estimate of the natural modes of excitation.

### 2.2.4 Excitation Mechanisms In BHA Dynamics

Many physical sources induce excitation mechanisms.

Mass imbalance, for instance, causes excitations primarily in the lateral direction that are in the order of 1 x RPM. This lateral excitation yields a smaller or secondary axial excitation that is of the order 2 x RPM, since one lateral cycle causes a fixed end to cycle axially twice. Torsional excitations of the order 1 x RPM and 2 x RPM are also induced [Besaisow 1986]. A bent pipe, for instance, can cause a mass imbalance mechanism.

Misalignment of the drill string or buckling of the BHA under compression causes lateral excitations of 1 x RPM primarily. Misalignment also causes axial and torsional excitations of 2 x RPM. If the drilled formation is not perfectly flat at the bottom, asymmetric supports also induce a 2 x RPM component in lateral excitation [Blake 1972]. Asymmetric supports tend to induce bending stress fluctuation at twice the lateral excitation due to moment of inertia variations.

The tricone bit causes primarily a 3 x RPM axial excitation mechanism [Deily 1968]. Since the bouncing axial motion causes fluctuating levels of torque, a torsional 3 x RPM excitation mechanism is also induced [Besaisow 1986].

Another excitation mechanism is the shaft whirl or rotational walk mechanism. Initial eccentricity of a bent drill string, or the combination of drill string sag due to gravity and high compressive loads, due to weight-on-bit, causes a dynamic imbalance [Vandiver 1989]. The sections of the BHA touching the hole tend to walk backwards, due to rubbing contact with the hole. Assuming no slippage, the rotational walk frequency is $[D/(D-d)]$ x RPM where $D$ is hole diameter and $d$ is drill string diameter. This mechanism only occurs with assemblies where the drill string can buckle and touch the hole [Besaisow 1986].

### 2.2.5 Natural Modes of Vibration of BHA

Several authors have derived analytical models for oil well drill string vibration, in an effort to evaluate the natural resonant frequencies, in several modes of vibration. Different modeling approaches were presented.

The accuracy of the analytical solutions depended on the assumptions made, and the drill string boundary conditions, mainly at the bit-rock interface [Bailey 1960], [Besaisow 1986], [Dareing 1968], [Huang 1968], [Paslay 1963].

**Axial and Torsional Vibrations of the Drill String**

The analytical solutions for the axial and torsional vibrations of the drill string have been investigated by Dareing and Livesay [Dareing 1968] who analyzed both cases in the context of petroleum engineering. The natural frequencies in the axial direction were obtained by solving the longitudinal wave equation, described by:

$$\frac{\partial^2 U}{\partial x^2} = \frac{1}{c^2}\frac{\partial^2 U}{\partial t^2}$$

where $U(x,t)$ is the axial deflection occurring at distance $x$ at time $t$, $c$ is the speed of propagation of longitudinal waves in the material, e.g. 5135.88 m/s for steel. The final solution of the wave equation depended on the boundary conditions assumed. Most authors assumed boundary conditions fixed at top and free at the bit rock interface.

In a similar manner, the torsional vibrations were obtained by solving the torsional wave equation, described by:

$$\frac{\partial^2\theta}{\partial x^2} = \frac{1}{c^2}\frac{\partial^2\theta}{\partial t^2}$$

where $\theta(x,t)$ is the torsional deflection occurring at distance $x$ at time $t$, $c$ is the speed of propagation of torsional waves in the material, e.g. 3246.12 m/s for steel.

**Lateral mode vibration**

A simple model for obtaining the natural frequencies in the lateral direction is described by Euler's beam equation. Assuming negligible shear and rotation, the Euler equation for vibrating beams of uniform cross section is expressed as:

$$EI\frac{\partial^4 y}{\partial x^4} - M\frac{\partial^2 y}{\partial t^2} = 0$$

where $y(x,t)$ is the lateral deflection occurring at distance $x$ at time $t$, $E$ is the material modulus of elasticity, $I$ is the moment of inertia and $M$ is the applied moment. The final solution of the beam equation depends on the boundary conditions assumed.

**Experimental results**

Besaisow et. al. [Besaisow 1986] collected data from the monitoring of two wells to verify the excitation mechanisms and the predicted resonant frequencies, using three different models. The first model used was based on a finite element eigenvalue solution algorithm developed by Paslay [Paslay 1964] for the ARCO Oil and Gas Co. The second is a general purpose finite element model with frequency response capabilities. The third uses simplified beam and wave equations (lumped parameters).

The results showed that the simple lumped parameter equations compared reasonably well for the axial and torsional vibration modes, but the axial resonance modes predicted by the three models deviated by up to 15 percent from the experimental results. The difference was stated to be caused by the bit-rock interaction condition, which was not modeled.

The finite element models performed best in predicting lateral resonant frequencies, although Besaisow et al. explain that the lateral modes are highly dependent on the boundary conditions of the sections prone to vibration. The simplified equations did not predict all the lateral modes that were significant.

Allen [Allen 1987] believes that lateral vibrations are the major cause of BHA failures. Data was gathered on thirteen bottom hole assemblies, which had been subjected to failures. In each case, the operator concluded from post failure inspection, that lateral vibration of the BHA was a likely cause of the failures. For the majority of the cases, computer models based on finite element analysis confirmed the presence of destructive lateral vibrations, and the absence of destructive axial and torsional vibrations. In two BHA failure cases, the computer model predicted that neither lateral, torsional nor axial vibrations would present a threatening vibration condition, however, the recurrence of failures in the two holes, indicated that some kind of destructive vibration could have been the cause of failure.

## 2.3 Drilling Automation

The main objectives of previous attempts to develop control strategies for drills, in the petroleum and mining industries, were aimed at maximizing production rates at minimum cost. These theories were based upon a combination of historical data and empirical techniques for selecting optimum weight-on-bits and rotary speeds. This approach required an economic evaluation of the variables involved, i.e. drilling rate, bit bearing wear, tooth wear and cost. Rotary torque was also monitored at all times and maintained within preset maximum or minimum limits by continuously adjusting rotary speed and bit weight.

In the mining industry and particularly for surface blasthole drills, these attempts resulted in the design of "automated drill control" packages by manufacturers (Bucyrus-Erie Ltd., Gardner-Denver Ltd., Marion-Indresco Inc.) to fulfill the immediate needs of the mining industry. By the mid-seventies, these automated control packages were available, based on solid state electronic technology [Currier 1972], [Li 1974]. The control strategies used were constraint violation initiated, with "normal" operating conditions restored through feedback control using appropriate sensors, current-limit devices and actuators. Operating limits were set by the mine, based on expected ground conditions, bit life and desired production rate.

## 2.4 Industrial State-Of-The-Art

### 2.4.1 Bucyrus-Erie Control System

A research program was conducted by Bucyrus-Erie Ltd. to automate an electric rotary blasthole drill in northern Quebec in 1969 [Currier 1972]. In limited field trials, a blasthole drill was modified for automated control during the drilling cycle. The automation mode began only after the drill had been positioned and leveled, and stopped when the bit reached its preset depth. Based on results from these trials it was concluded that:

1. Production footage using automation exceeded that from the past;
2. Bit costs per foot were significantly less than the best previous cost records in the same type of material;
3. Periods of severe vibration due to operator attempts to force progress through difficult ground were reduced.

It was indicated, however, that an overall increase in maintenance time occurred with the installed automation package. Furthermore, longer term tests were seen to be necessary to refine the system (hardware and logic), towards eventually reducing downtime and increasing machine availability. The original system incorporated electronic transducers and current-limit devices which fed back drill performance data to a central controller. The system would respond to the monitored signals when preset drilling and machine parameters were exceeded, through adjustments (individually or combined) to weight-on-bit and water injection rate, rotary speed and bailing air supply [Currier 1972], [Li 1974]. This initial work formed the basis for the commercial development of an automated drilling control package by Bucyrus-Erie. This system was offered as an integral component on both 60R and 61R Series III drills as early as 1971.

A modern Programmed Drilling Control (PDC) automation package is currently being offered as a factory installed option on Bucyrus-Erie's new 49R and 59R drills, implemented using a programmable logic controller (PLC) platform. The new product line of drills features drilling functions driven by electric direct current motors, powered by high-end programmable solid state drives. The PLC system is linked to a graphical display that replaces the mechanical gauges used in older machines, and provides the necessary user-interface to the drill operators.

In order to drill in automatic mode, the operator has to set the maximum allowable limits for weight-on-bit, rotary speed, rotary torque, rate of penetration, bailing air pressure and vibration. When drilling in automatic mode, the Programmed Drill Control would maintain the drilling variables within the preset limits, and then stop drilling when the user specified depth is reached. An automatic leveling mechanism and an alarm reporting screen are also included in the system.

**Vibration Control**

Two transducers, measuring drill mast velocity in the horizontal and vertical directions, are mounted at a mid point location of the drill mast, on the B-E 49R and B-E 59R. The PDC reacts to the measured signals, by adjusting weight-on-bit and rotary speed. When unable to compensate, the PDC lifts the rotary head, resets weight-on-bit, and then resumes the drilling process from that point. If unsuccessful after several attempts, the PDC stops drilling and generates a buzzing sound, requesting assistance from the operator.

Field visits to the Iron Ore of Canada mine, Labrador city, New Foundland, and to the Fording Greenhills Operation, Elkford, B.C., where several Bucyrus-Erie 49R drills were in operation, showed that the vibration control scheme had some limitations, when operating under diverse drilling situations and conditions.

### 2.4.2 Harnischfeger P&H Control System

Similar systems were also developed by Gardner-Denver for their line of GD-100/120 rotary blasthole drills. The Gardner-Denver *programmed control package* offered several different hardware configurations depending upon the need of the customer. The basic control hardware operates by initially setting targets for variables such as rotary speed, weight-on-bit and rate of penetration, to which the system would then seek to attain. The machine operator would set the drill bit on the bench, turn on the bailing air, set the desired depth of hole and initiate the automatic sequence.

Once automatic control was set, the drill would collar for a preset number of minutes, then the system would attempt to achieve the target levels of the variables. As the weight-on-bit, rotary speed and rate of penetration increased at a controlled rate, the feedback of torque, vibration and bailing air pressure responses due to changing ground conditions, would result in modifications to the control system. If torque exceeded its preset value, while weight-on-bit and rate of penetration were at acceptable levels, the controller would begin to reduce weight-on-bit at a controlled rate while allowing rotary speed to still seek its previously set value. If bailing air pressure began to rise, the controller would also reduce weight-on-bit and begin to limit the rate of penetration. If vibration levels (measured in both axial and lateral directions) increased above preset thresholds, the rotary speed only would begin to be reduced at a controlled rate. The system would eventually stabilize at some value of rotary speed, weight-on-bit and rate of penetration which was as close to the originally preset limits as possible. This basic automation system was available, not as retrofit equipment, but only as a factory installed option on new drills [Beardsley 1990].

In 1991, the Harnischfeger P&H Corporation acquired the large rotary blasthole drill product line from the Gardner-Denver Mining & Construction Division. Major improvements to the GD100/120, now identified as P&H 100B/120A, include the electrical drilling functions. The direct motors are driven by programmable digital DC drive systems, using a similar technology to the BE-49R/59R.

A standard PLC control system, named P&H Commandd™ Control, Integrates all control and display functions on the drill. The system controls all the major drilling functions including rotary, hoist, pulldown, propel, bailing air, auto level and auto lubrication (greasing system). Drill status, systems faults, fault history, PLC I/O status, data logging and automated drilling functions are among the information that can be displayed on a color screen, mounted above the operator's console.

The automatic drilling control algorithm is based on the same logic as the GD120, however, without vibration control. The operator enters the desired feed rate and rotary speed, as well as limits for the drilling variables of torque, bailing air pressure and pulldown force. When either limit for bailing air pressure, pulldown or rotary torque is exceeded, the feed rate is decreased. In automatic drilling mode, the rotary speed remains equal to the user-set reference. This system does not incorporate any vibration control.

### 2.4.3 Marion-Indresco Control System

The Marion-Indresco control system for the M-4 and M-5 crawler rigs was based on consideration that automation of only the primary drill functions was necessary to optimize drill performance, and that such a system should serve to enhance rather than substitute for the operator's skills. The Marion-Indresco system thus controls only the variable of weight-on-bit, based on limits of torque and bailing air pressure. Limits for each of these are preset into the system, and are determined based upon ground conditions, projected rotary bit life and desired rate of production. The system was aimed at achieving maximum productivity in terms of increased drilling footage with lower downtime and maintenance costs, while reducing operator abuse of the equipment [Li 1974].

**Conclusion**

Few drill manufacturers are currently offering surface blasthole drills with automation packages. Of those available, only one drill manufacturer (Bucyrus-Erie) is offering an automatic drilling system which includes vibration control. Field experience with the Bucyrus-Erie 49R blasthole drill indicated that the vibration control strategy, as implemented has limited success when drilling in variable ground condition.

## 2.5 Control Theory Review

### 2.5.1 System Identification

A control system architecture consists of a process to be controlled, called the *plant*, and the *controller* or *compensator*. The plant may also contain sensors for measurement of plant dynamics. In a control design exercise, the development of the original plant model is one of the most important and probably the most difficult aspect of control engineering. Many control problems turn out to be directly related to the use of an incorrect plant model [Houpis 1985].

A plant mathematical model can be generated based on considerations of the physics of the process, and the interaction between the various physical factors and elements that affect or contribute to the process. The model is valid within the established set of constraints and assumptions.

Further validation of the model can be obtained by collecting experimental data measured at the inputs and outputs of the process, sampled at speeds that exceed the estimated dynamics of the system. By applying iterative signal processing techniques to the measured input output data, the parameters of the model can be identified with reasonable accuracy. A good reference on the subject can be found in [Ljung 1987].

For the present control objectives, the drill's mechanical actuators need to be modeled, parametrized, and then identified experimentally, based on field input-output measurements.

### 2.5.2 Digital Control

The decline in the cost of digital hardware over the past years has made digital control implementation more economical and accessible to a broader range of applications. Such applications include industrial process control, robotics, guidance and control of aerospace vehicles, numerical manufacturing machines, as well as biomedical applications.

### 2.5.3 Feedback Controllers Structure

In the general context, the function of a controller is to achieve a desired response from a system, irrespective of the effect of internal (plant) and external (environmental) changes. The control objectives may be stated as [Palm 1983]:

- Minimizing steady state error.
- Minimizing settling time.

- Achieve other transient specification, such as minimizing the maximum overshoot and reduce rise-time.

For the vibration control problem, the primary objective is to minimize severe overshoots in the variables due to transitions between rock layers of different hardness, while keeping the steady state error close to zero.

### 2.5.4 PID Controllers

The most popular controllers are Proportional Integral Derivative (PID) controllers. PID controllers produce a control signal based on the error signal between the desired set-point and the actual output [Astrom 1984].

**Proportional Control**

A proportional controller generates a control signal proportional to the error signal. The proportionality constant is the *proportional gain*. Proportional control gives a zero control signal for zero error. Therefore, a stable system with proportional control would reach an equilibrium in which the control signal no longer changes, allowing a constant steady state error to exist. Increasing the proportional gain reduces the steady state error but adversely affect the system's stability.

**Integral Control**

An integral controller produces a signal that is proportional to the time integral of the error. More important, the type of the system is increased by one, improving the steady state error by one order; that is, if the steady state error to a given input is constant, the integral control reduces it to zero (provided the system is stable) [Kuo 1991]. However, because the system has increased by one order, it may become less stable than the original system.

**Derivative Control**

A derivative control produces a signal proportional to the derivative of the error signal. Since the derivative of the error represents its slope, derivative control can be seen as an anticipatory kind of control. For instance, large overshoots are predicted ahead of time and proper correcting effort is made. It is apparent that derivative control produces a signal *only* if the steady state error is not constant with respect to time. Therefore, derivative control are never used alone.

### PID Control

From the previous assertions, proportional control used with derivative control would add damping to the system, but the steady state response is not affected. Using PI control alone could add damping and improve the steady state error at the same time, but the rise time and settling time are penalized. This leads to the motivation of using a PID controller so that the best properties of each of the PI and PD are utilized.

The PID controller can be modeled as:

$$u(s) = [K_P + \frac{K_I}{s} + K_D s]\ e(s)$$

where $u$ is the control signal, $e$ the error defined as $e = u_c - y$ where $u_c$ is the set-point reference and $y$ the process output. $K_P$, $K_I$ and $K_D$ are the proportional, integral and derivative gains respectively.

### 2.5.5 Controller Implementation

Controllers connected in series with the plant are the most common because of their simplicity in implementation, depending on the nature of the process. In applied process control, a PID controller is usually implemented with the derivative control acting on the output variable of the process, which is first filtered [Eitelberg 1987]. Additional features need to be implemented when using integral control, such as integral windup prevention, integral preload, and bumpless transfer when switching from manual to automatic control. These features are essential to safe and effective operation in practice [Astrom 1984].

# Chapter 3 ANALYSIS OF DRILL VIBRATION

## 3.1 Blasthole Drill Rig Vibration

Several differences exist between petroleum and mining drilling using tricone bits, where the primary difference is the length and composition of the drill string. In petroleum drilling, the drill string contains collars and other heavy components, where vibration can cause costly Bottom Hole Assembly failures. In surface mining operations, the drill is much larger and heavier than the drill string (composed of drill pipes, bit-sub and bit), where vibration of both the drill and the drill string are of concern.

An idle leveled drill (i.e. raised on its jacks), vibrates under the effect of various rotating machinery, mainly electric or diesel operated, prime movers driving the bailing air compressor, hydraulic pumps, and, in the case of drills with electric drilling functions, direct current generators (e.g Bucyrus-Erie 60/61R, Gardner-Denver GD100/120). The vibration levels on these drills are typical of rotating machinery, which are generally non destructive.

While drilling a hole, the drill string can be subjected to severe vibrations, which subsequently results in severe vibration of the machine itself. If no corrective action is taken, the vibration can severely damage the drill.

It is apparent that the most critical drill vibrations are transmitted to the drill rig from the drill string, and therefore machine vibration can be attenuated by controlling the drill string vibrations.

### 3.1.1 Excitation Mechanisms in Tricone Blasthole Drilling

The same excitation mechanisms in BHA dynamics apply to blasthole drilling, namely mass imbalance, drill string misalignment, drill string rotational walk and tricone bit excitation.

The excitation mechanisms and their frequencies (Chapter 2) are summarized in the table below:

| Physical Mechanisms | Primary Excitation(s) | Secondary Excitation(s) |
|---|---|---|
| Mass Imbalance or Bent Pipe | 1 x RPM Lateral | 2 x RPM Axial<br>2 x RPM Torsional<br>2 x RPM Lateral |
| Misalignment | 1 x RPM Lateral<br>2 x RPM Lateral | 2 x RPM Axial |
| Tricone Bit | 3 x RPM Axial | 3 x RPM Torsional |
| Rotational Walk | D/(D-d) x RPM Lateral | 2D/(D-d) x RPM Axial |

**Table 3.1:** Drill String Excitation Mechanism Frequencies

In order to explore the possibility of controlling drill string vibration by adopting a similar approach to that suggested for oil well drilling, the drill string natural frequencies need to be estimated in the axial, lateral and torsional directions. Critical speeds can then be estimated and avoided while drilling.

In the case of the Ingersoll-Rand DM45E drill, a drill string can be composed of a maximum of five drill rods, available on the drill's carousel. For such a condition, a total of five sets of natural frequencies need to be computed, i.e. one set for every possible drill string assembly configuration.

The following sections will estimate the natural frequencies of the drill string, and how they are also affected by the rotary head position and drill string length.

## 3.2 Axial And Torsional Vibration Of Drill String

The drill pipes used in the DM45 were 7.62 m (25 ft.) long, with 133.35 mm (5.25 in.) and 158.75 mm (6.25 in.) inner and outer diameters respectively. The natural frequencies of the drill string in the axial and torsional directions were obtained using a finite element analysis package, MSC-PAL, used for the purposes of a mechanical engineering undergraduate course at McGill University. The drill string length was augmented by 1.37 m. (4.5 ft.) to account for the rotary head spindle sub, bit sub and the bit, modeled as an extended length of the drill pipe. Each additional drill pipe increased the length of the drill string by 7.62 m (25 ft.).

The natural frequencies of the axial vibrations are shown in Table 3.2, assuming a free boundary condition at the bit, while Table 3.3 assumes the bit to be fixed. Table 3.4 shows the natural frequencies of the torsional mode, with the bit assumed free to rotate. The fixed bit boundary condition is not considered, since it reflects the condition of a stalled bit.

When compared with the excitation mechanism frequencies, the natural frequencies as obtained for the axial and torsional modes remain quite high with respect to average rotary speeds encountered in blasthole drilling. For example, a typical rotary speed of 120 RPM translates into a rotational frequency of 120 (rev/min) / 60 (sec/min) = 2 Hz.

| **Drill string** | **1st mode (Hz)** | **2nd mode (Hz)** |
|---|---|---|
| **1 pipe** | 136.25 | 423.61 |
| **2 pipes** | 71.72 | 217.48 |
| **3 pipes** | 48.83 | 147.14 |
| **4 pipes** | 37.01 | 111.31 |
| **5 pipes** | 29.80 | 89.55 |

**Table 3.2:** Axial Natural Modes of Vibration as Computed; DM45 Drill String; bit assumed free

| Drill string | 1st mode (Hz) | 2nd mode (Hz) |
|---|---|---|
| 1 pipe | 267.89 | 535.78 |
| 2 pipes | 142.91 | 285.81 |
| 3 pipes | 97.44 | 194.88 |
| 4 pipes | 73.92 | 147.85 |
| 5 pipes | 59.55 | 119.11 |

**Table 3.3:** Axial Natural Modes of Vibration as Computed; DM45 Drill String; bit assumed fixed

| Drill string | 1st mode (Hz) | 2nd mode (Hz) |
|---|---|---|
| 1 pipe | 80.71 | 242.71 |
| 2 pipes | 43.67 | 131.11 |
| 3 pipes | 29.94 | 89.84 |
| 4 pipes | 22.78 | 68.34 |
| 5 pipes | 18.31 | 55.14 |

**Table 3.4:** Torsional Natural Modes of Vibration as Computed; DM45 Drill String; bit assumed free

## 3.3 Lateral Vibration of Drill String

In the lateral direction, the drill string is fixed at the rotary head and constrained at the deck level by the centralizer bushing, as illustrated in Fig. 3.1. The solution for the natural frequencies depends upon the drill string boundary conditions, and the centralizer bushing constraint. Since the rotary head can move along the length of the mast, the position of the centralizer bushing with respect to the rotary head is continuously changing.

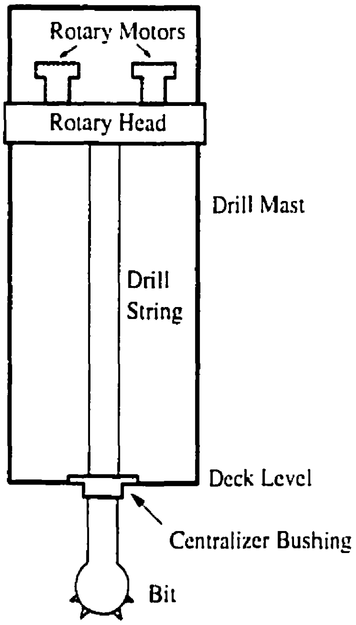


**Figure 3.1:** Illustration of centralizer bushing effect

By modeling the centralizer bushing as a pin, the drill string becomes fixed at the rotary head and pinned at the centralizer bushing level, e.g. at a distance $0<x<7.62$ m., since the head can slide over this length along the mast. The total length of the drill string includes the spindle sub, bit sub and the bit.

Using the finite element analysis package MSC-PAL, the natural frequencies of the first three modes were estimated, at 0.5 m. incremental displacements of the rotary head, assuming three different boundary conditions at the bit level; *free, fixed and pinned* (the actual boundary condition is an impedance, with parameters depending on the bit rock interaction).. The results are included in Appendix A. The results for the free bit boundary condition are also shown in Fig.3.2 and Fig.3.3. The ordinate scale on the right is given in counts per minute (cpm), which corresponds to revolutions per minute (rpm).

Figures 3.2 and 3.3 indicate that the drill string natural frequencies are affected by the number of pipes, as well as the rotary head position and the bit boundary condition. They decrease when additional drill pipes are added, and their rate of change, with respect to the rotary head position, becomes smaller. The natural frequencies as obtained fall well within typical operating ranges of rotary speed. Therefore, it is possible to excite the drill string into lateral vibration resonance while drilling .

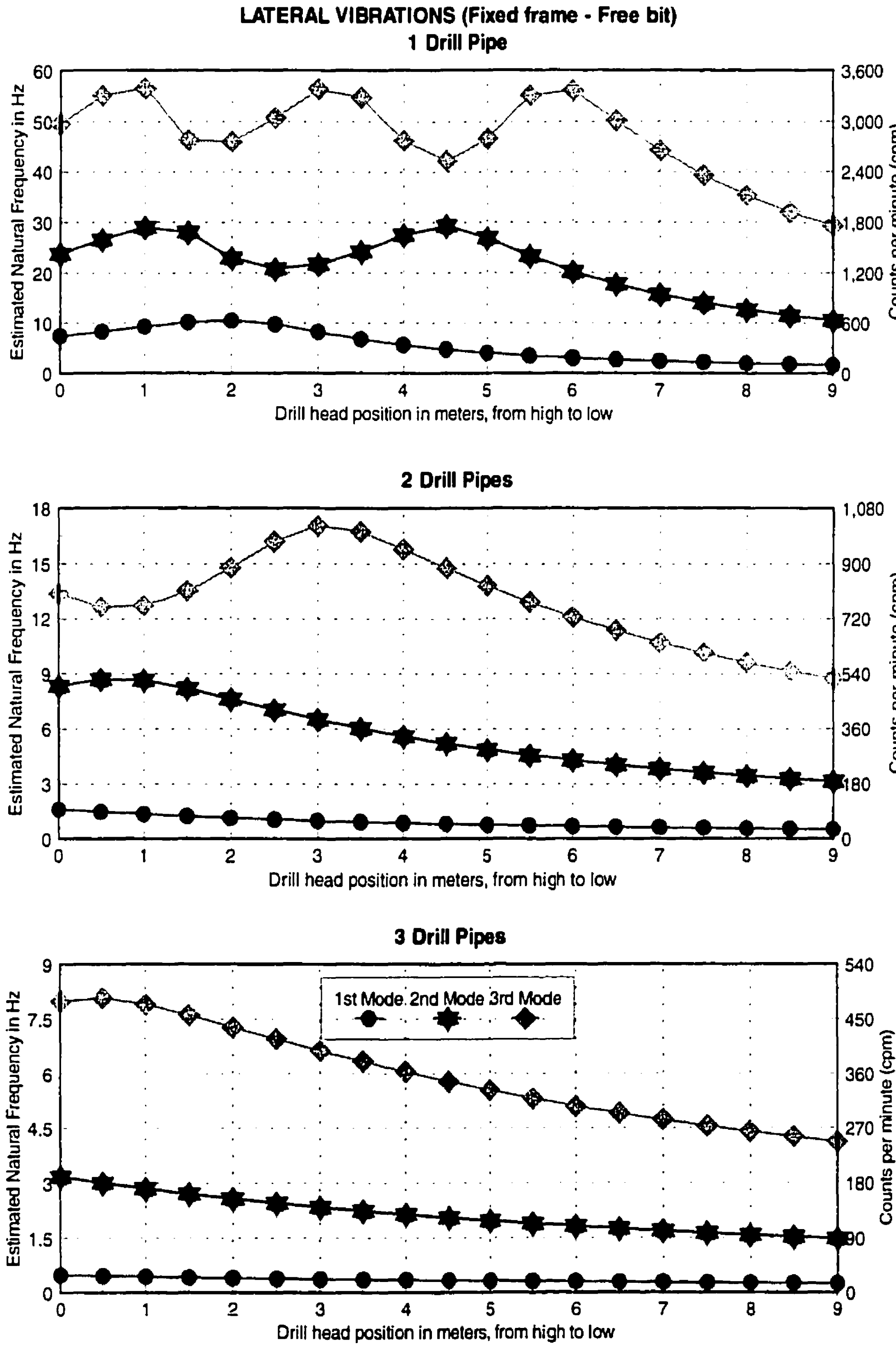


**Figure 3.2:** Lateral Natural Modes of Vibration as Computed; DM45 Drill String; bit assumed free

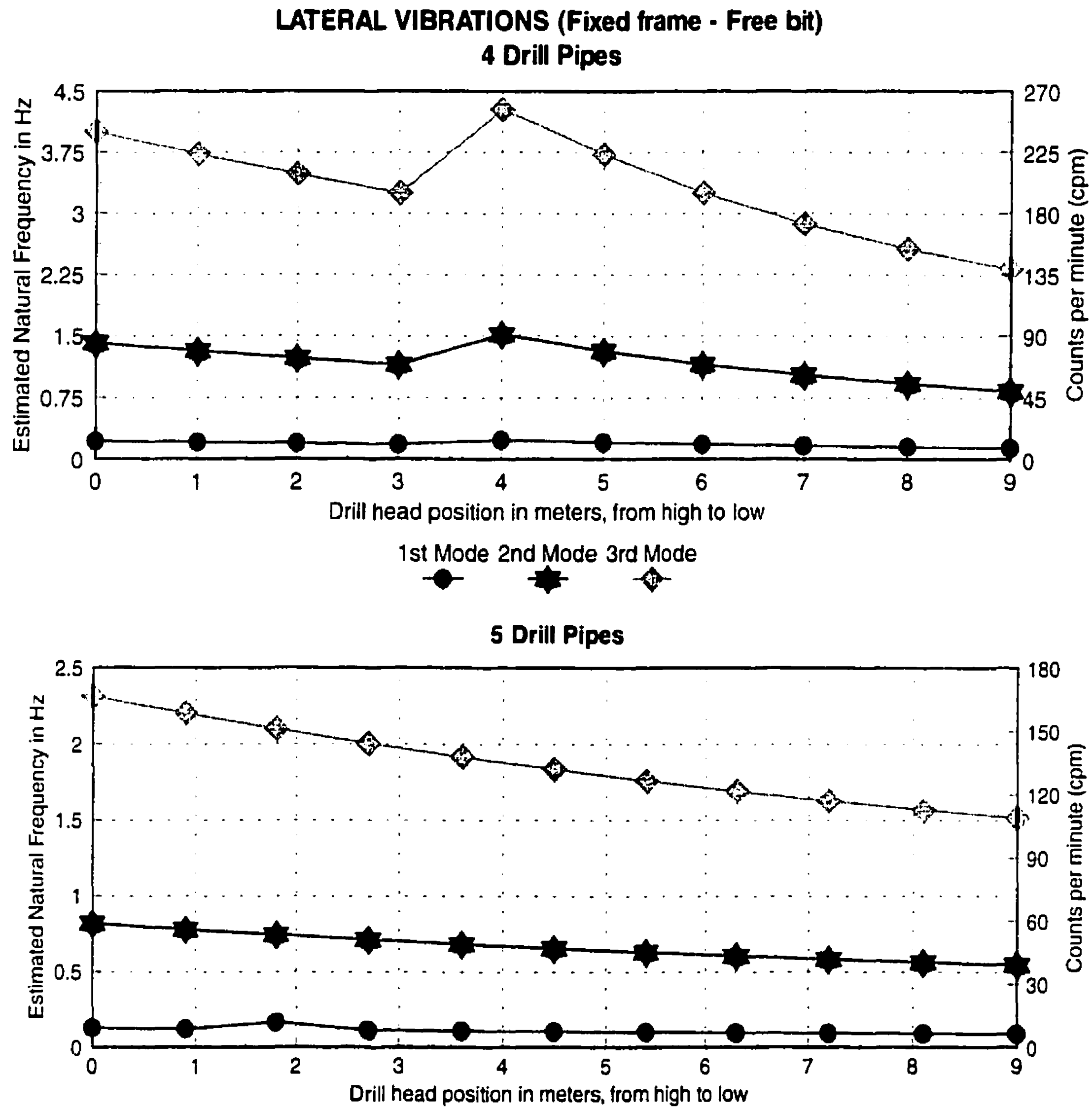


**Figure 3.3:** Lateral Natural Modes of Vibration as Computed; DM45 Drill String; bit assumed free

### 3.3.1 Experimental Determination of Natural Frequencies

The validity of the analytical results was verified by conducting structural resonance tests on a drill string composed of a single drill pipe, at the Ingersoll-Rand Rotary Drills testing facility, Dallas, Texas, in May 1992. The instrumentation needed to experimentally obtain a structure's natural frequencies consisted of an *impact hammer*, a *Frequency Spectrum Analyzer* and *acceleration transducers* with appropriate signal conditioning units.

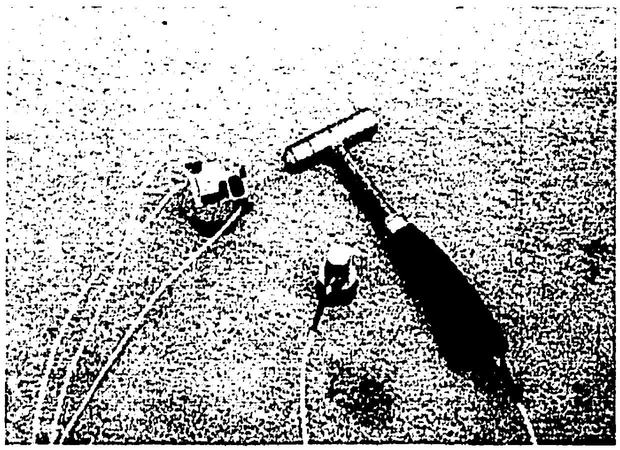

**Figure 3.4:** From left to right: Triaxial accelerometer, uniaxial accelerometer and impact hammer

Impact hammers (Fig. 3.4) are small hammers used to excite structures and machines with an impulse. The width of the impulse depends on the hammer striker tip and upon the material and stiffness of the system to which the hammer is applied. The striker tips are interchangeable and are usually made of steel, aluminum, plastic or rubber. The impulse function in the time domain is obtained from the output of a force transducer embedded in the head of the impact hammer. Additional weights can be added to the head to generate larger impulse amplitudes. As an example, the width of the impulse obtained from the output of a steel-tipped impact hammer striking a concrete floor is about 0.2 millisecond.

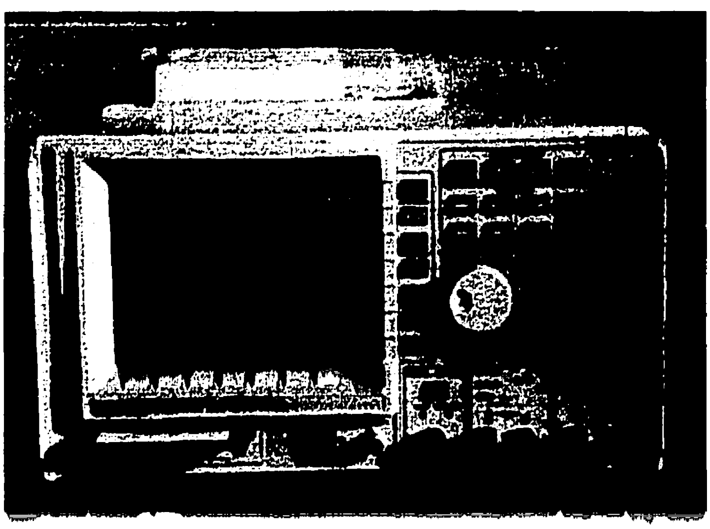

Figure 3.5: Advantest Fast FourierTransform Spectrum Analyser

Upon impact, the structure responds by vibrating, with an amplitude of oscillation greatest at frequencies close to the structure's natural frequencies. A spectrum analyzer (Fig. 3.5) is a measuring instrument that shows the structure's amplitudes of oscillation at those different frequencies in a plot called a *frequency spectrum*, computed using a digital signal processing technique known as the Fast Fourier Transform (FFT). The highest oscillation amplitude on the frequency spectrum indicates the natural frequencies of the structure.

For the factory DM45 test drill, the bit was lowered into a 3.48 m (10 ft.) pit below the machine, and the natural frequencies were measured at 0.45 m (18 in.) incremental displacement of the rotary head. The results, shown in Fig. 3.6, are at an offset from analytical estimates, nonetheless they follow the same trend. Thus it appears that the trends of the estimated natural frequencies are valid. The estimated frequencies, however, have some margin of error.

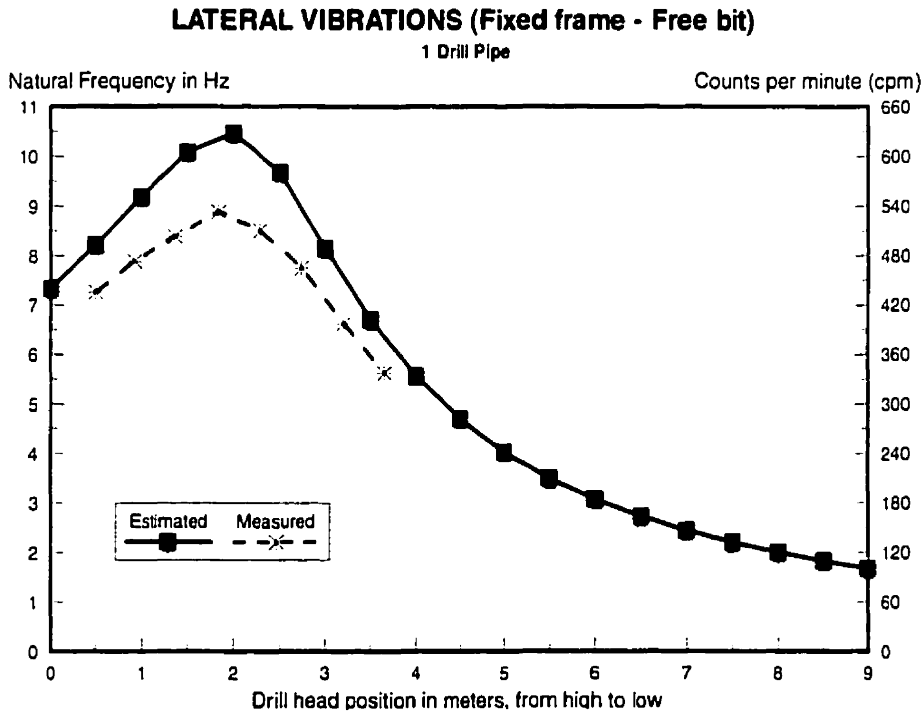


**Figure 3.6:** Estimated and experimental natural frequencies of a 7.62 m. DM45 drill string

## 3.4 Conclusions

The studies previously conducted in oil well drilling yielded encouraging results, with good approximations of natural frequencies for BHA assemblies. Although the accuracy was in some cases within 20%, and some modes of resonance were not predicted, a large number of BHA failures were avoided.

In the case of blasthole drilling, the drill string natural frequencies, as computed in the axial and torsional modes, were found to be too large to be excited by typical operating drilling rotary speeds. In the lateral modes, the natural frequencies fall well within drilling rotary speed ranges. Therefore, only critical speeds that generate lateral resonance need to be avoided.

The lateral mode natural frequencies, however, depend on several factors, mainly the boundary condition at the bit and the rotary head position along the mast. Furthermore, the estimated natural frequencies did not consider the non-linear effect of backlash, due to the clearance of the centralizer bushing and the rotary head guides. These factors are continuously changing during the course of drilling a hole, thus shifting the natural frequencies to a different range.

For practical implementation of such a model based control strategy, accurate estimate of natural frequencies would need to be generated, adapted to the machine specifics, such as design and steel pipe geometry. This would require a powerful computer on board the drill, to continuously compute natural frequencies, while drilling, and therefore enact adjustments on rotary speed. A look up table could be used, however such a table would have to be recalculated and updated every time a new geometry was introduced in the drill string, e.g. new pipe of different length.

It is apparent that such preventive approach represented by resonant frequency prediction is not viable for blasthole drilling. A more practical and less expensive solution is needed. This solution needs to be portable to different types of machines, robust and insensitive to steel pipe geometry, machine aging, bit and centralizer bushing wear. Such an approach can be implemented by adopting a "reactive" control strategy, e.g. one that actuates rotary speed based on feedback measurements of the drilling variables, as opposed to the preventive approach of avoiding critical speeds.

A typical methodology for designing a feedback control strategy is to devise a model for the process to be controlled. Subsequently, this model would be used to design a controller, run computer simulations until a stage of readiness for implementation, and to finally test it on an actual machine under controlled conditions. Based on observations during field tests, the controller is refined and tuned until the desired machine performance is achieved.

The following chapters of this thesis will endeavour to fulfill such objectives.

# Chapter 4 EXPERIMENTAL FIELD TESTING

## 4.1 System Modeling

A feedback control design approach consists of understanding the interaction between the various components of the drilling process, leading to modeling the process. The model can then be used to formulate a control strategy, and also to build a computer simulator that simulates drilling, which can assist in testing and fine-tuning the envisioned control strategies.

The drilling process consists of the machine mechanics that generate rotary speed and weight-on-bit based on the operator's setpoints. The bit rock interface produces penetration rate, torque demand, vibration, bailing air pressure rise and other secondary variables, based on these setpoints. A block diagram model of the overall system is shown in Fig. 4.1.

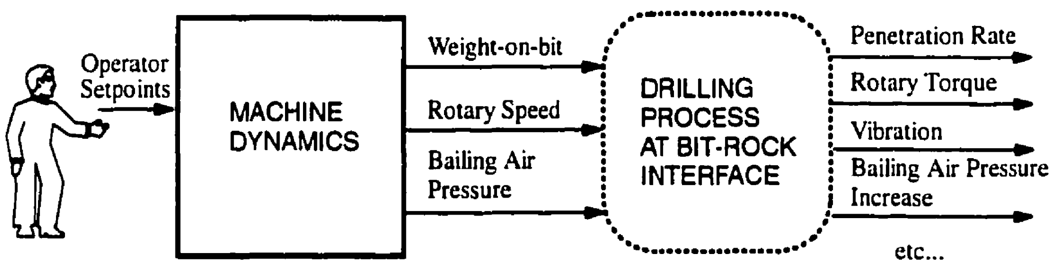


**Figure 4.1:** Modeling the overall drilling process

While the machine actuators can be modeled as linear systems, the bit-rock interface is nonlinear and has complex dynamics. In addition, certain aspects of the mechanical structure of the machine also exhibit nonlinear behavior.

For the present control objectives, a very detailed model of the system is not possible nor necessary, due to the complicated non-linearities that are difficult to assess and characterize analytically. However, a good approximation that can describe the drilling process will be modeled, and will be sufficient to design and simulate a control strategy.

### 4.1.1 Modeling Machine Actuators

The actuators of interest are the hydraulic cylinders of the feed system that produce weight-on-bit, and the hydraulic rotary actuator that produces bit rotation, in the case of the DM45E drill. Modeling is based on mechanical considerations as well as hydraulic fluid flow-pressure relationships (other makes of blasthole drills use electric actuators, e.g. Gardner-Denver, Bucyrus-Erie).

System identification techniques can be applied to experimentally measured input-output data [Ljung 1987]. For the feed system, the relevant data consists of the feed cylinders hydraulic input pressure and the actual weight-on-bit. The rotary actuator necessitates the measurement of the hydraulic input flow and pressure, as well as the actual bit rotary speed.

### 4.1.2 Modeling The Bit-Rock Interface

Modeling the bit-rock interface consists of modeling the penetration rate, torque and vibration. As described in the literature review, several authors have suggested models for penetration rate and torque, however all their models were based on empirical results with initial approximations generated from an analysis of the physics of the process. The vibration models presented were mainly focused on predicting natural frequencies.

### 4.1.3 Need for Experimental Testing

Since the bit-rock interface models are based on empirical data, field testing and data logging is necessary. In parallel, the experimental tests needed for the mechanical actuators identification can be conducted. Field testing will in addition provide a better understanding of the drilling process.

## 4.2 Field Testing

Field tests were conducted at the Lafarge quarry, Alpena, Michigan, during the period June 17 to June 24 1992, where a fully instrumented DM45E was tested. The instrumentation involved design, procurement of new hardware and software, assembling hardware, writing software, machining, welding, testing and calibrating transducers. The initial instrumentation set-up and testing were run on a DM45 drill at the Ingersoll-Rand Garland test facility during the period of April-May 1992. The actual field tests were conducted as a joint effort between the Canadian Center for Automation and Robotics in Mining (CCARM-McGill) and Ingersoll-Rand Co. Rotary Drills division personnel.

### 4.2.1 Instrumentation Overview

The variables of interest and the way they were measured is described in the following.

**Weight-on-bit:**

By measuring the hydraulic pressure at the input of the hydraulic cylinders, denoted by "Feed Pressure" in this thesis. The feed pressure generates a proportional force on the bit, that can be calculated.

The proportional relationship between feed pressure and weight-on-bit was obtained experimentally by measuring both the feed pressure and the actual weight-on-bit. The weight-on-bit was measured using a 50,000 lbs. load cell, shown in Fig. 4.3, positioned below the drill's first steel pipe.

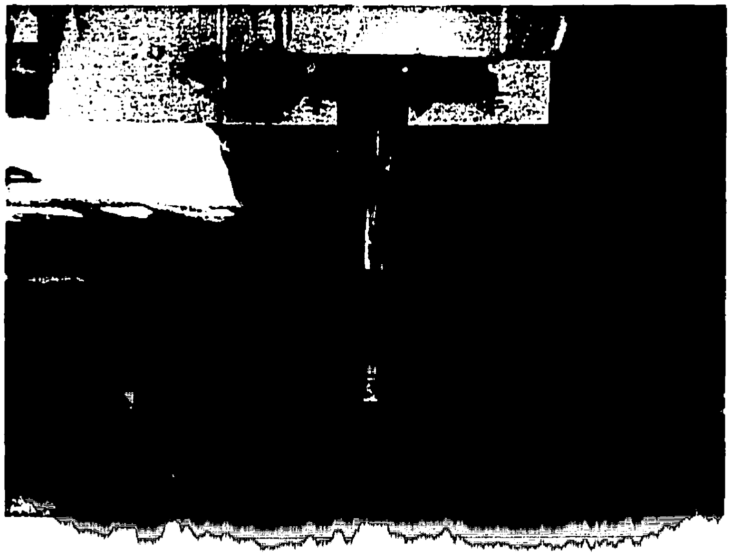

**Figure 4.3:** 50 Klbs. load cell used to measure actual weight-on-bit.

**Rotary speed:**

By using a DC tachogenerator coupled to the spindle through direct contact. The rotary motors hydraulic flow was also measured using a flow transducer.

**Rotary Torque:**

By measuring the hydraulic pressure into the hydraulic rotary motor, also denoted by "Rotation Pressure". The rotation pressure, minus the output pressure from the motor, is proportional to the mechanical torque produced by the motor at the shaft. At no load, i.e. when not drilling, this torque must overcome viscous damping, dry (Coulomb) friction, and also drive the inertial load of the drill string. Thus the rotation pressure needed to rotate the spindle at a steady state rotary speed is referred to as the "no-load rotation pressure". The increase in rotation pressure while drilling produces the torque delivered to the rock at the bit-rock interface, referred to as "Disturbance Torque". Thus, in terms of pressures, the portion of the rotation pressure that generates the disturbance torque is referred to as "Disturbance Pressure". A telemetry system that was designed to independently measure the actual spindle torque and bending of the drill string failed to generate the appropriate signals due to several technical difficulties encountered at the test site.

**Depth:**

By using a potentiometer (CELESCO) actuated by the extension of a steel cable connected to the rotary head. The potentiometer was fixed onto the upper frame of the mast.

**Penetration Rate:**

By smoothing and then differentiating the depth signal.

**Axial, Lateral, and Transverse vibration of rotary head:**

By using a triaxial strain-gauge accelerometer fixed onto the rotary head. Fig. 4.2 illustrates those directions with respect to the tower.

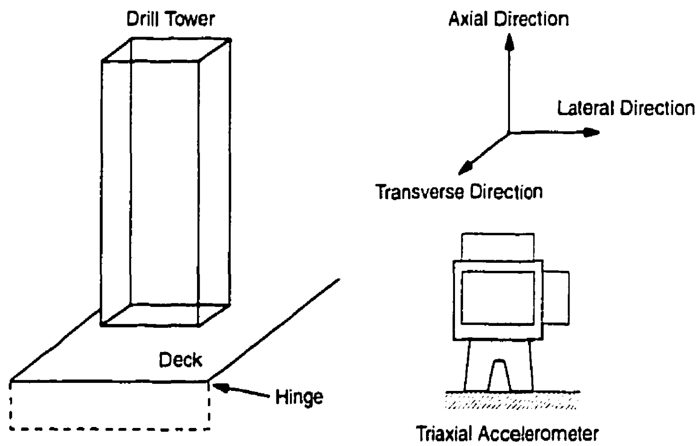


**Figure 4.2:** Orientation of accelerometers with respect to drill tower

**Lateral Vibration of tower, near operator cab:**

By using a strain-gauge accelerometer mounted onto the tower, one meter above the table. A similar accelerometer that was mounted to measure vibration in the axial direction malfunctioned, and could not be replaced.

**Fluid Flow into Rotary Motor:**

By using a turbine-based flow transducer with appropriate signal conditioning. However, the flow transducer saturated at nearly 90 gpm, corresponding to a rotary speed near 130 rpm. The maximum operating speed of the tested DM45E was in the vicinity of 150 rpm.

**Bailing Air Pressure:**

By using a pressure transducer connected to the bailing air conduit.

**Number of drill pipes in drill string:**

The number of pipes in the drill string was needed to compute the actual depth, using the rotary head position signal. The number was generated by a power supply, set to produce an analog voltage where each volt corresponded to one drill rod (Ex. 3 Volts => 3 drill rods). The author incremented the voltage every time a steel pipe was added to the drill string.

**Power Source**

The majority of the sensors were strain-gauge based, and therefore powered and conditioned by a strain-gauge amplifier-conditioning unit. The remaining transducers were powered by DC-to-DC converters, converting the 24V available from the rig's batteries into the appropriate voltage levels required by the transducers.

**Data Logging**

The transducers signal were recorded using a Digital Audio Tape (DAT) recorder, model RD-200 PCM from TEAC. The unit records using DAT technology 16 analog signals of 2.5 KHz bandwidth each. Each tape can store data equivalent to two hours of recording, providing a convenient mass storage medium. An additional channel is reserved for recording external comments that the user enters by speaking into a hand held microphone. The recorder, supplied by CCARM-McGill, was conveniently powered by the 24V DC battery source available on the drill rig.

**Computerized Data Acquisition**

In addition to the recorder, the transducers' signals were wired to a computer system (Kontron Lite) equipped with a data acquisition card (Metrabyte-Keithley), and controlled by a user-programmable software (Viewdac™). The system was set to display all the measured quantities in their physical units, as well as other variables computed on-line, such as penetration rate. This set up offered the advantage of monitoring the progress of the testing methodology, and also pin-pointing occurrences of hardware failure .

In the field, except for the transducers, the instrumentation equipment was installed on a bench replacing the middle row seats of a rental van, as shown in Fig. 4.3.

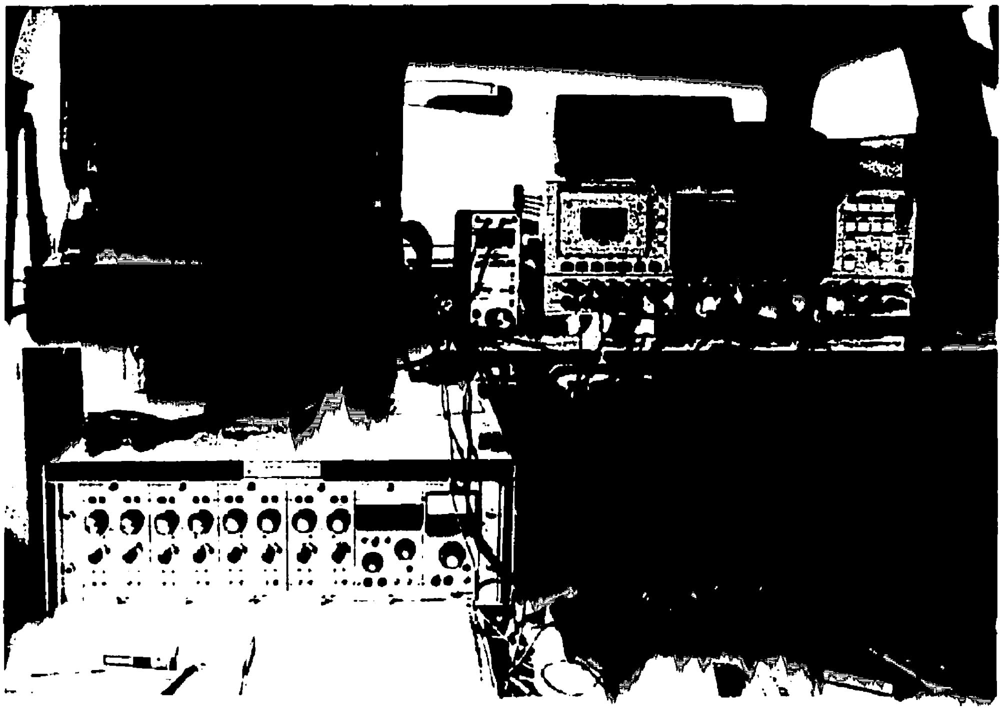

**Figure 4.3:** Data acquisition instrumentation in the field

### 4.2.2 Field Testing Summary and Methodology

A total of 17 boreholes were drilled at the Lafarge quarry during the period June 17 - June 26 1992. Ten boreholes were "normally drilled", i.e. according to standard operating practice at the site, while the remaining seven boreholes were drilled according to a pre-specified testing sequence. The majority of the boreholes were drilled at 20 degrees inclination, 28 ft apart, with an average drilled length of 100 ft. One borehole was drilled 48 ft. away from a cored hole, outside the graded area (Borehole XXTRA) using five drill pipes, at full length (near 115 ft.). Only one borehole (Borehole A1A) was drilled vertically, a 1000 ft. away from the graded area, and using the full length of five steel pipes. The vertically drilled borehole was completed in one hour, while nearly fifteen more minutes were needed for normally drilled inclined holes. The inclined holes used one third of the fifth drill rod full length.

The bit used was a new $7^{7/8}$ inch O.D. Baker-Hughes BH50J Model 924888. A new bit was used to reduce the bit dullness effect on data variability. The height of the highest carbide insert was approximately 0.43 inch. The centralizer bushing on the tested machine had an inner diameter of $6^{1/2}$ inches. The five drill pipes available on the machine's carousel had an outer diameter of $6^{1/4}$ inches and were each 25 ft. long.

The graded area hole pattern is shown in Fig.4.4. It consisted of two rows of inclined holes at 20 degrees, identified as rows A and B. Geological information supplied by the Lafarge quarry, showed the bench to consist of numerous limestone beds, of varying shale composition, and therefore of varying strength. These limestone beds seemed to be the most variable in the upper portion of the bench up to 58 ft. depth, where a thin (2 to 3 ft. thick) band of shale was found. Also, there was a shaly limestone unit at 34 to 39 ft. depth. During field tests, a geophysical logging company was subcontracted to provide gamma, caliper, density and sonic logs to confirm the geological characteristics of the test site.

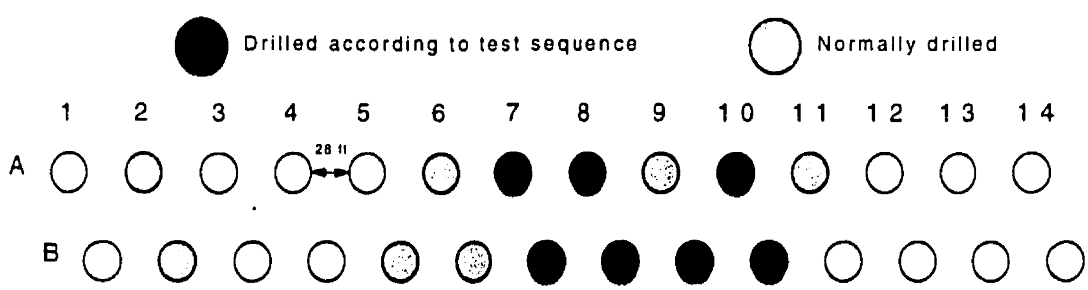


**Figure 4.4:** Bench borehole layout; Lafarge Quarry, Alpena, MI

The procedure for drilling the seven "test" boreholes consisted of maintaining feed pressure constant at levels of 500, 1000, 1500 and 2000 psi, while incrementing rotary speed gradually, to full scale. A period of 30 seconds approximately after each rotary speed increment allowed the system to stabilize at a steady state operating point. The same procedure was followed by maintaining rotary speed constant at several levels while gradually incrementing feed pressure. The steady state operating points, averaged over the 30 second interval, form experimental observations that can be used for analysing the steady state relationship between the drilling variables.

# Chapter 5 FIELD DATA ANALYSIS

## 5.1 Office Data Digitization Set-up

Field test data recorded on tape needed to be reproduced, then digitally sampled by a host computer, to allow for data manipulation and analysis.

During playback, the reproduced analog field signals were low pass filtered, using 4$^{th}$ order Butterworth filter blocks. The filter blocks ordered from Frequency Devices Inc., had a programmable cutoff frequency range of 1 to 255 Hz. Additional electronic circuitry was designed and assembled in-house to interface the filters with the host computer (Kontron Lite), enabling the filters to be programmed through the Viewdac software. Figure 5.1 illustrates the digitization set up.

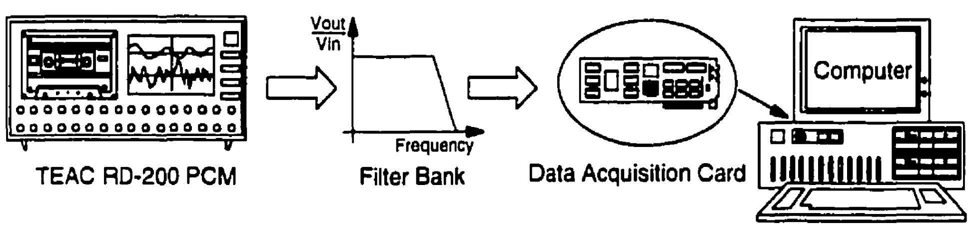


**Figure 5.1:** Recorded field data digitization set-up

## 5.2 Validation of Excitation Mechanisms

### 5.2.1 Time Domain Vibration

A section of field signals, where severe drill vibration occurred while drilling borehole B2 at length of 22.5 meters (74 ft.) is shown in Fig. 5.2. The signals were filtered at 50 Hz, then sampled at 200 Hz. The head axial, lateral, transverse and tower lateral vibration signals are displayed, as well as rotary speed and rotation pressure. The nominal feed pressure and rotary speed were set at 1500 psi and 140 rpm respectively, and remained unchanged during the 10 second interval.

At time 4 seconds, the vibration signals amplitudes increased, the rotary speed became less stable, and the rotation pressure increased in magnitude and ripple. The sudden change in rotation pressure could have been the result of a change in ground condition, as more torque is required to crush the new rock layer.

Since the boreholes drilled were geophysically logged, it was possible to examine the rock properties at 22.55 m depth for borehole B2. The geophysical logs of Young, shear and bulk moduli, as well as rock density for this hole are shown in Fig. 5.3 with respect to depth. The geophysical logs may not accurately coincide with the borehole lengths monitored by the test system. The reason for the discrepancy is explained by the inaccurate ground level referencing by the geophysical logging operator, because of the rock cuttings pile surrounding the borehole.

The geophysical logs clearly indicate a variation in geology, as indicated by decreases in the Young, shear and bulk moduli, starting from 20 m. borehole length. The sudden increase in these traces near 22 m. suggests a transition from a softer to a harder ground type. The decrease in the density log near 22 m. confirms the existence of a lower density band of shale interbedded with the limestone.

Based on these data, it therefore appears that the drill started to vibrate severely as the bit suddenly progressed from a soft to a harder rock type.

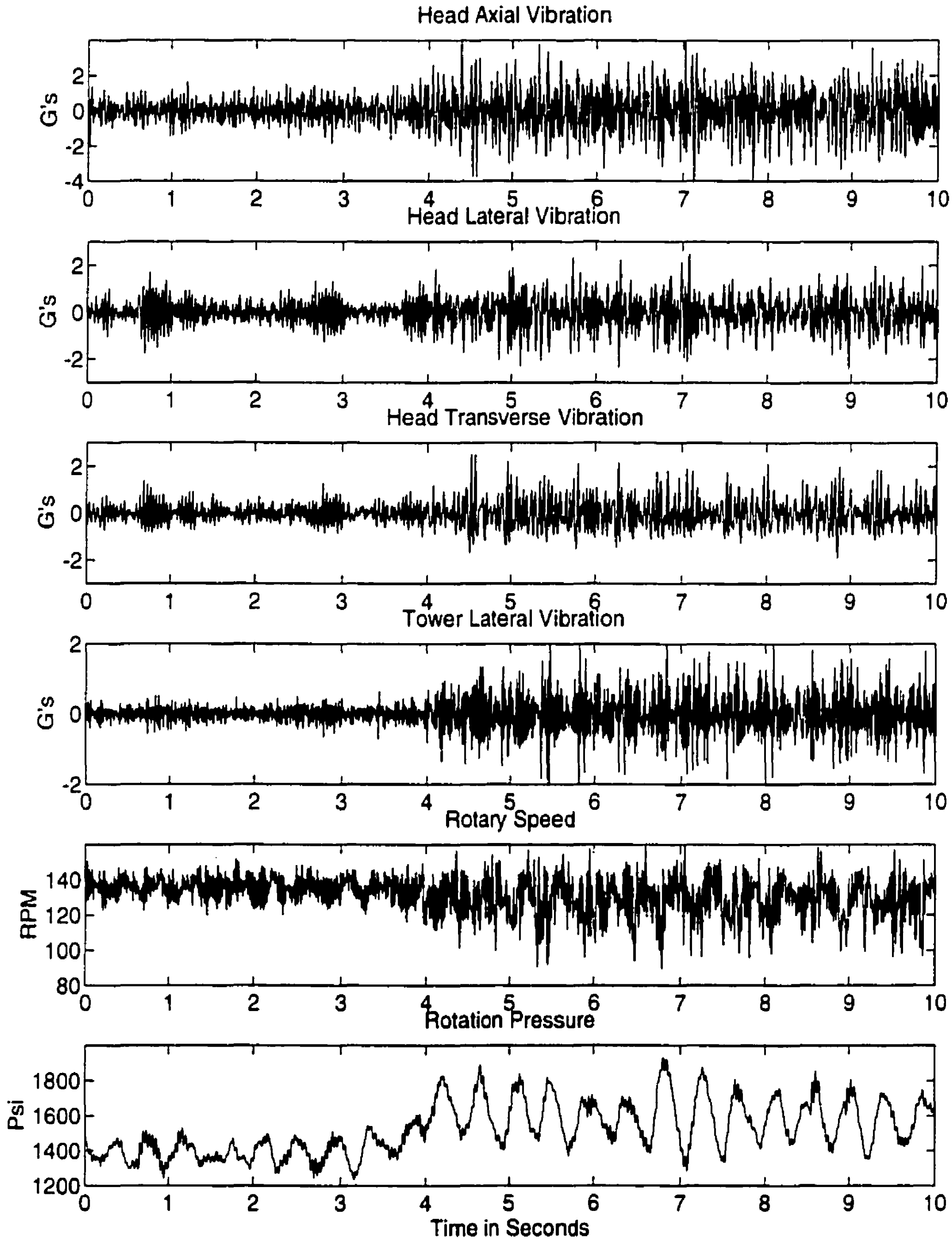


**Figure 5.2:** Time domain vibration, rotary speed and rotation pressure signals, borehole B2

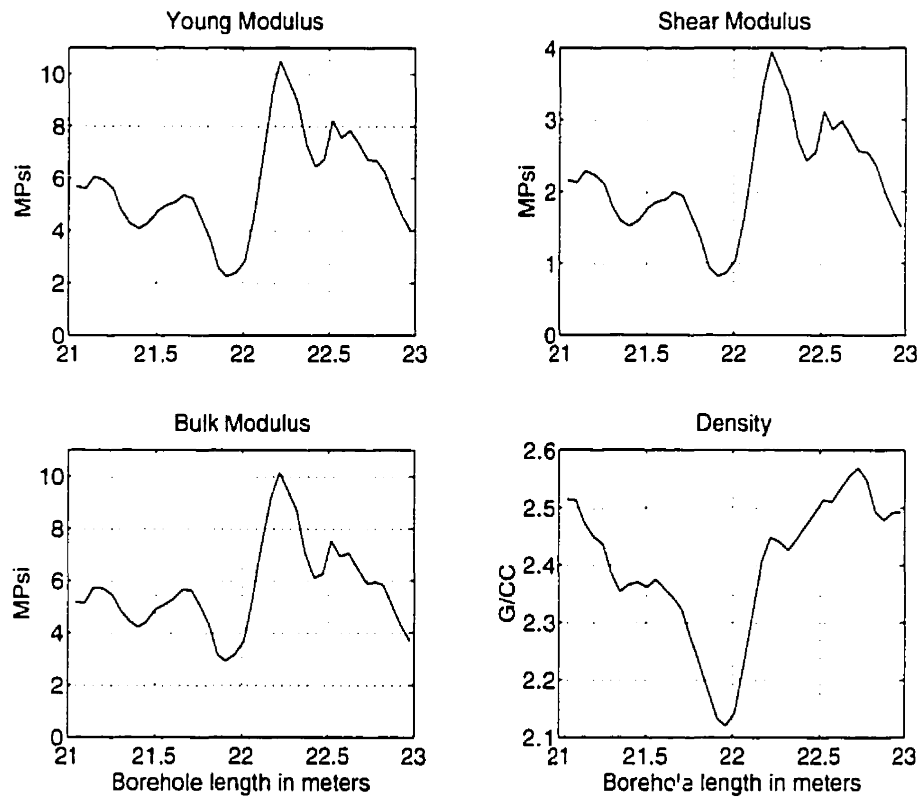


Figure 5.3: Geophysical logs of Borehole B2 near 22 meters length

The drill string natural frequencies could also be verified. At time 4 seconds, the head position was at 1.67 m (5.5 ft.), with four drill pipes loaded in the drill string. The estimated lateral mode natural frequencies were then extrapolated from the data in Appendix A, at a head position of 1.67 m., with 4 drill pipes in the drill string, for the three bit boundary condition cases. The results are summarized in the table below:

| | **Free Bit Case** | **Pinned Bit Case** | **Fixed bit Case** |
|---|---|---|---|
| **1st Mode** | 0.24 Hz (14.4 RPM) | 0.80 Hz (48 RPM) | 1.35 Hz (81 RPM) |
| **2nd Mode** | 1.25 Hz (75 RPM) | 2.80 Hz (168 RPM) | 3.65 Hz (219 RPM) |
| **3rd Mode** | 3.60 Hz (216 RPM) | 6.20 Hz (372 RPM) | 7.10 Hz (427 RPM) |

**Table 5.1:** Estimated lateral mode natural frequencies at a head position of 1.67 m, 4 drill pipes

The closest possibility to the rotary speed of 140 RPM is the second mode of vibration, for the pinned case, yet at an error of 20%.

### 5.2.2 Frequency Domain Analysis

A frequency domain analysis was conducted on the vibration data acquired before the occurrence of severe vibration. Vibration frequency power spectra were computed by integrating the acceleration signals twice, to obtain displacement, then by applying Fourier transforms onto the time domain displacement signals. The power spectra graphs are shown in Fig.5.4.

The head axial vibration power spectrum exhibits several peaks, the largest at the primary 3x RPM ( 6.99 Hz) tricone bit excitation. A secondary 2x RPM (4.66 Hz) mass imbalance and misalignment excitation is also visible, as well as a 1x RPM (2.33 Hz) excitation. Artifacts of the 2x RPM and 3x RPM are also apparent at 4x RPM (9.32 Hz) and 6x RPM (14 Hz). Finally, a less enhanced peak at 2D/(D-d)x RPM (22.6 Hz) is representative of a minor rotational walk mechanism.

The tower lateral and both head lateral and transverse vibration power spectra show a largely dominant 1x RPM excitation, due to the effects of mass imbalance and misalignment. Peaks at 3x RPM and 6x RPM are also visible.

The power spectrum of the vibration signals, after the occurrence of severe vibration, was then computed and shown in Fig. 5.5. In the case of the head axial vibration, the 1x, 2x, 3x, 4x and 6x RPM peaks are no longer isolated, but the vibration power has increased and largely intensified over the first 20 Hz range of the spectrum. Since no dominant peaks can be observed, no resonant condition can be stated to exist.

A similar observation can be made for the other three vibration power spectra, where the vibration power has also intensified in the low frequency range, below 20 Hz. In addition, the head lateral and transverse vibration have maintained a clearly dominant peak at 1x RPM, with larger amplitude than before the occurrence of severe vibration. The increase can be justified by an aggravation of the mass imbalance or misalignment effects, or possibly because of a resonance condition that was not analytically estimated. Finally, the tower lateral power spectrum shows an increase in vibration power at a frequency of D/(D-d), suggesting a strong rotational walk mechanism.

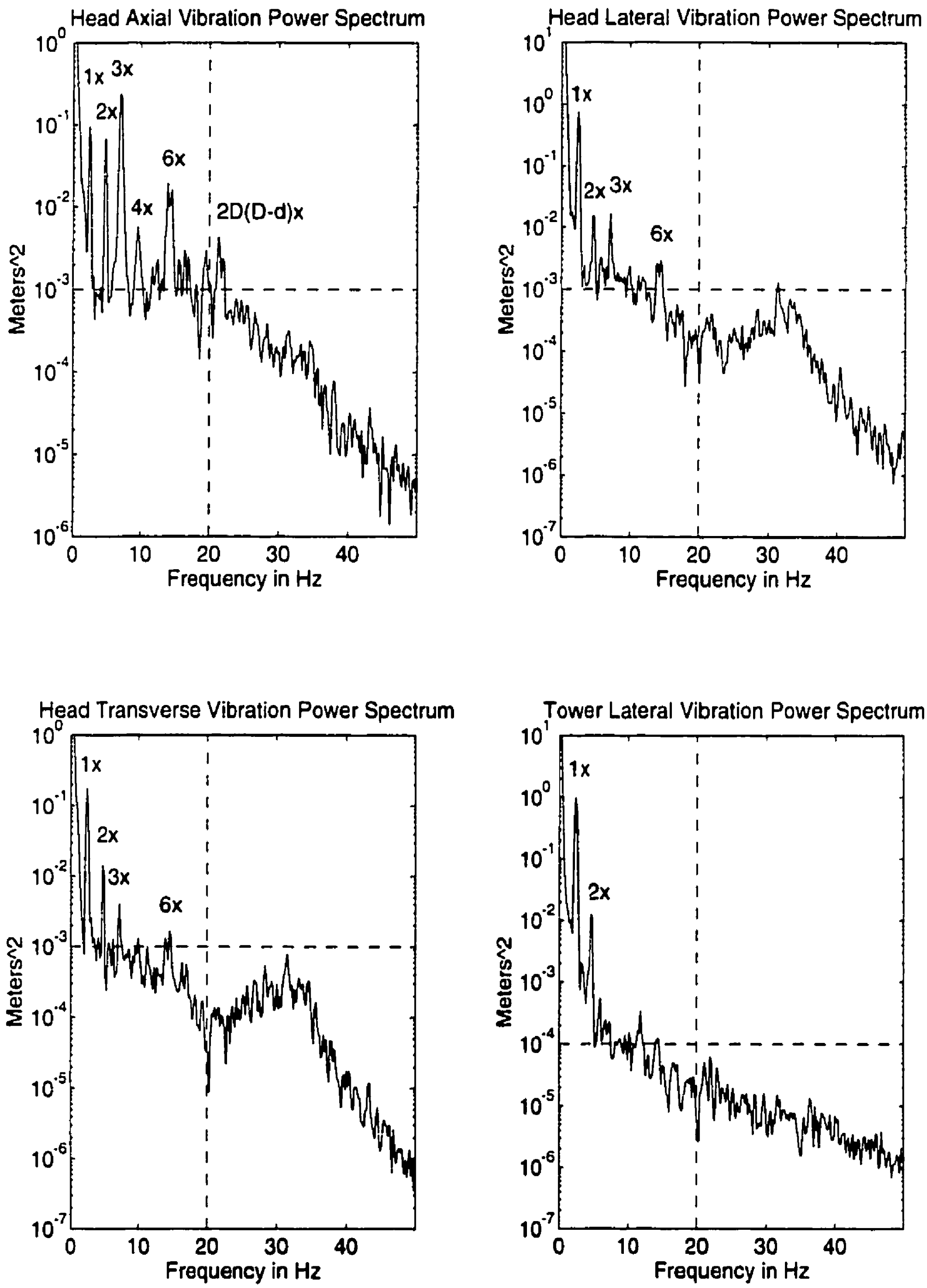


**Figure 5.4:** Power Spectrum of vibration signals before severe vibration occurrence

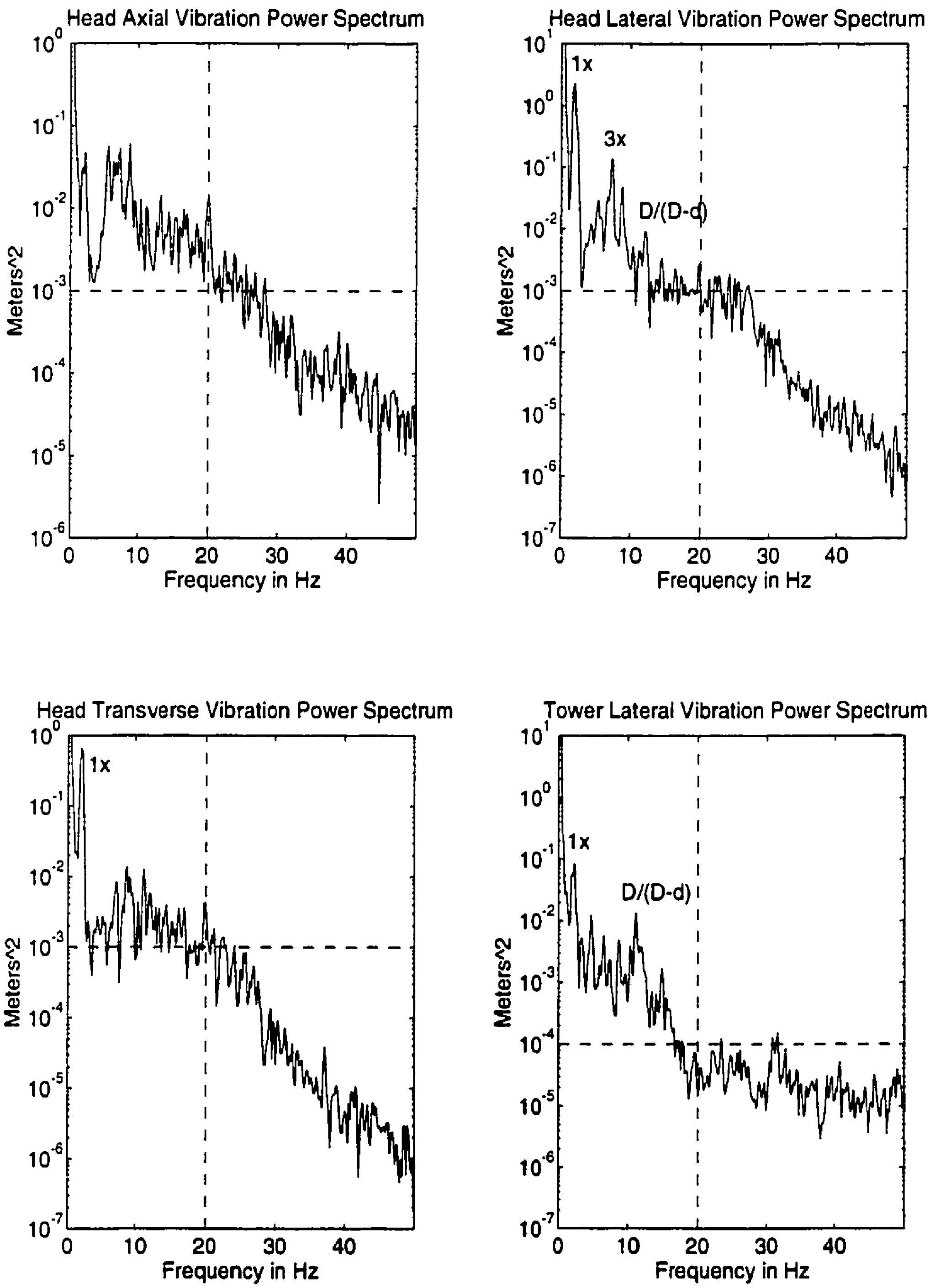


**Figure 5.5** Power Spectrum of vibration signals after severe vibration occurrence

## 5.3 Analysis of Strip Charts Data

Strip chart records of the monitored blastholes were generated, allowing convenient visualization and analysis of the experimental data. The procedure followed consisted of filtering field analog signals at 30 Hz, which secured a filter flat response in the band 0-20 Hz. The data was then digitized by taking a set of 60 samples over a second interval (60 Hz sampling), repeated every 3 seconds. Each set of 60 samples/second was further reduced to represent a single data point, by computing their Root Mean Square (RMS) in the case of vibration signals, or their mean, in the case of the remaining signals. The 3 second interval was chosen because of hardware computational speed limitation.

Using the rotary head position measurement, and the number of pipes in the drill string, the actual depth was computed. Subsequently, the sampled data was reordered to correctly delineate the hole profile.

Strip chart records of the data mentioned above is found in Appendix B, listed in the following sequence: Boreholes A9, B2, B9, A1A, XXTRA. Strip chart records of all the drilled holes can be found in [Ingersoll-Rand 93]. Due to technical difficulties encountered when playing back the recorded tapes, mainly due to dust particles caught on the tape during field testing, some sections of data were lost, and therefore have been represented by straight line segments in the strip charts. Borehole A1A is the only vertical borehole.

Borehole XXTRA was drilled with feed pressure and rotary speed constant at 1460 psi and 101 rpm respectively, throughout the entire borehole length. This feature offers the advantage of observing the behaviour of the other variables, over the drilled length. The vibration strip chart records are shown in Fig. 5.6

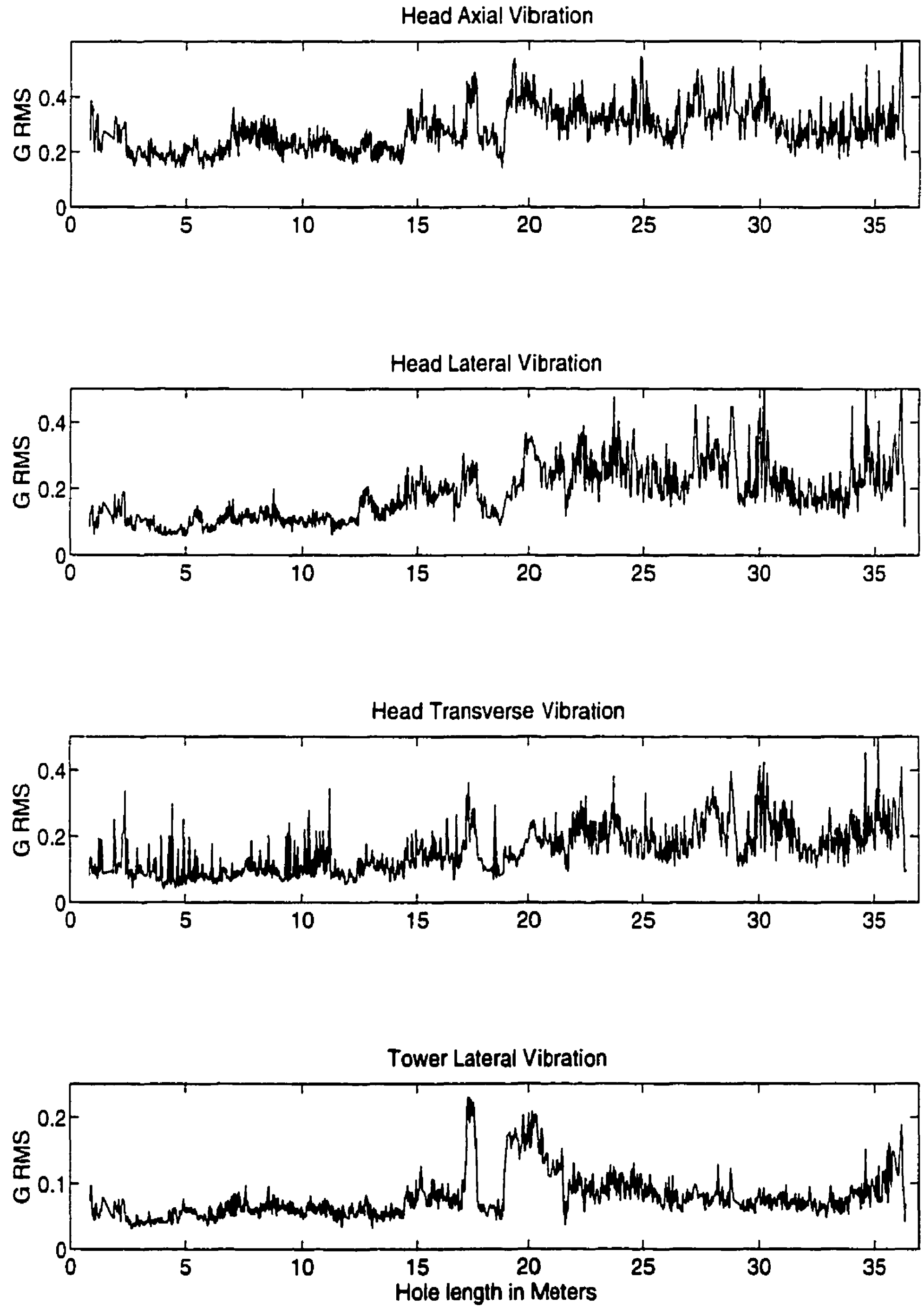


**Figure 5:6** Borehole XXTRA vibration strip chart records

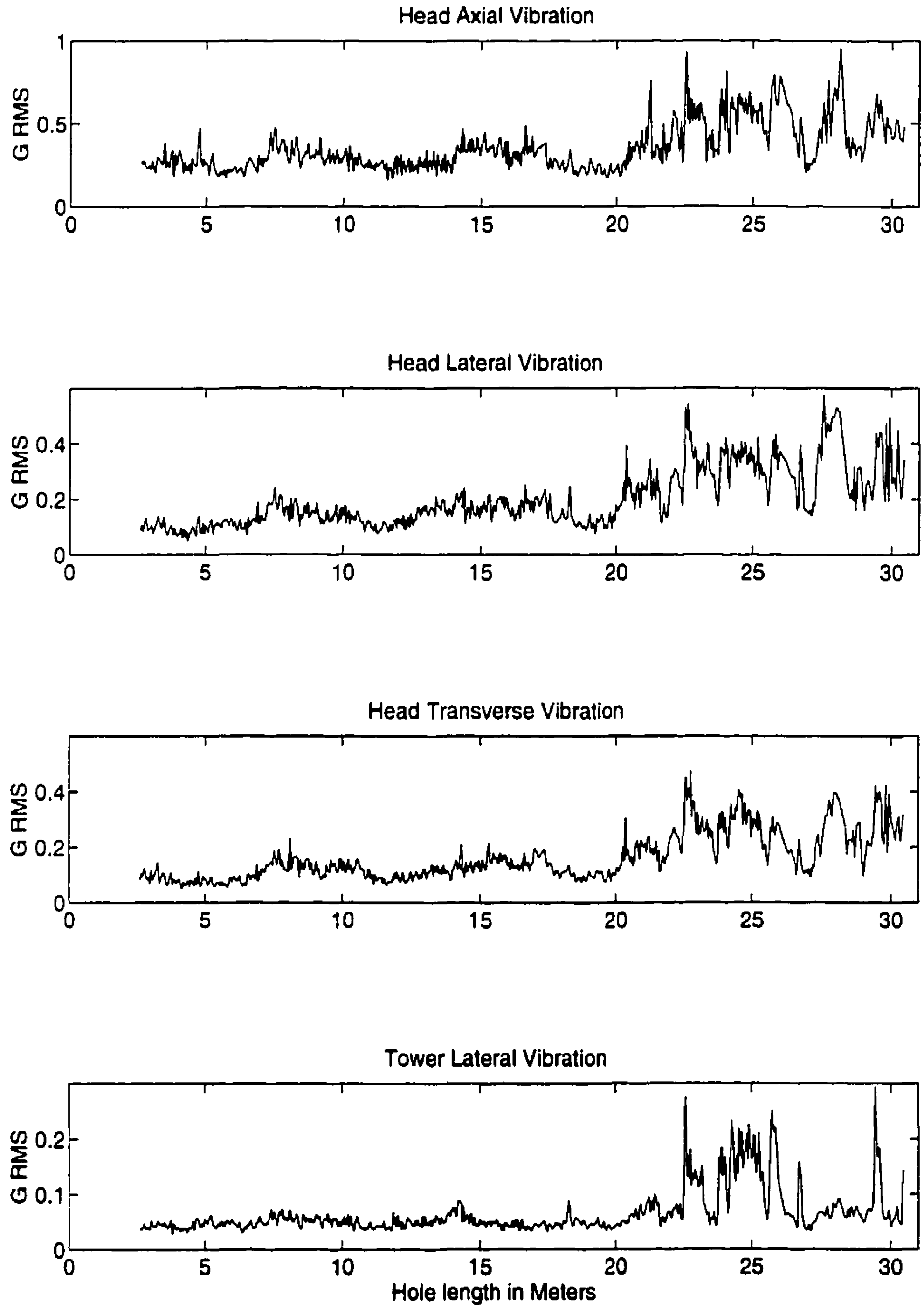


**Figure 5.7:** Borehole B2 vibration strip chart records

It is apparent that vibration levels increased with the addition of drill pipes. Since natural frequencies become lower, mainly in the lateral mode, the drill string tends to vibrate at larger amplitudes under low frequency excitations. In addition, longer drill strings are prone to eccentricity effects, increasing mass imbalance excitation mechanisms. For reference, the third, fourth and fifth drill pipes were added at hole lengths near 15m (50 ft.), 23m (74.5 ft.) and 30.5m (100 ft.) respectively.

It can also be noted that the tower experienced severe lateral vibrations near 17m (55 ft.) and in the range 19m to 22m (62 to 71 ft.), while the vibration level at the head in the three measured directions did not significantly exceed the vibration base line.

A similar observation can be made about borehole B2 (Fig.5.7), at depth exceeding 23m (74.5 ft.), after the fourth pipe was added. All four measured vibrations were significantly high. However, at depths 27m to 28m (88 to 91.5 ft.), high level of vibration at the rotary head can be observed, with no significant vibration at the tower.

Similar observations can be made about the remaining boreholes, such as borehole B9, in which feed pressure and rotary speed were adjusted according to the test methodology followed during field testing. At a depth near 20m (66 ft.), the vibration level at the tower increased by an approximate factor of 7, while the rotary head vibration levels increased with less proportions. At depths near 25m to 27m (81 to 88 ft.), the tower vibrated excessively, while the head vibration did not exceed the baseline (Borehole B9, Appendix B).

Borehole A9 was normally drilled, according to the operator's practice. The strip charts indicate that feed pressure remained constant near 1550 psi, while rotary speed was varied by the operator. The head vibration in the lateral and transverse directions remained within acceptable limits. However, the strip charts show several instances where the tower vibration level increased, while the rotary speed (or flow) strip chart shows that the operator has reacted to those vibrations by decreasing rotary speed (Borehole A9, Appendix B).

It was observed in general that the operator reacted to severe vibrations by reducing rotary speed. During field testing, an attempt to reduce vibrations by reducing feed pressure was unsuccessful. Reducing vibration by increasing feed pressure was not attempted.

### Conclusion

It appears from field data that vibration levels increase with longer drill strings, and that it is possible to encounter situations of high vibration at the rotary head with little or less significant vibrations at the tower, and vice-versa. It is also possible to have high vibration levels in both the rotary head and tower. Finally, the data shows that reducing rotary speed reduces vibration levels.

## 5.4 Analysis of Steady State Data

### Averaging Steady State Data

The steady state data points were obtained from the seven "test" boreholes drilled, as described in section 4.2.2. The strip chart data points were averaged, over the approximately 30 second interval of each steady state test. A total of 384 steady state data points were obtained.

The axial vibration at the rotary head plotted against rotary speed (Fig. 5.8) shows that the steady state vibration levels increase with higher rotary speeds. These vibration levels may be large enough in some mining environments to force an operator to drill at slower rotary speeds.

The lateral and transverse vibration at the rotary head and the tower vibration do not show a similar trend to the axial vibration. The main reason being the dependency of steady state vibration on the number of drill pipes in the drill string. Longer drill strings intensify mass imbalance excitation, in addition to lowering natural frequency characteristics, which reduce dampening of low frequency excitation at the bit rock interface. The same steady state vibration data was plotted against feed pressure, as shown in Fig.5.9. For similar reasons, no particular trend could be observed.

Nevertheless, the plots have the merit of displaying the range of acceptable steady state vibration while drilling a hole, which makes them useful in determining vibration thresholds that would trigger a controller to react.

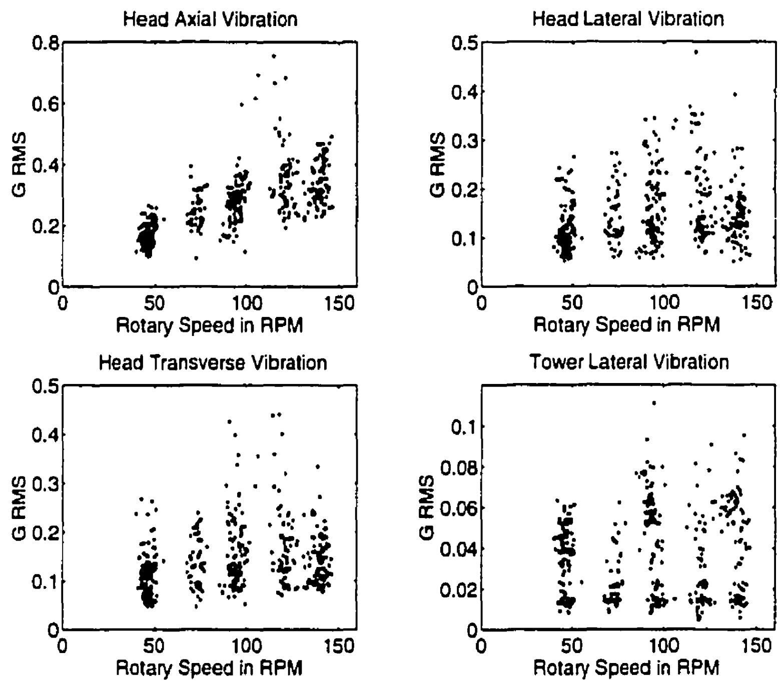


**Figure 5.8:** Steady State vibration levels plotted against rotary speed.

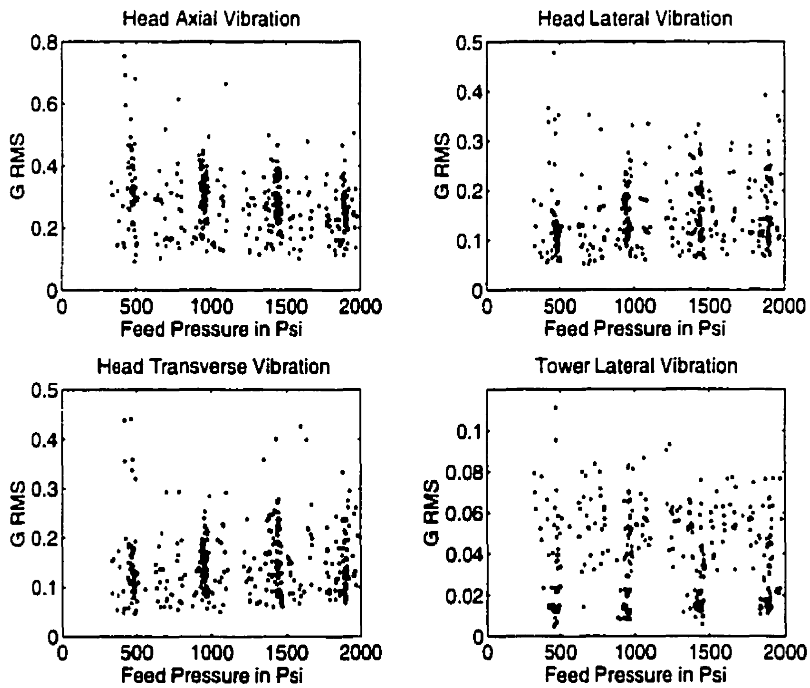


**Figure 5.9:** Steady State vibration levels plotted against feed pressure.

## 5.5 Conclusion

### 5.5.1 On Excitation Mechanisms

The validity of the excitation mechanisms, as summarized in Table 3.1 has been confirmed by the results thus presented. Frequency domain analysis of the vibration signals measured while drilling normally, confirmed the presence of 1x, 2x, 3x, 4x and 6x RPM excitation mechanisms. Since typical drilling rotary speeds do not exceed 150 RPM, or 2.5 Hz, then 6 x 2.5 = 15 Hz is the largest excitation frequency in typical tricone drilling situations for the specified conditions.

During instances of severe vibrations, Fourier power spectral analysis has indicated that vibration power is mostly intensified in the low frequency band, below 20 Hz. For control purposes, whether a resonance condition has occurred or not, the vibration power measurement will be confined within the band 0-20 Hz.

By filtering frequencies above 20 Hz, undesirable high frequency vibration, generated by rotating machinery on the drill rig, is attenuated, leaving destructive vibration power confined within the band 0-20 Hz to be considered, for control implementation. A good discrimination between destructive and non destructive vibration is obtained. In addition, the advantage of a smaller bandwidth signal is slower sampling speed requirements on the controller, which accordingly reduces computational overhead.

In the segment of data reviewed, severe drill vibration occurred as the bit was progressing from soft to harder ground. Since bit penetration rates are higher in softer ground, the bit contact at the soft/hard interface resulted in a mechanical coupling between the bit and ground of different nature, which resulted in reflected energy into the drill string and the machine structure. The reflected energy is usually dissipated in the form of heat and vibration. In the reviewed case, vibration levels could not be dampened, adversely affecting the bit coupling with the drilled rock. Consequently, a smaller proportion of energy generated at the bit was crushing the rock, leaving the remaining energy to be dissipated in heat and vibration.

In tricone drilling, between 60 and 90% of the total bit energy is generated by the rotary motors. The effect of reducing rotary speed serves the purpose of reducing the energy level at the bit, which at the same time reduces the magnitude of any reflected energy, or vibration.

Although the reviewed case is not representative of all drilling vibration situations, it demonstrates that the primary origin of the exciting force which leads to drilling vibration is the interaction taking place at the bit rock interface, and the manner in which that interaction is affected by changes and irregularities in the material being drilled. Given a certain exciting force at the bit-rock interface, the nature and amplitude of the resultant vibration which occurs will depend on the resonant properties of the drill string and the drill itself. Reducing rotary speed will ultimately reduce the power of the exciting mechanism, as well as any resulting vibration.

### 5.5.2 On Relationship Between Vibration and Other Variables

The steady state values of head lateral and transverse vibrations increase with extending borehole length, since longer drill strings have lower natural frequencies, and therefore a higher tendency to vibrate when forced with low frequency excitations.

The data has shown that although vibration levels at the rotary head and tower can be simultaneously quite severe, it is also possible to have situations of independent high vibration levels at the rotary head or at the tower. A vibration control strategy must address the head and tower vibration independently.

The steady state axial vibration at the rotary head plotted against rotary speed showed that the vibration levels increased at higher rotary speeds. These vibration levels may be sufficiently large to dictate the selection of rotary speed, below the machine's maximum speed capability. Conversely, reducing rotary speed attenuates vibrations in all directions.

# Chapter 6 MODELING THE DRILLING PROCESS

## 6.1 Modeling Machine Actuators

The actuators of interest for this work are the hydraulic cylinders of the feed system that produce weight-on-bit, and the hydraulic rotary actuator that produces bit rotation, in the case of the DM45E.

The actual machine uses manual valves to actuate the mechanical actuators. If automation is to be implemented, electric servo-valves would have to replace the present manual valves. The servo-valve transfer function depends on the servo type to be selected.

### 6.1.1 Identifying The Feed Actuator Dynamics

The model for weight-on-bit consists of the feed cylinders dynamics. The tests were conducted by measuring the feed cylinders input pressure with the actual weight-on-bit measured by a fixed load cell.

The testing procedure consisted of gradually incrementing the feed pressure in a staircase manner. The step transitions were useful in identifying the system's dynamics, while the steady state levels helped in determining the static relationships. For system identification purposes, the initial step starting from zero was discarded, to reduce stiction effects.

The system identification procedure was based on a parametric ARX-model fit to sampled input-output data at 100 Hz [Ljung 1987], using the tools provided by the *Matlab System*

*Identification Toolbox* [Matlab ] software package. The transfer function identified follows a first order behavior described as follows:

$$F(s) = \frac{223.66}{s + 12.9}$$

$$\omega_n = 12.9 \text{ rd/s}, f_n \cong 2 \text{ Hz}$$

The static relationship between feed pressure and weight-on-bit is described by the following equation:

$$\text{Weight-On-Bit} = 17.248 * \text{Feed\_pressure} + 844.44 \quad \text{lbs}$$

Figure 6.1 shows a plot of feed pressure, actual and simulated weight-on-bit using F(s). The discrepancy between the two signals, in the form of local dips that can be observed at times 2, 4 and 5.5 seconds is due to hydraulic components that were not yet assembled on the machine, whose main functionality was to drain the hydraulic oil from the pulldown cylinders. As a result, the hydraulic pressure in the cylinders would not drop without the assistance of a mechanic.

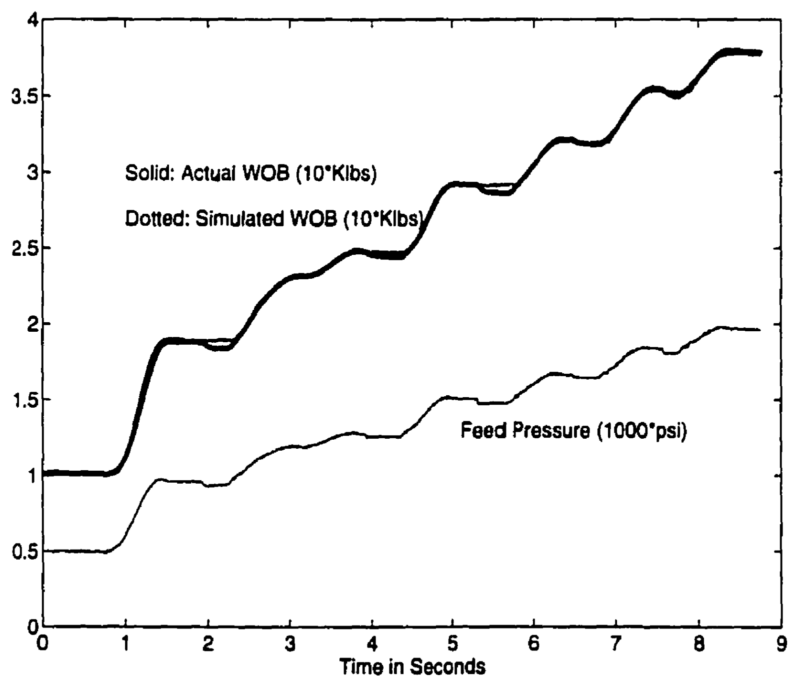


**Figure 6.1:** Actual and simulated weight-on-bit signals

### 6.1.2 Modeling the Rotary Actuators

The rotary actuator consists of the hydraulic motor and transmission system. Modeling is based on a flow-pressure relationship, and also by equating the produced torque with the mechanical load at the spindle, past the gear reduction box. Neglecting motor cross port leakage, the following equations can be written [Watton 1991]:

$$Q_{in} = \frac{D_m N}{G_r} + \frac{P_{in}}{R_e} + C\frac{dP_{in}}{dt}$$

$$Q_{out} = \frac{D_m N}{G_r} + \frac{P_{out}}{R_e} - C\frac{dP_{out}}{dt}$$

$$\frac{D_m(P_{in} - P_{out})}{G_r} = T_{dist} + B_v N + J_m\frac{dN}{dt}$$

where

$Q_{in}$, $Q_{out}$, $P_{in}$, $P_{out}$ are input and output hydraulic flow and pressure,

$N$ is the spindle rotary speed,

$R_e$ is the motor leakage resistance,

$C$ is the line and motor capacitance

$D_m$ is the motor displacement,

$G_r$ is the gear reduction ratio,

$T_{dist}$ is the disturbance torque,

$B_v$ is viscous damping coefficient,

$J_m$ is the drill string moment of inertia.

To simplify the model, the output pressure is assumed constant (actually equal to the hydraulic tank pressure, observed during field testing to vary by ±50 psi). This assumption further eliminates the output flow variable. Computing the Laplace transforms of the presented equations, the rotary system can be represented by block diagrams as shown in Fig.6.2, under the proposed assumptions.

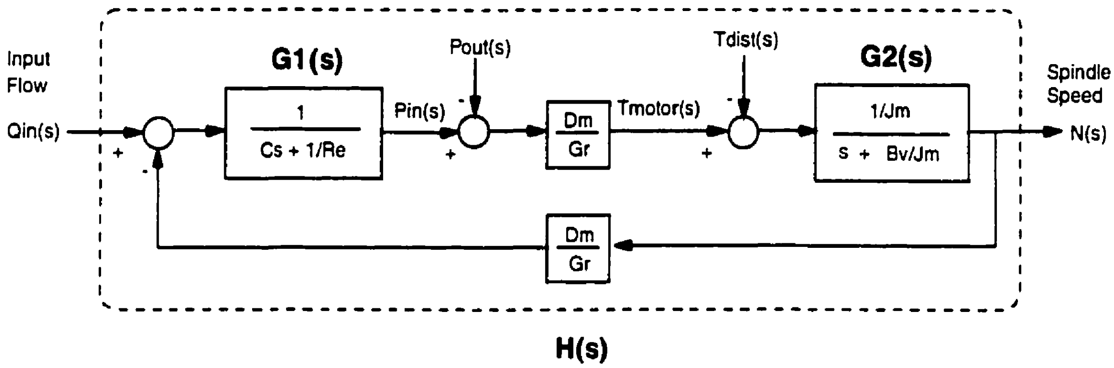


**Figure 6.2:** Block diagram of the rotary hydraulic actuator system

The blocks in Fig.6.2 were identified using parametric model identification techniques, applied to field test data. The measured variables were hydraulic input flow and pressure (rotation pressure) as well as the rotary speed at the spindle (i.e. past the gear box). The tests conducted consisted of varying the hydraulic input flow in a square wave manner, ranging from 25 to 75% of full input range, where the best linear behaviour is obtained, stiction effects minimized. The 75% upper limit was dictated by the flow sensor that saturated near 90 gpm (i.e. near 130 rpm).

The test analog signals were filtered with an analog $4^{th}$ order Butterworth filter at 50 Hz cutoff frequency, then sampled at 150 Hz. The sampled data was further filtered digitally using a $128^{th}$ order linear phase FIR filter [Oppenheim 1989], using the *Matlab Signal Processing Toolbox* [Matlab], at 20 Hz cutoff, to eliminate high frequency uncertainty. The overall transfer function relating hydraulic fluid flow to rotary speed was identified using a parametric ARX-model fit to sampled input-output data [Ljung 1987], using the *Matlab System Identification Toolbox*, as follows:

$$H(s) = \frac{8.6s + 702}{s^2 + 5.8s + 488} = \frac{8.6(s + 81.63)}{(s + 2.9 + j21.9)(s + 2.9 - j21.9)}$$

$$\omega_n \cong 22 \text{ rd/s}, f_n \cong 3.5 \text{ Hz}, \zeta = 0.13$$

Using the same approach, with $T_{dist}(s) = 0$, G2(s) was identified as:

$$G2(s) = \frac{1.46}{s + 4.4754}$$

$$\omega_n \cong 4.48 \text{rd/s}, f_n \cong 0.7 \text{ Hz}$$

The transfer function described by G1(s) could not be accurately identified by the parameter estimators, although different parametric models were used (ARX, ARMAX, Box-Jenkins and Instrument Variables), due to highly oscillatory dynamics (low damping) and noise. A better result was obtained by computing G1(s), using the identified transfer functions for G2(s), H(s) and the known G3(s). The calculated G1(s) was obtained as follows:

$$G1(s) = \frac{8.6s^2 + 740.48s + 3141.73}{0.9882s^2 + 0.0152s + 15.62} = \frac{8.7(s + 81.62)(s + 4.475)}{(s + 0.00769 + j3.98)(s + 0.00769 - j3.98)}$$

$$\omega_n \cong 3.97 \text{rd/s}, f_n \cong 0.63 \text{ Hz}, \zeta = 0.002$$

Note that G1(s) is described by a second order system, instead of a first order system as predicted analytically. The higher order model is more adequate since it can account for the dynamics of the fluid transport lines, since the flow and pressure sensors were 11.5 m. (38 ft.) away from the hydraulic motor.

The following static relationships were also obtained:

$$N = 1.45 \times Q_{in}$$

and

$$P_{\_no\_load} = 4.95 \times N$$

where $P_{\_no\_load}$ is the rotation pressure required to drive the spindle at speed $N$, when the bit is rotating in air, i.e. no load.

Figure 6.3 shows the actual and simulated rotary speed signals, while Fig.6.4 and Fig. 6.5 show the transfer function Bode plot and step response respectively. The simulated rotary speed matches well with the actual signal, validating the identified model.

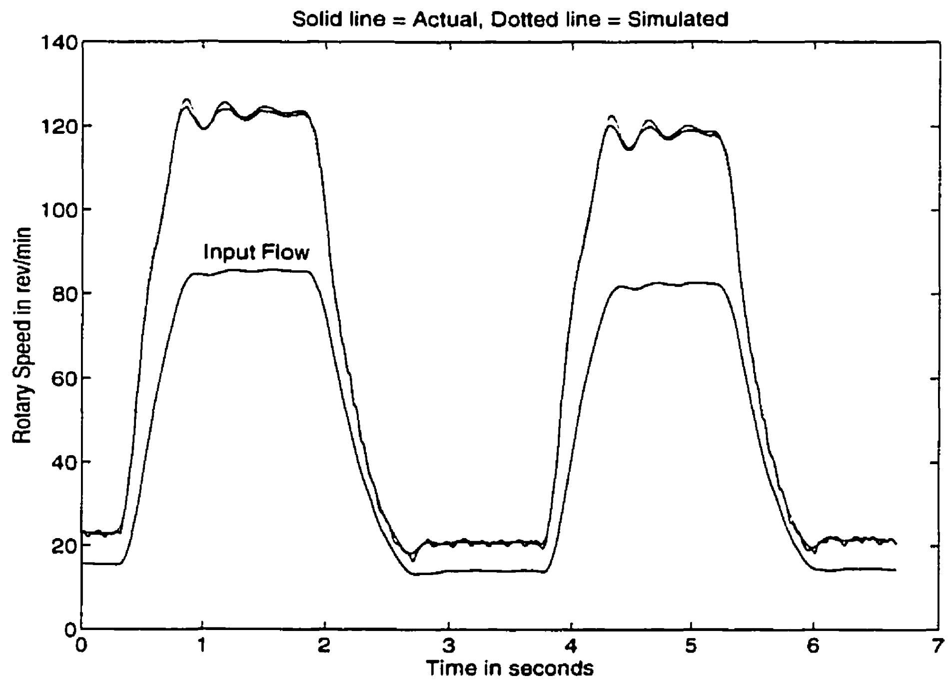


**Figure 6.3:** Actual and simulated rotary speed signals

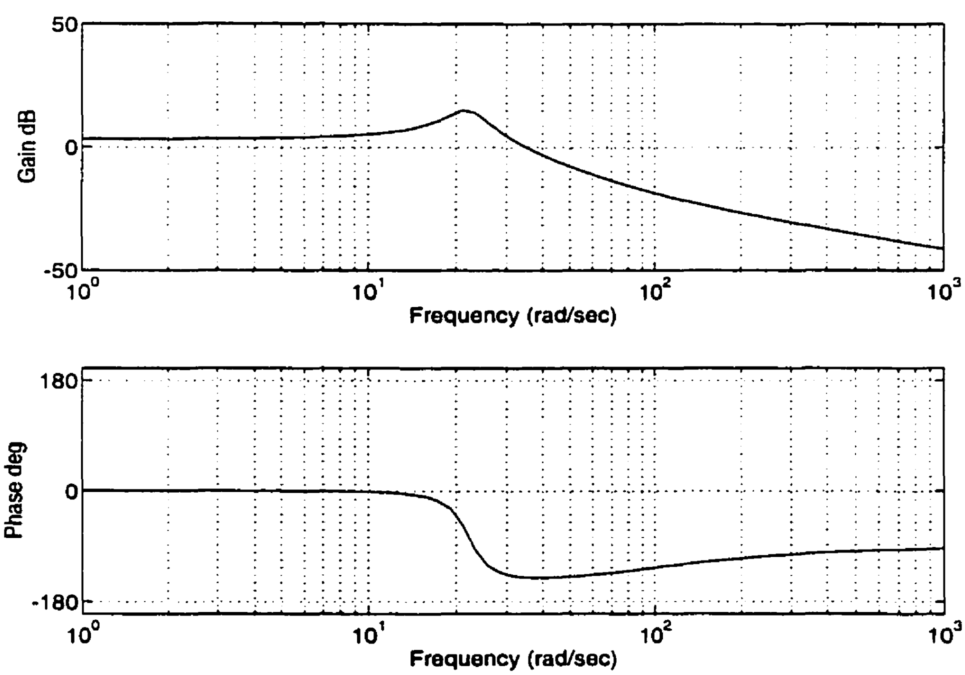


**Figure 6.4:** Bode Plot of Rotary Actuator

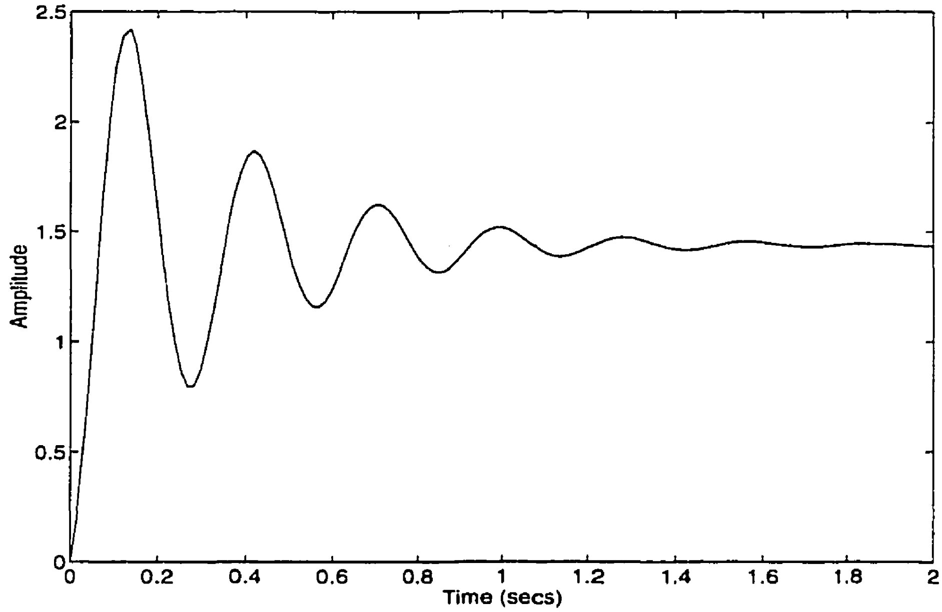


**Figure 6.5:** Step response of rotary actuator system

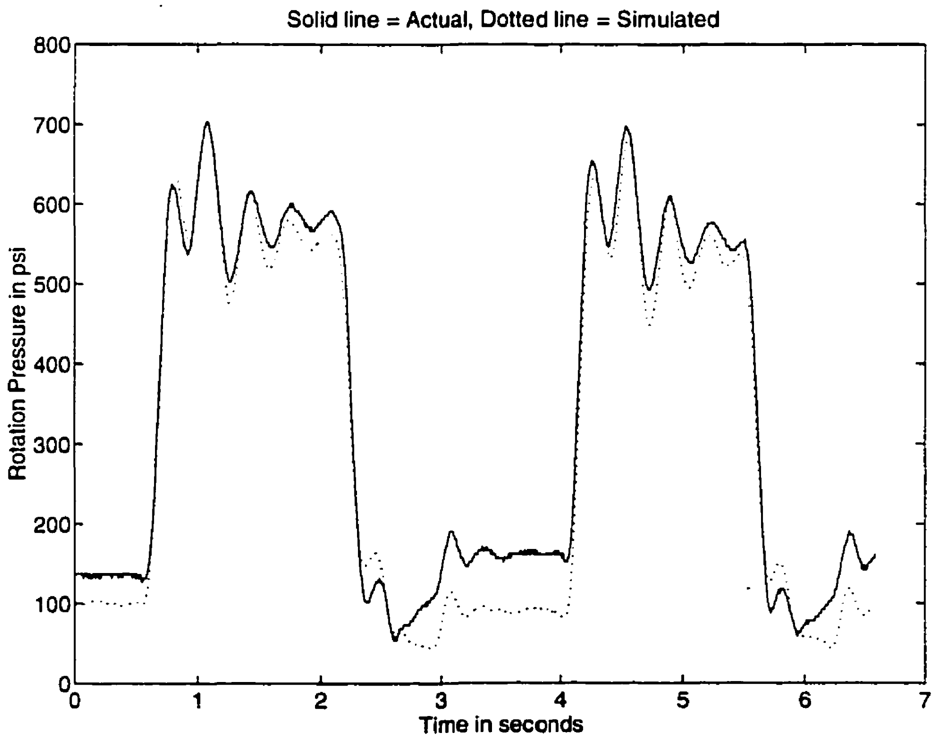


**Figure 6.6:** Actual and simulated rotation pressure signal

Figure 6.6 shows the actual and simulated rotation pressure signals. The discrepancy between the simulated result and the actual rotation pressure at the low pressure end is due to the tank return pressure that is not zero, since all the hydraulic circuits on the drill dump the hydraulic oil back to the tank. The theoretical model assumed a zero tank return pressure to simplify the analytical model.

## 6.2 Modeling the Bit-Rock Interface

### 6.2.1 Modeling Vibration

For the purpose of designing and simulating a controller, a mathematical model describing vibration behaviour needs to be developed. The study on drill string resonance has indicated that the natural frequencies dependence on several factors, and the fact that they were continuously changing, made them unsuitable for modeling. In addition, field data has shown that ground irregularities contributed to the vibration buildup.

It is therefore impossible to design a deterministic mathematical model that can accurately simulate vibration under all possible drilling conditions. For the purposes of control simulation, a model for vibration has to meet two requirements:

1. It must have a dependency on rotary speed, and,
2. severe instances of vibration can occur at any time, while drilling a hole.

Based on energy considerations, the amount of power supplied by the machine to the bit is consumed in crushing the rock. However, the energy transfer does not occur at 100% efficiency, which results in some energy dissipated in the form of heat, and another portion reflected back through the drill string, dissipated in the form of vibration.

The amount of the reflected energy depends on the drilling conditions and the bit-rock impedance damping. Such reflected energy cannot be predicted in a deterministic manner, as observed from field data. It is therefore proposed to model it using a reflection factor $\alpha$, which when multiplied with the total power delivered to the bit, gives a value of reflected power in the form of vibrations. If $\alpha=0$, then no power is reflected, and for $\alpha=1$, all bit power is reflected. Under a constant value of $\alpha$, the reflected power will depend on the total power produced at the bit, in which rotary speed forms a large contribution. By reducing rotary speed, the total bit power is diminished, which in turn decreases vibration power.

**Bit Power**

The power available at the bit consists of a translational and a rotational component, as described by the following equation:

$$\text{Bit Power} = W_{bit} \times PR + 2\pi \times Torque_{bit} \times \omega$$

where $W_{bit}$ is the actual weight-on-bit, $PR$ is rate of penetration, $Torque_{bit}$ and $\omega$ are the actual bit torque and rotary speed respectively. Typically, the rotational component accounts for 60 to 90% of the consumed power in crushing the rock [Schivley 1987]. For example, a Gardner-Denver GD-120 drill is equipped with one or optionally two 135 HP rotary motor(s), and a single 35 HP pulldown motor.

**Bit Power Reflection Factor**

The steady state reflection factors were computed by dividing the vibration steady state data points by the total power available at the bit. Thus four reflection factors were obtained, one for each direction on the rotary head, and one for the tower. Graphs showing the computed reflection factors plotted against rotary speed are shown in Fig 6.7. The reflection factor plots versus rotary speed show no correlation between the two, but are inconclusive, mainly because the variable of depth is not accounted for. Graphs of reflection factor versus feed pressure (Fig. 6.8) show that the former decreases with an increase in feed pressure. Low feed pressures result in poor coupling between the bit and rock, therefore producing higher reflected power. In terms of drilling efficiency, low reflection factors denote that a higher fraction of the generated power is used in crushing the rock. This result is most apparent in the reflection factor computed for the head axial vibration.

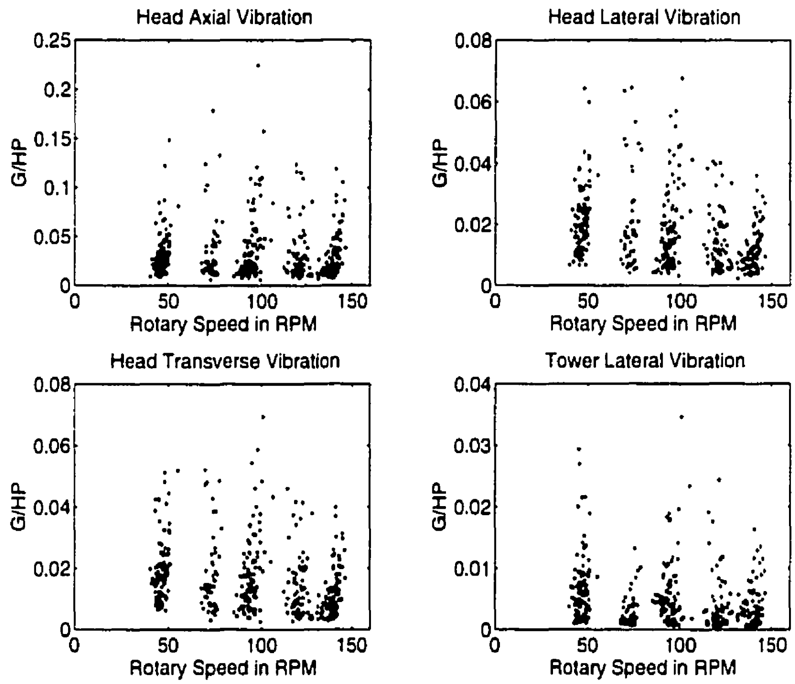


**Figure 6.7:** Head and tower power reflection factor, versus rotary speed

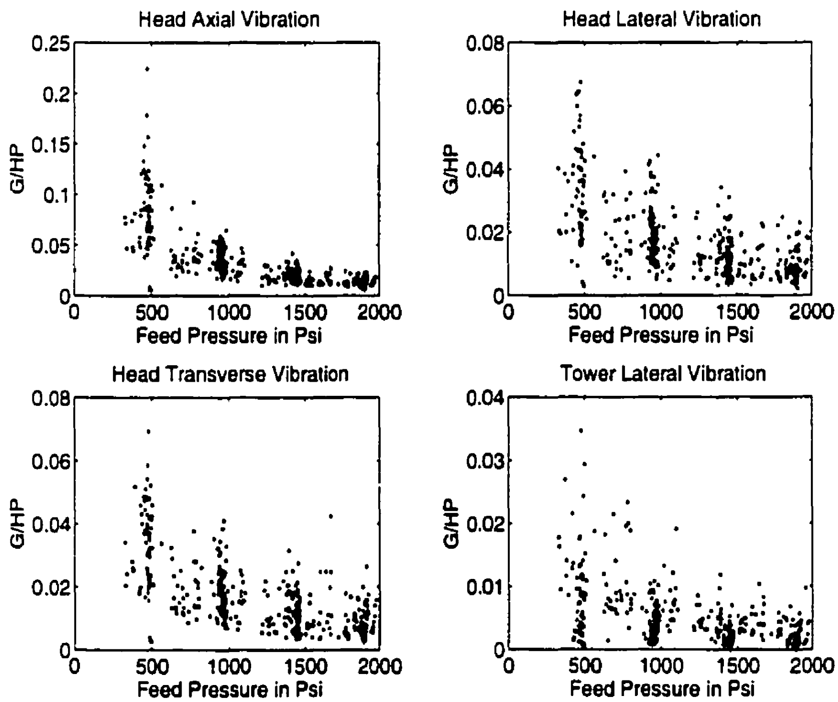


**Figure 6.8:** Head and tower power reflection factor, versus feed pressure

### Statistical Analysis of Reflection Factors

The reflection factors as computed are treated as random signals, and therefore mean and variance values were extracted for each vibration direction, with results listed in Table 6.1. The cross-correlation between the four reflection factors were also computed, and are summarized in Table 6.2. The results do not show a strong correlation between the tower and the head power reflection factors, in agreement with the conclusion obtained earlier from the analysis of strip chart data. However, the correlation between the reflection factors at the head is high, mainly between the lateral and transverse directions. It thus appears that reducing vibrations in one direction at the rotary head would reduce vibration in the other two.

The vibration can be simulated by generating reflection factors, in the form of random signals with mean and variance as listed in Table 6.1. Severe instances of vibration could be simulated by superimposing occasional pulses with amplitudes representing 50 to 80% reflection factors. The reflection factors multiplied by the total power at the bit give a measure of vibration at the head and the tower.

| Reflection Factor | Mean | Variance |
|---|---|---|
| Head Axial Direction | 0.0343 | $8.836*10^{-4}$ |
| Head Lateral Direction | 0.0174 | $1.5088*10^{-4}$ |
| Head Transverse Direction | 0.0168 | $1.3314*10^{-4}$ |
| Tower Lateral Direction | 0.0048 | $2.38*10^{-5}$ |

**Table 6.1:** Power reflection factors mean and variance

| Head Axial | Head Lateral | Head Transverse | Tower Lateral | Cross-Correlation |
|---|---|---|---|---|
| X | X | | | 0.86 |
| X | | X | | 0.86 |
| | X | X | | 0.93 |
| X | | | X | 0.47 |
| | X | | X | 0.49 |
| | | X | X | 0.46 |

**Table 6.2:** Cross-correlation factor between reflection factors in each measured location and direction.

Finally, since the bit power equation depends on bit penetration rate and disturbance pressure, models for penetration rate and disturbance pressure must also be developed.

### 6.2.2 Empirical Penetration Rate Model for the DM45E

Due to the bench geology at Alpena, the penetration rate data set is restricted to the rock type of limestone. The penetration rate model presented by Maurer is non linear, however it can be linearized by consolidating the rock constant $K_{r}$ with the bit diameter constant $D^{z}$. By taking the natural logarithms on both sides, we obtain:

$$\ln(PR) = \ln K^{*} + x\ln(WOB) + y\ln N$$

The above equation is linear, therefore the use of linear regression is possible. Using a least squares regression applied to 352 steady state data points [Draper 1981], the following empirical equation was obtained:

$$PR = 1.2478 \times 10^{-6} \times (WOB - 4300)^{1.0068} \times N^{0.9281} \text{ (ft/min)}$$

A figure of merit for the fit success is described as $R^{2}$, representing the proportion of total variation about the data mean, and is equal to 1 for a perfect fit. For the penetration rate fit, $R^2$ was equal to 0.8416.

The constant subtracted from the weight-on-bit was adjusted to 4300 lbs, to achieve the best linear relationship between weigh-on-bit and penetration rate. This constant exists because of the minimum threshold weight-on-bit required before the bit inserts penetrate the rock, as well as the non-zero hydraulic tank return pressure.

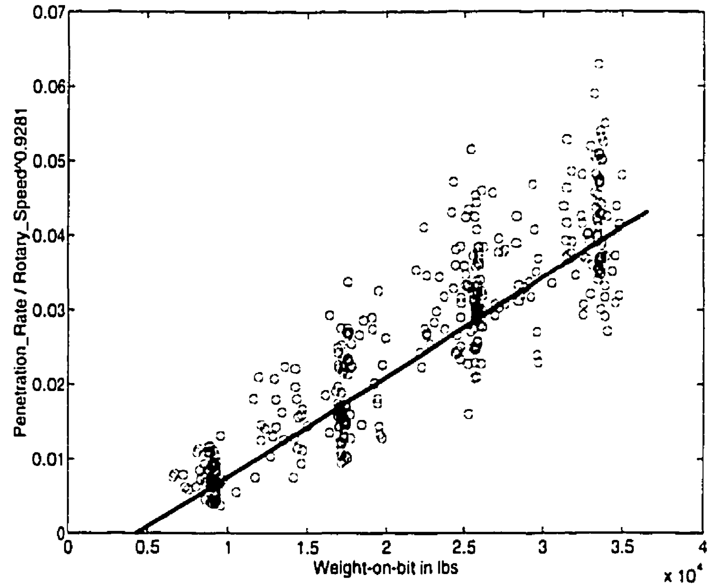


**Figure 6.9:** Empirical model fit of penetration rate steady state data

Figure 6.9 shows the steady state data, with a solid line representing computed penetration rates using the obtained empirical equation.

### 6.2.3 Empirical Torque Model for the DM45E

Because of the hydraulic nature of the rotary actuator, the disturbance pressure ($P_{\_dist}$) is the component of the rotation pressure that generates torque at the bit. The remaining component ($P_{\_no\_load}$) overcomes dry and viscous friction and drill string inertia. The two components are summed up to form the total rotation pressure ($P_{\_rot}$). The disturbance pressure was empirically modeled, by applying a non-linear regression, similar to the penetration rate model, to 348 steady state data points ($R^2 = 0.8675$), as:

$$P_{\_dist} = 0.0157 \times (WOB\ )^{1.0686} \times N^{-0.0761} \text{ (psi)}$$

The model shows a weak correlation with rotary speed, however, it offers an improved fit over the model $T = \alpha\,(WOB)^n$ presented in Chapter 2.

The no-load rotation pressure was identified as:

$$P_{\_no\_load} = 4.95 \times N \quad \text{(psi)}$$

Finally, the rotation pressure is obtained from:

$$P_{\_rot} = P_{\_no\_load} + P_{\_dist} \quad \text{(psi)}$$

Figure 6.10 shows the steady state data, with a solid line representing computed disturbance pressure using the obtained empirical equation.

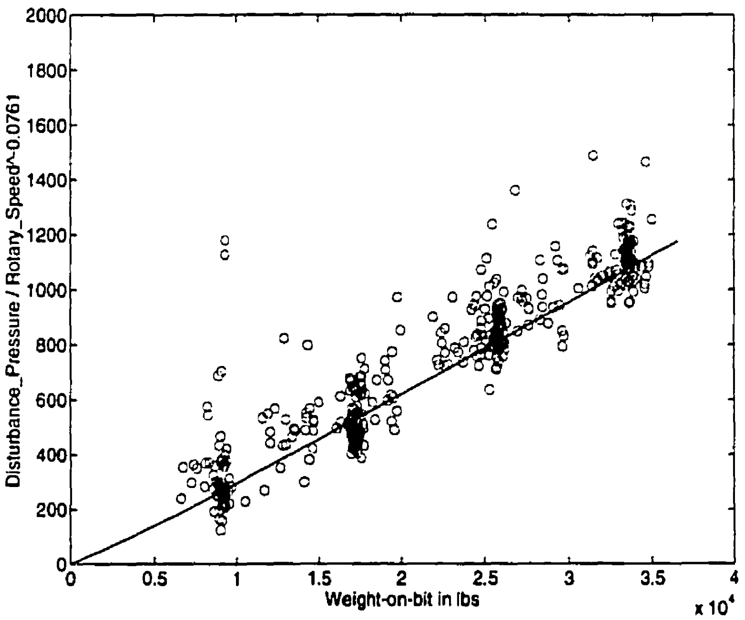


**Figure 6.10:** Empirical model fit of disturbance pressure steady state data

## 6.3 Building A Drilling Simulator

### 6.3.1 Simulation Software: Simulink™

The bit-rock interface in the plant is inherently nonlinear, and as such, the development of a simulator requires a simulation language capable of handling nonlinear systems. The simulation environment chosen is a nonlinear simulation module called Simulink™, that runs under a mathematical package called Matlab™ [Matlab]. Simulink is a powerful tool that offers good programming flexibility, and runs on a variety of computers and operating systems. The drilling simulator for this work was developed using a personal computer running Microsoft Windows 3.11™.

### 6.3.2 Drilling Simulator Block Diagram

The drilling simulator block diagram is shown in Fig.6.11. The $N_{\_servo}$ and $W_{\_servo}$ are respectively the servo-valve input signals for rotary actuator hydraulic flow (Q) and feed pressure (W) demand. The dynamics of the machine will implement the identified transfer functions with the addition of saturation blocks to represent the physical limitations of the actuators. The hydraulic servos are modeled as rate limiters, where the output follows the input at a rate that saturates at a preset level. Once the servos have been specified, their transfer function would replace the rate limiters.

The bit-rock interface reads as inputs rotary speed, feed pressure and an index corresponding to a pre-programmed rock layer type. The only pre-programmed rock layer is limestone, however future revisions of this simulator could include other rock types, as well as variations of mechanical properties within one rock type. The simulated bit-rock interface computes penetration rate (PR) and disturbance pressure ($P_{\_dist}$) using the empirical equations determined from field data. Vibration is generated by computing the total bit power, multiplied by a randomly distributed power reflection factor, generated as white noise with mean and variance computed from field testing data. Figure 6.12 illustrates the vibration model. Two vibration signals are generated, one at the tower and another as the rotary head lateral vibration.

In addition, a pulse that is generated repetitively is superposed with the power reflection factor signal, simulating instances of severe vibrations. Depth is also computed by integrating the penetration rate, and also used as a pointer to the data structure containing an optional stored rock strata, if rock related simulations are needed.

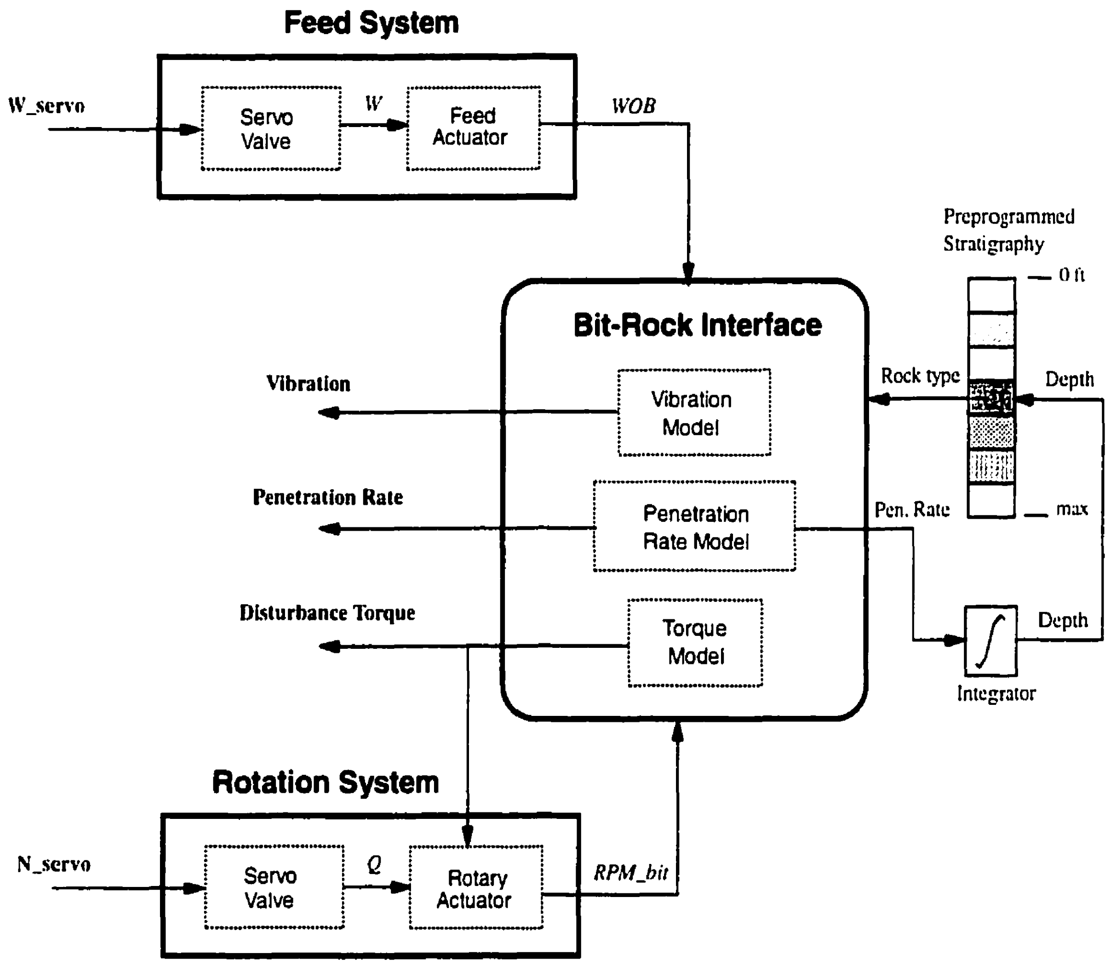


**Figure 6.11:** Drilling Simulator block diagram to be implemented in Simulink

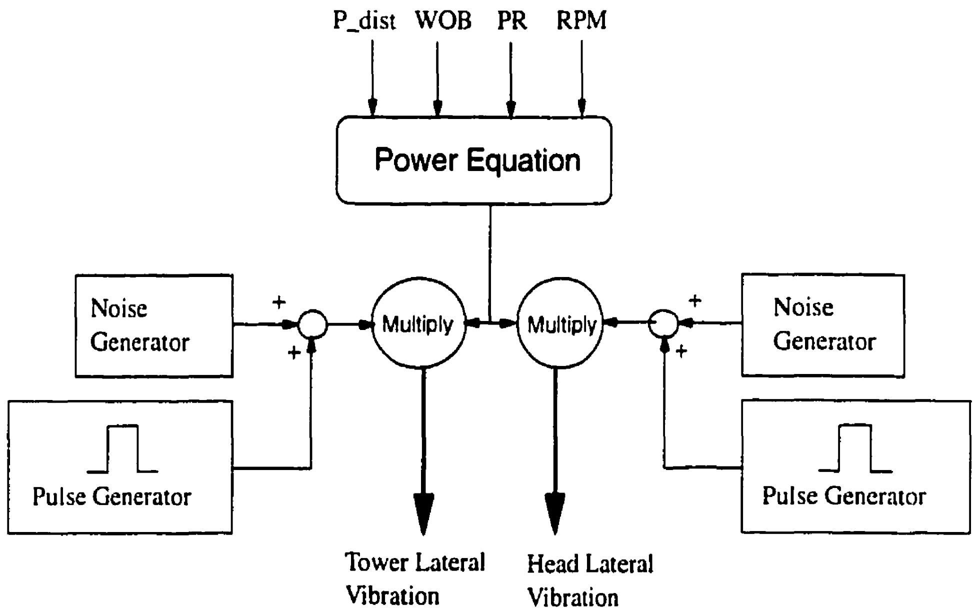


**Figure 6.12:** Block diagram of simulated vibration model

## 6.4 Conclusion

### On vibration reflection factors

A new variable was computed, termed the "reflection factor", obtained by dividing the steady state vibration by the total power available at the bit, in the four measured vibration directions. In terms of energy transfer efficiency, low reflection factors denote that a higher fraction of the generated power is consumed in breaking the rock.

The reflection factor formed the basis of the vibration model proposed, where a random variable is generated and multiplied by the bit total power to generate vibration. Models for penetration rate and torque were also obtained.

A model for simulating drilling has been subsequently developed and implemented as a software program. The drilling simulator will enable testing and evaluation of control schemes and strategies.

The topic of specifying, designing, testing and tuning a control strategy is covered in the following chapter.

# Chapter 7 CONTROLLER DESIGN AND SIMULATION

## 7.1 General Considerations

The development of an algorithm for drilling vibration control is based on the nature of the controlled process, which, for the current work is nonlinear. Linear feedback with nonlinear switching control would be combined to achieve the desired behavior.

Based on the results presented earlier, it became clear that reducing vibration can be achieved by reducing rotary speed. Vibrations are transmitted to the drill through two points of contact: the rotary head and the centralizer bushing.

To maintain an acceptable level of vibration, vibration amplitude measured near those two points of contact should not exceed maximum preset limits, within the machine's mechanical limitations and the operator's comfort as well. An appropriate control reaction consists of reducing rotary speed, whenever one or more of the preset limits has been exceeded, to initially lower, then maintain (regulate) the measured vibration level at the preset limit. The controller keeps regulating the vibration levels until the exciting source at the bit rock interface becomes weaker, enacting the controller to automatically (and gradually) restore the full rotary speed.

In addition, the weak correlation between the tower vibration near the centralizer bushing and the rotary head vibration indicates that a reliable control strategy must be able to react to any feedback vibration signal independently of the other measured signals.

A description of this control strategy is depicted in Fig.7.1. Consider for example the case where:

- feedback_signal_1 = Head Axial Vibration,
- feedback_signal_2 = Head Lateral Vibration,
- feedback_signal_3 = Head Transversal Vibration,
- feedback_signal_4 = Tower Lateral Vibration, etc...

Assume that at time $t_k$, the vibration at the head in the lateral direction and at the tower exceed the maximum acceptable preset limit. The controller would therefore compute R2 and R4, the respective amounts of rotary speeds to be reduced from the current setpoint. The total amount to be reduced is then Rtotal = R1+R2+R3+R4+...+Rn, with R1=R3=...=Rn = 0. The full rotary speed is restored when all the R# are null.

Note that this strategy is modular in the sense that it can be expanded to include feedback signals from rotation and bailing air pressures, as well as other signals if deemed necessary.

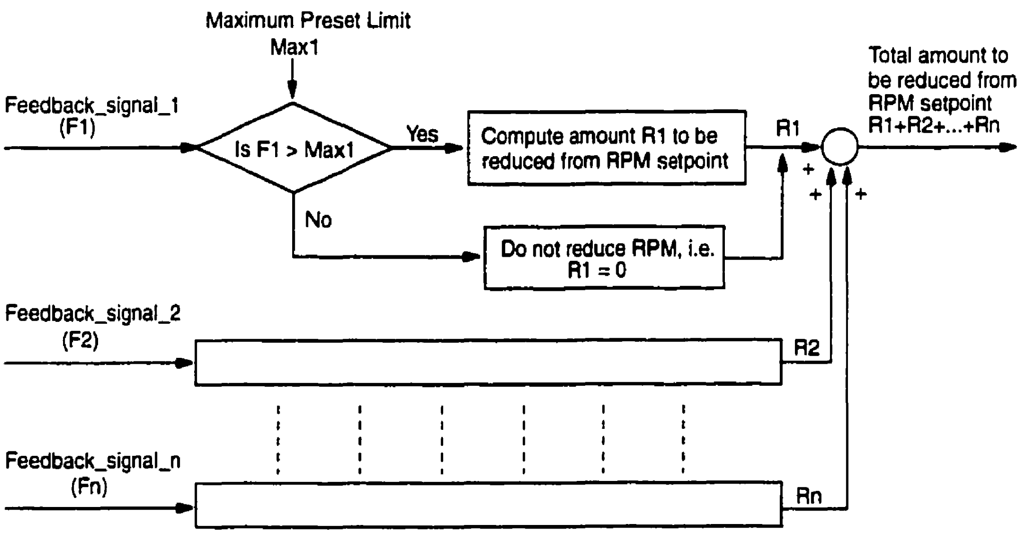


**Fig 7.1:** General Description of Control Strategy

## 7.2 Compensator Requirements and Design

The control strategy as presented is in essence a closed-loop feedback system, with non-linear switching since it is not activated if none of the feedback signals exceeded its preset limit. When the feedback loop is activated, the rotary actuator system (Servo-valve and Motor(s)) sees a step change in its actuating input signal. Thus the step response (by definition, the response of a system with respect to a unity step input) of the rotary actuator must be analyzed and compensated if necessary.

A compensator is a transfer function added in series with a dynamic system, in order to modify the system's dynamic response. The step response of the Lafarge DM45E (single motor) rotary actuator is shown in Fig.7.2. A large overshoot can be observed, before the system reaches steady state after 1.5 seconds.

Since the proposed closed loop feedback system is activated whenever the feedback variables exceed preset setpoints, then its effect can take the form of step variations in the rotary speed setpoint. A series compensator is therefore needed, to dampen the open loop step response of the rotary actuator, and reduce the overshoot. This would result in a smoother response, when the controller is activated.

A first order lag was connected in series with the rotary actuator and simulated. The simulation results showed that a first order lag with a time constant of 0.25 seconds dampened the overall open loop rotary actuator system's step response, without altering the steady state settling time. The simulated open loop step response of the compensated system (compensator and rotary actuator) is shown in Fig. 7.2.

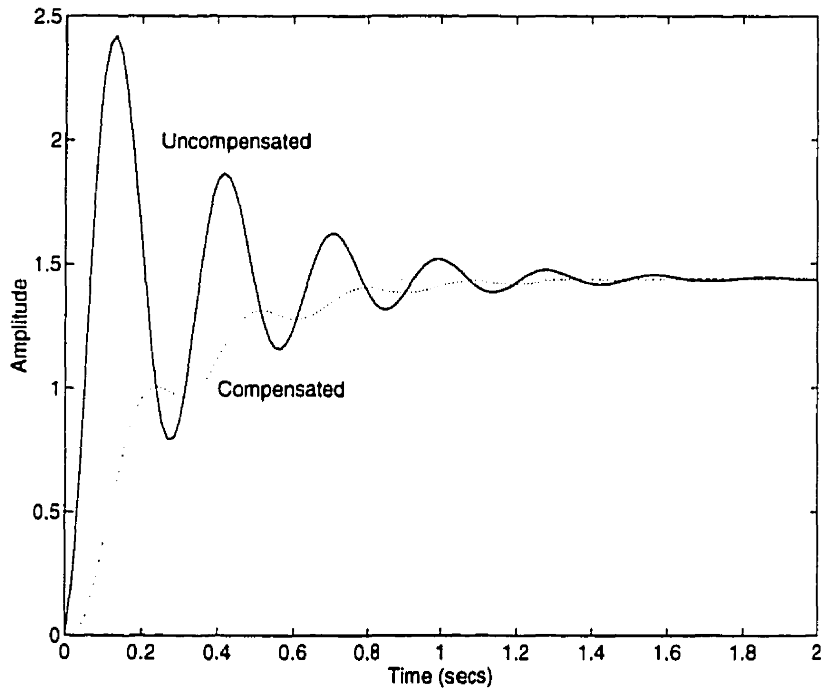


**Figure 7.2:** Open loop Step response of rotary actuator with and without compensator

## 7.3 Feedback loop design

The design of a continuous time feedback closed loop control system, that implements the strategy introduced in Fig.7.1 is illustrated in Fig 7.3. The $N_{setpoint}$ is the nominal desired rotary speed, during normal operation. In the absence of constraints, f(s) is equal to zero and the demanded rotary speed $N_{dem}(s)$ is equal to $N_{setpoint}$. The compensator block generates the servo-valve actuating signal $N_{servo}(s)$. The rotary actuator system produces the rotary speed N(s) at the bit rock interface.

Each feedback signal is subtracted from its preset maximum threshold value, producing an error signal, that is positive when the feedback signal exceeds the preset threshold value. The error signal is then multiplied by a proportional gain (constant), to compute the amount R#(s) to be reduced from $N_{setpoint}$. The inner loop saturation block limits the amounts R#(s) between zero and $N_{setpoint}$ - Minimum(N), where Minimum(N) is the lowest rotary speed at which the controller is allowed to drive the machine.

The logic is also described in the following pseudo-code:

feedback_error_1 = Feedback_1 - Maximum threshold

If feedback_error_1 > 0 Then R1 = Kp1 * feedback_error_1

0 < R1 < saturation limit

The total sum of the feedback loops is computed and bounded:

Total_feedback_sum = R1+R2+...+Rn

0 < Total_feedback_sum < saturation limit

The bounded total sum of the feedback loops is filtered with a single pole low pass filter LP(s), to smooth out instantaneous transitions of the total_feedback_sum, from zero to a positive value, or from a positive value to zero, when all the feedback signals become lower than their maximum threshold limit. The low pass filter was given an arbitrary time constant of 0.2 second (i.e. f(s) becomes close to zero after 0.6 seconds).

For example, assume $N_{setpoint}$ = 100 rpm and Minimum(N) = 30 rpm, then the maximum amount of rotary speed that the controller can subtract from $N_{setpoint}$ is 70 rpm. The saturation block preceding the low pass filter limits the amount $R_{total}(s)$ between zero and $N_{setpoint}$ - Minimum(N).

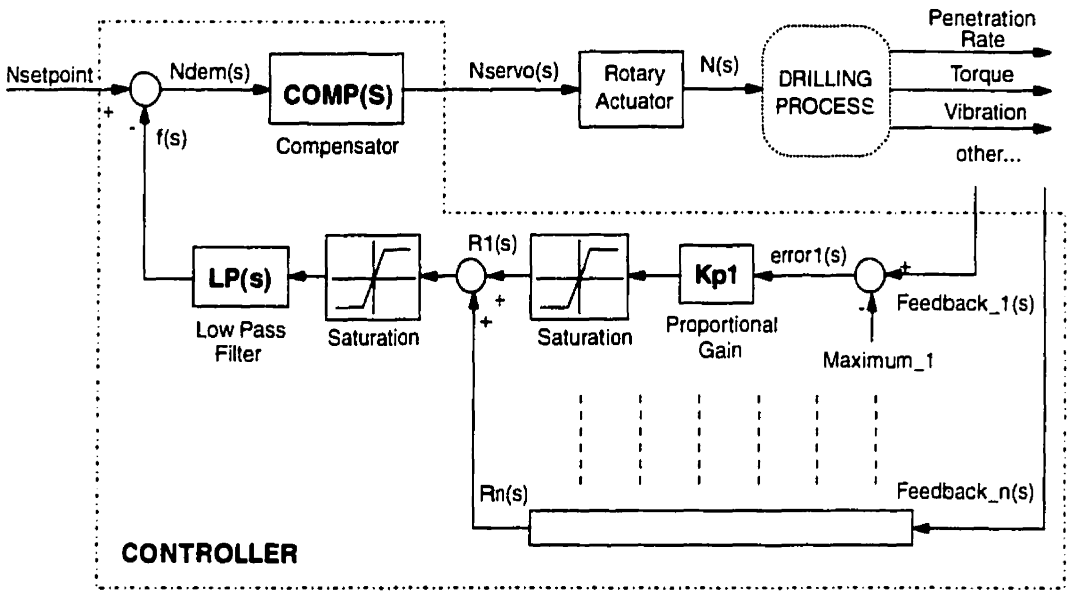


**Figure 7.3:** Closed loop implementation of rotary actuator control strategy

## 7.4 Simulation Results

The controller, as described by Fig. 7.3 was added to the drilling simulator, within the Simulink environment. It implemented two feedback loops, with feedback signals being the Head and Tower_lateral Root Mean Square (RMS) vibration signal, filtered at 20 Hz. The Head_lateral signal from the rotary head was chosen for feedback since it was observed that reducing head vibration in one direction reduced vibration in the other two. The tower vibration was chosen because of the weak correlation between the tower and head vibrations.

The computer simulation was conducted over a time interval of 12 seconds. Figure 7.4 shows the simulated head and tower vibrations over the simulation interval, prior to controller implementation. Excessive vibrations were simulated to occur at the head, at time 3 to 5 seconds, while heavy tower vibrations developed from time 4 to 6 seconds. Time 4 to 5 seconds is a vibration occurrence overlap between the two feedback signals. Finally, less than excessive vibrations occur at the head from time 8 to 10 seconds.

The solid line in the vibration signals graphs represents the threshold limit that would trigger the controller to respond by reducing rotary speed. The weight-on-bit remained constant at

35,000 lbs during the simulation time, and $N_{setpoint}$ was 150 rpm. Figure 7.4 also shows rotary speed and rotation pressure.

Since the simulator run started with a rotary speed step transition from 0 to 150 rpm, the first two seconds of the displayed data exhibit the step response behaviour of the compensated rotary actuator. The graphs shows a steady state rotary speed value below the setpoint of 150 rpm, due to the torque loading effect at the bit, resulting in a drop in rotary speed.

The controller was subsequently implemented, with Kp1 and Kp2 both tuned by trial and error to a gain of 2000. The simulation results are shown in Fig. 7.5. The vibrations at the head and tower quickly converged to their respective threshold levels, however they remained within a steady state error that is inversely proportional to the controller gain Kp#, an inherent characteristic of proportional gain controllers. Subsequently, increasing Kp# reduces the steady state error, but also speeds up the controller response, which adversely affects the stability of the system (instability refers to a situation where the system starts to oscillate until a limit cycle is reached or the system fails). In an actual application, the steady state error could be compensated for, by setting lower than ideal threshold limits, by an amount near the steady state error. Alternatively, an integral controller could be used. However, it further complicates the tuning of the controller.

The graph of simulated rotary speed shows how the latter was driven by the controller, below the nominal rotary speed. The ripple observed in the rotary speed signal is due to the head lateral vibration signal that oscillated about the threshold limit of 0.3 G rms, which triggered the controller to reduce rotary speed occasionally. The response of the rotation pressure is also shown in Fig. 7.5.

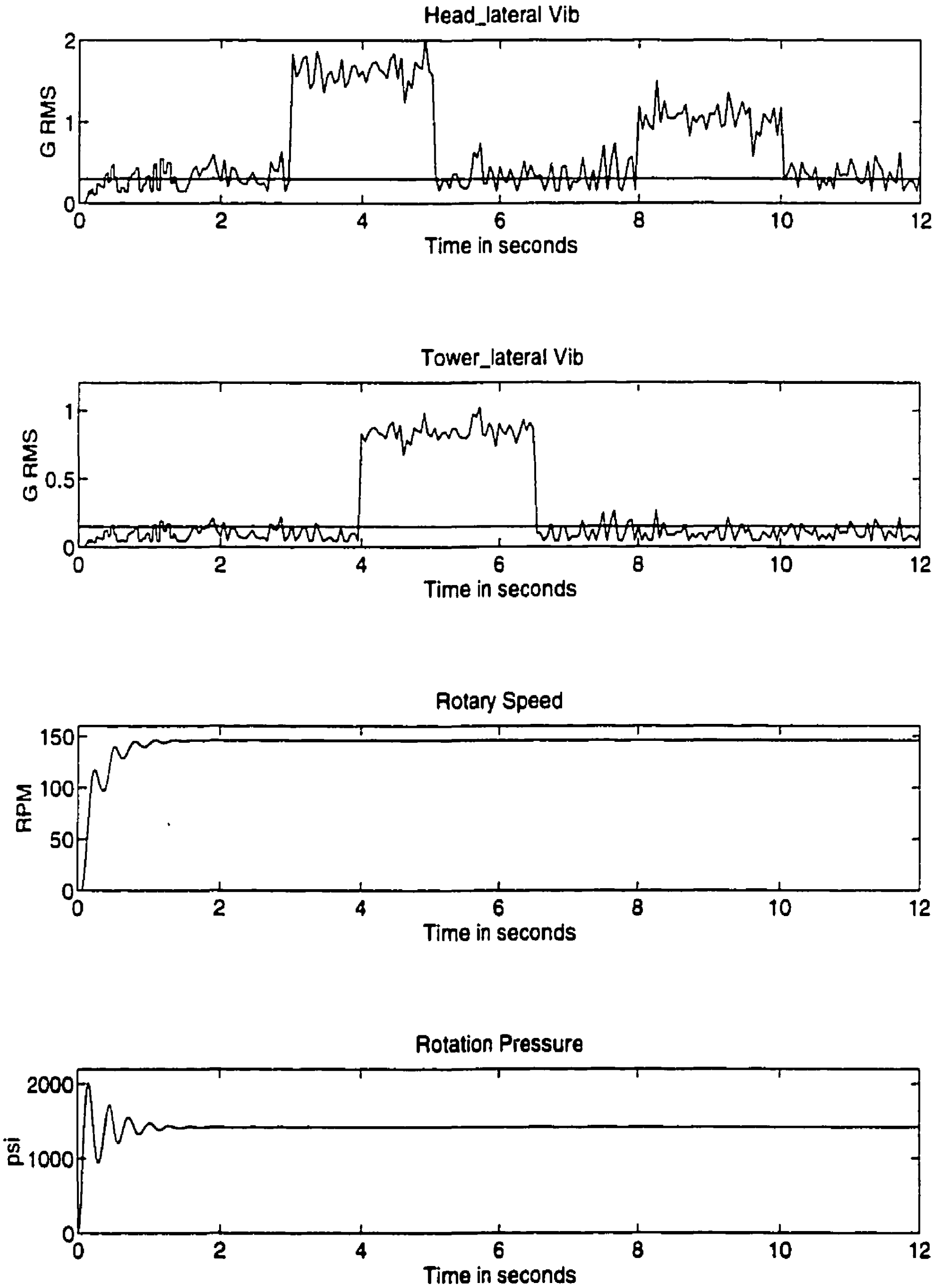


**Figure 7.4:** Simulation of drilling vibration, prior to feedback control loop implementation.

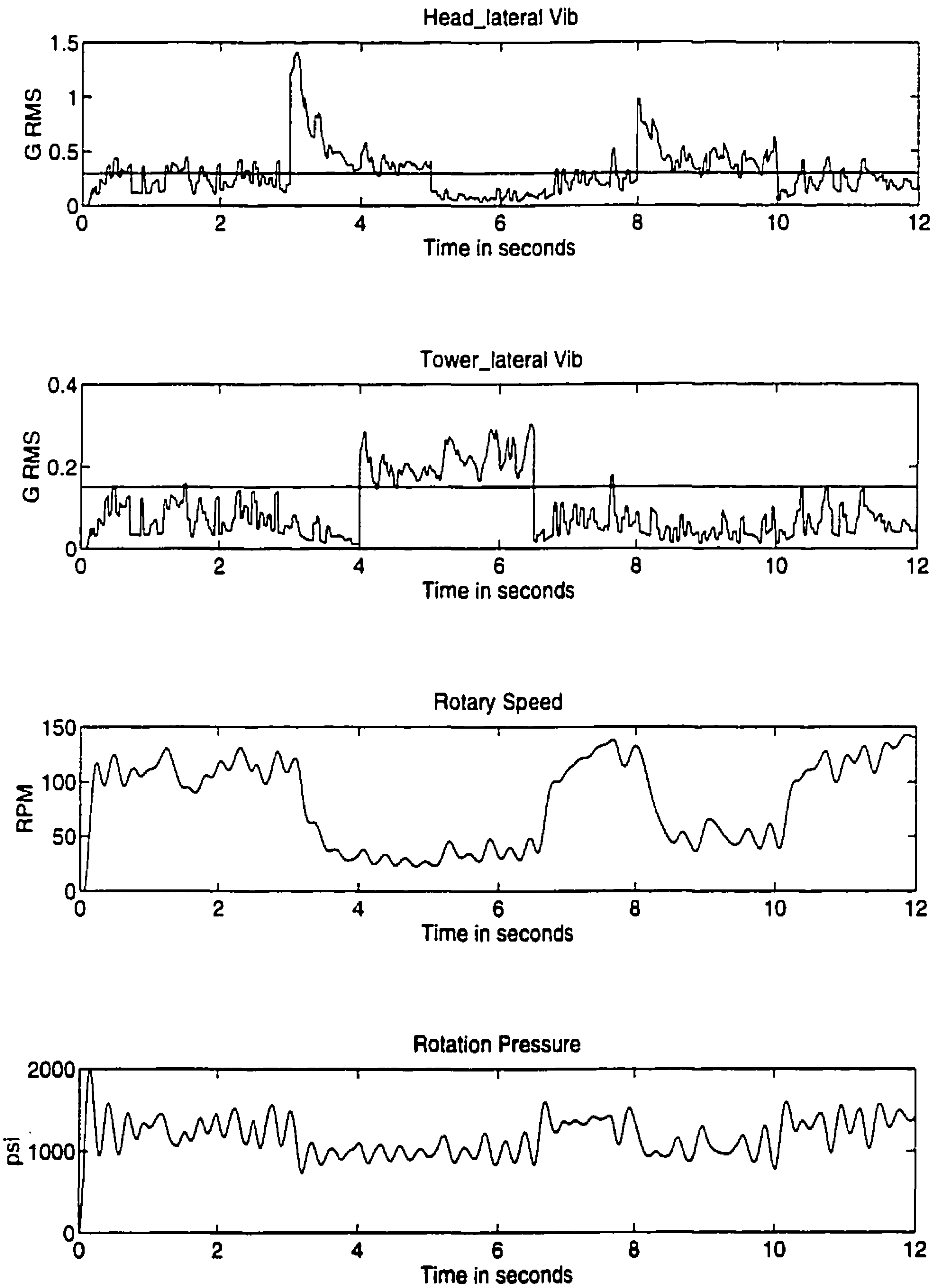


**Figure 7.5:** Simulation of the continuous controller, with Kp1 = Kp2 = 2000.

## 7.5 Simulation Of Discrete-Time Controller

The controller as implemented and simulated in the previous section is a *continuous time* controller. Modern controller implementation is based on digital computers, where a discrete-time counterpart system emulating the continuous time compensator is required. A characteristic of discrete-time systems is the *sampling time* (Ts), which represents the time elapsed before a new sample or output is read by, or generated to the system. A discrete-time system approaches a continuous time system when, at the limit, Ts is 0. The *sampling frequency* is the inverse of the sampling time, i.e. 1/Ts.

After a sampling frequency has been specified, then discrete-time transfer functions, counterpart of the continuous time functions are computed and simulated. The discrete-time transfer functions can then be implemented using a computer for control applications.

### 7.5.1 Discretization of controller

The selection of a sampling rate is a complex engineering function depending upon many factors and compromises. As a rule of thumb, the sampling frequency for a single-rate sampling control system is chosen to be 5 to 10 times larger than the bandwidth of the controlled process [Houpis 199?]. For the current implementation, the crossover frequency of the rotary actuator system is approximately 3.5 Hz, which yields a sampling frequency of 35 Hz. The sampling time is therefore 1/35 or approximately 0.03 seconds. A 0.03 seconds sampling time was therefore chosen for the discrete controller implementation. The discretization method used a Tustin transformation method, which approximates z-domain transfer functions from the s-domain transfer functions.

### 7.5.2 Simulation of Discrete Controller

The discrete controller was implemented in the simulator and simulated. The simulation results are shown in Fig. 7.6, and closely match the continuous controller results.

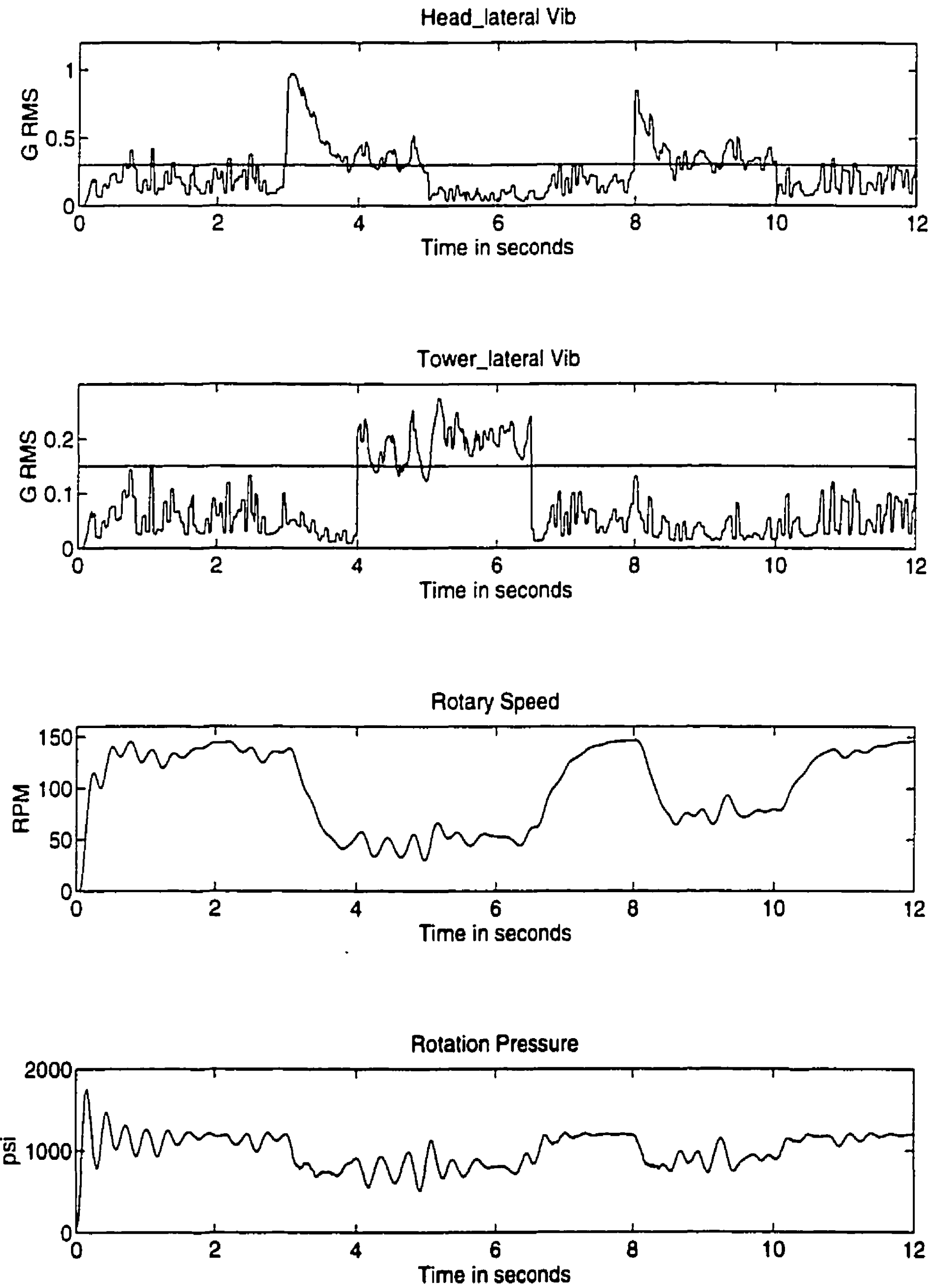


**Figure 7.6:** Simulation of the discrete controller, sampling time Ts = 0.03 sec, Kp1 = Kp2 = 2000.

In order to show the effect of the sampling rate selection, the continuous time controller was digitized using a sampling time of Ts = 0.3 second, i.e. ten times slower. The simulation results of the new discrete time controller are shown in Fig. 7.7. The degradation in performance can be observed in the rotary speed and rotation pressure signals, which exhibit high ripple content. In addition, the vibrations were not properly damped as in the continuous case controller.

**Effect of variations in feed pressure**

In order to verify the stability of the system with respect to variations in feed pressure (i.e. weight-on-bit), the 0.03 second sampling time discrete controller was simulated, with feed pressure varying in a sine wave manner, ranging from 285 to 1975 psi, with a frequency of $1/\pi$, e.g. the weight-on-bit cycled between 5760 lbs and 34900 lbs. The range of feed pressure was chosen to cover the extreme cases that the drill could generate. The frequency was chosen to provide a feed pressure cycle of 3 seconds, to simulate 4 full cycles of feed pressure variations within the simulated time of 12 seconds. In practice, such high speed and wide variations of feed pressure are not realistic nor desirable, as they subject the bit and the drill tower to cyclic stress that can reduce their useful life. For simulation purposes, the implemented feed pressure variation represents a worst case situation, that would validate the vibration controller, under real drilling applications.

The simulation results show that the vibration controller started reducing rotary speed at time t = 3 seconds. At time t = 5 seconds, the feed pressure started to drop, resulting in a drop in rotation pressure and penetration rate. At the same time, rotary speed was quite low. The bit power calculated was low, thus generating low vibration at the tower, below the threshold level of 0.15 G rms. Consequently, rotary speed started rising again, until time t = 6 seconds, when feed pressure started rising as well, driving the tower vibration back beyond the threshold level. Subsequently, the vibration controller was activated, and started to reduce rotary speed again.

In conclusion, the simulation showed that the controlled drilling process remained stable, under large variations in feed pressure. The results of this test validate the objective of designing a vibration controller that can operate in conjunction with another controller - or the drill operator - varying weight-on-bit, in an independent manner.

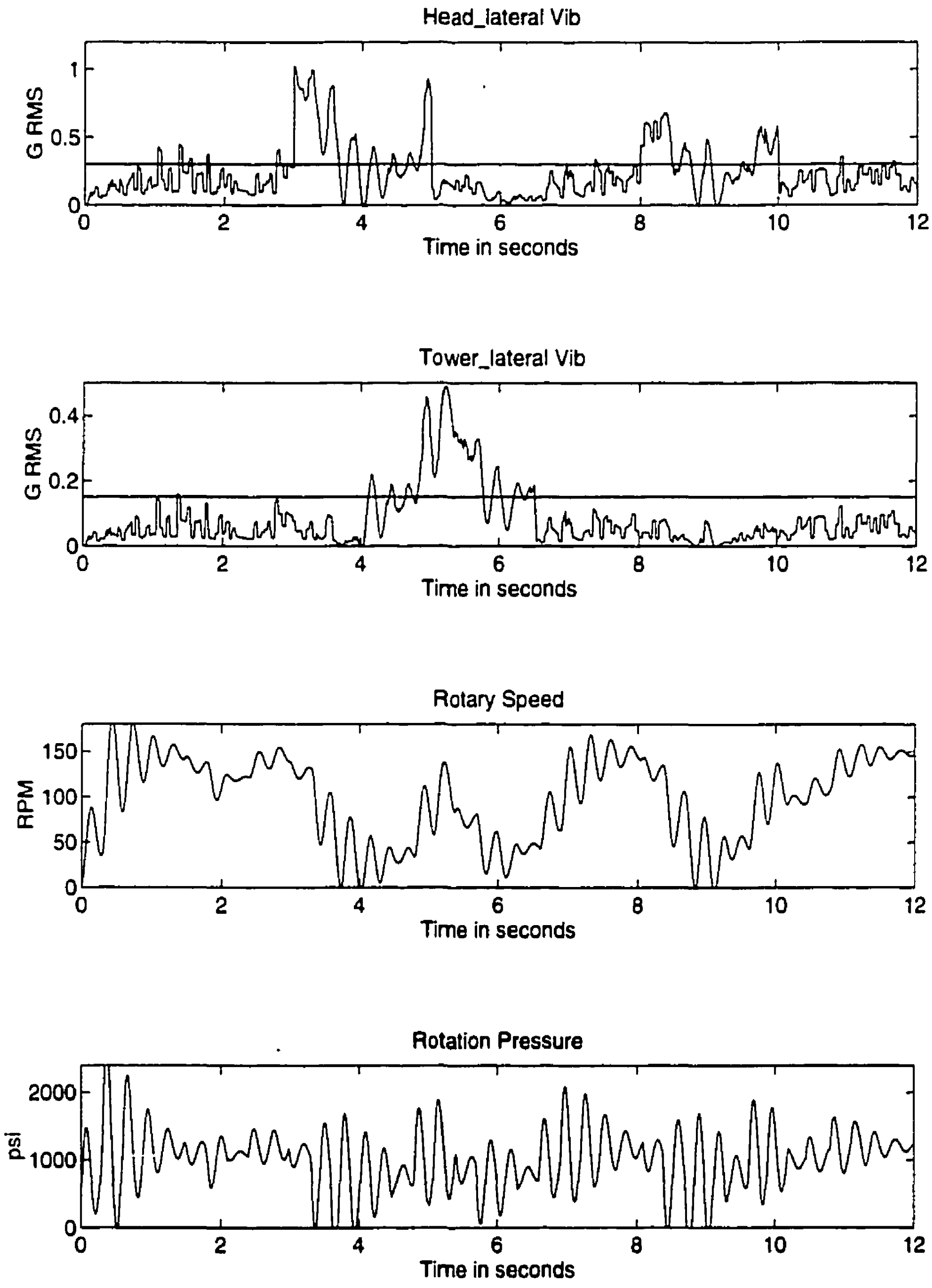


**Figure 7.7:** Simulation of the discrete controller, sampling time Ts = 0.3 sec, Kp1 = Kp2 = 2000.

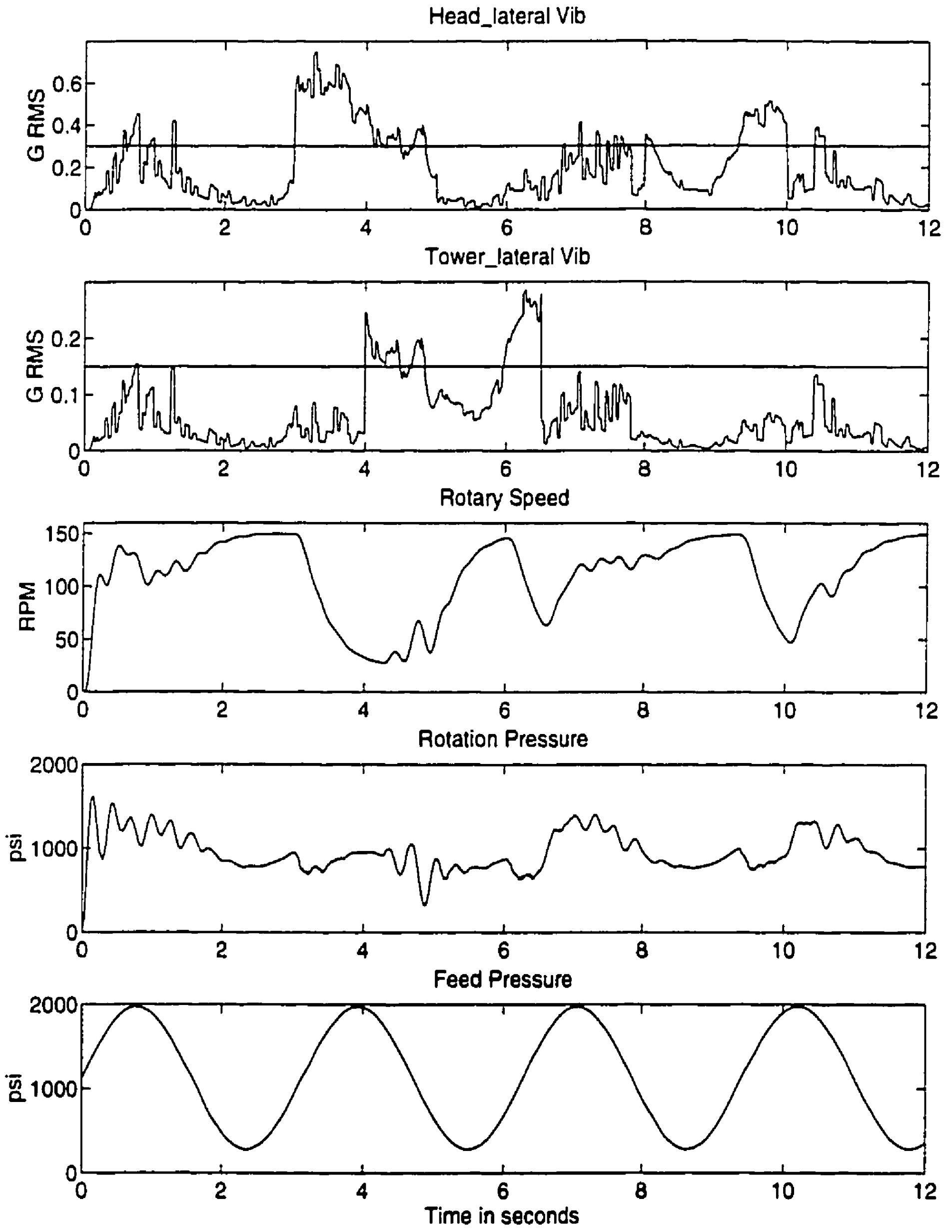


**Figure 7.8:** Simulation of discrete controller, sampling time = 0.03 sec, Kp1 = kp2 =2000, variable feed pressure

## 7.6 Conclusions

A vibration control strategy was designed and interfaced with the drilling simulator, then tuned and simulated. Severe levels of vibration were simulated to occur on the head and the tower, both in the lateral direction.

The simulation results showed that the proposed controller was able to dampen vibration, and to restore the rotary speed to its nominal operating range, once the vibration has been dampened. The results also show that controlling vibration based solely on variations of rotary speed is a viable technique.

The proposed controller, based on a robust fixed gain proportional type controller, appears to be adequate for this application. The sampling rate for implementation of this controller is likely to be in the region of 30 Hz.

The sensitivity of the control loop with respect to variations in feed pressure initiated by the drill operator, is negligible. The controller is also robust with respect to a parallel feedback loop controlling feed pressure, provided its bandwidth does not exceed $1/\pi$ Hz.

The further validation and refinement of the proposed controller requires closed-loop control experimentation on actual machines operating under a variety of field conditions.

# Chapter 8 FIELD TESTING OF CONTROLLER

## 8.1 Field Test sites

The control strategy proposed in previous Chapters was implemented and field tested at the Quintette Coal Operation, and the Bullmoose Operating Corporation mines, both in British Columbia, Canada. The work started in late 1993, and was completed by the end of 1994. The two mines are located in the Canadian Rocky Mountains, where coal layers are extensively faulted and folded. Drilling through variable ground is common, and therefore rock conditions can vary from very hard to very soft (coal). Due to such varying drilling and operational conditions, the mines had shown interest in automating their drilling machines.

## 8.2 Quintette Operating Corporation

### 8.2.1 Drill : Gardner-Denver GD-120

The drill at the Quintette Coal Operation was a Gardner-Denver model GD-120, rated to provide 120,000 lbs of weight-on-bit. The GD-120 was equipped with a hydraulic motor for the pulldown motion, while a DC electric motor provided bit rotation.

**Feed Mechanism**

The weight-on-bit mechanism consisted of a hydrostatic transmission, where both motor and pump were of fixed displacement. A hydrostatic transmission is a hydraulic circuit in which a pump, driven by a prime mover, supplies hydraulic flow into a motor, at the system's set pressure. Fixed displacement pumps and motors operate at a constant fixed flow, as opposed to variable displacement pumps and motors, where the hydraulic flow can be stroked from minimum to maximum rated capacity. A mechanically controlled directional valve determined the bit's direction of motion, by reversing the hydraulic flow into the motor. The desired pulldown pressure was set by the operator through manual adjustments of the relief valve that diverted excessive hydraulic flow back into the tank.

**Computer Control of Pulldown Pressure**

In order to electrically control the pulldown pressure, the mechanically adjusted relief valve had to be replaced by a proportional valve that could be electrically controlled. The operator's pressure control knob was also substituted with a joystick type control handle that generated an output voltage to the proportional relief valve. The directional valve was also upgraded to provide electrical control over hydraulic flow direction, by using an electric switch controlled by the operator. This enabled electric control over the direction of motion, e.g. upward or downward.

**Rotation Mechanism**

The rotation mechanism is based on the Ward-Leonard speed control system. A prime mover drives a direct current (DC) generator, whose generated voltage supplies a DC motor, having a separately excited (constant) field current. The generator's field current is controlled by solid state rectifiers, that read a voltage reference dialed by the operator. By controlling the generator field current, the generator's output voltage is therefore controlled. Since the rotary motor is powered by the generator, its rotation speed depends on the generator's output voltage. Thus by adjusting the generator's field current, one could control the motor's rotation speed.

**Computer Control of Rotary Speed**

The rotary speed could be computer controlled by substituting the operator's speed reference voltage with a computer generated analog reference. Appropriate current and voltage amplifiers were selected to fulfill the interfacing requirement. In addition, a set of computer controlled relays were installed in order to energize the motor's field current, as well as the solid state rectifiers.

### 8.2.2 GD-120 Drill Instrumentation

#### Transducers

The GD-120 was instrumented with transducers to measure the variables of pulldown pressure, rotary speed, rotary torque, air pressure, depth and penetration rate, axial and lateral vibration of the rotary head, as well as the lateral vibration of the tower, near the cab.

The pressure measurements were obtained using pressure transducers, while depth and penetration rate were calculated using a quadrature optical encoder connected to the pulldown chains shaft. The rotary speed and torque were calculated by measuring the motor's armature voltage and current, through high voltage isolation amplifiers.

Vibration was measured with piezoresistive type accelerometers, conditioned by an electronic circuit that filtered the acceleration signals at the low pass frequency of 35 Hz. The Root-Mean-Square over a 0.5 sec. time constant of the filtered signals were subsequently generated with an electronic converter. Table 8.1 summarizes the various sensors used to instrument the drill.

| Measurement Description | GD-120 Instrumentation |
|---|---|
| Pulldown Pressure | Pressure Transducer |
| Air Pressure | Pressure Transducer |
| Rotary Speed | Isolation Amplifier |
| Rotary Torque | Isolation Amplifier |
| Depth and Penetration Rate | Optical Encoder |
| Head Axial, Head Lateral and Tower Lateral Vibration | Piezoresistive Accelerometers |

**Table 8.1:** Description of GD-120 instrumentation

In addition to the sensors, three power supplies were needed to power the various instrumentation on the drill.

### Programmable Logic Controllers

Programmable Logic Controllers (PLC) are widely used at mines for diverse applications, ranging from process control at their plant processing facility, to automatic lubrication of drills and shovels. The drills at Quintette were already equipped with one PLC, and the mines had shown interest in extending their capability to provide automatic drilling control.

The GD-120 used for this work was equipped with an Allen-Bradley PLC model SLC5/03. The PLC was expanded through the addition of input and output cards, to fulfill the required additional Input/Output capability. Discrete input cards were used to measure switch contact closures, while discrete output cards controlled the directional valves and related solenoid valves. Analog cards were used to read the instrumentation analog signals, while analog output cards generated the control signals to the drill's actuators. The analog output control signals were amplified before powering the electric actuators on the drill. An additional high-speed-counter card was added to each PLC for the purpose of decoding the encoder signal.

The PLC was programmed using Ladder Logic programming software supplied by Allen-Bradley. The control logic component of the PLC program was written by the author.

### Rugged Computer With Display

A rugged industrial computer was used to provide the user interface and display. The computer was linked to the PLCs through a serial link interface, that provided a two way communication between the computer and the PLC. Figure 8.1 illustrates the system's overall architecture. The computer was programmed using the C programming language, running under the QNX real-time operating system, by software engineers at Aquila Mining Systems Ltd. The computer was also used as a data logger, for the purposes of logging actuator dynamic tests, as well as logging the measured variables while drilling a hole, for subsequent data analysis.

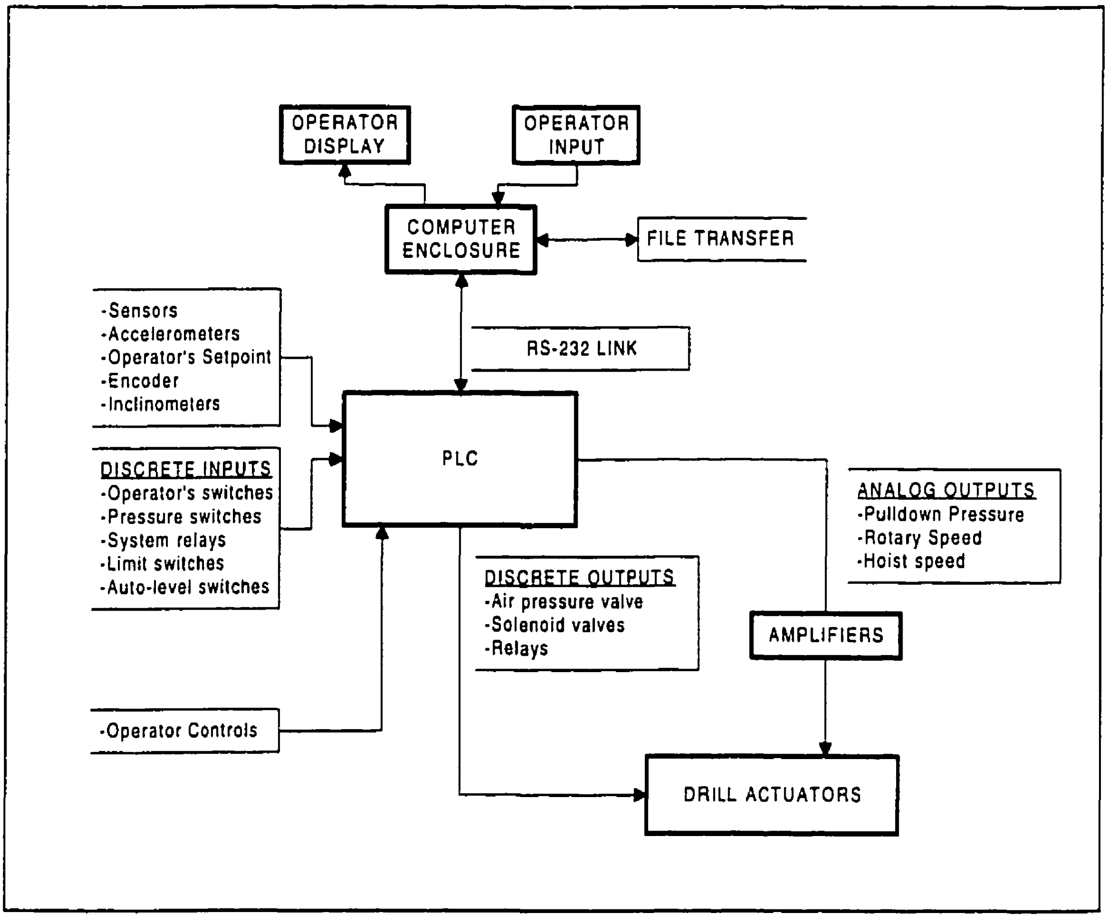


**Figure 8.1:** Implemented system architecture for automatic drilling control

### 8.2.3 Implemented Control Logic

#### Operator Drilling Procedures

Once the drill has been positioned and leveled, the operator engages the automating drilling system by entering the hole number, the target depth, as well as the desired collaring distance. Subsequently, the drill rig automatically drills the hole until the preset depth is reached.

Prior to the installation of the automatic drilling system, the mine engineers had specified setpoints for pulldown pressure and rotary speed for collaring and drilling, based on their experience with the bench geology and their requirements for total footage drilled by a single bit before failure. The setpoints were to be respected during normal manual drilling operations. The operator would reduce these setpoints in the event of severe vibration, or when the drill experienced other difficulties, such as a rise in the bit air pressure, rotary torque, or other exceptional condition.

Based on the mine requirements, the control logic for automatic drilling was to follow the manual drilling procedures. Therefore the setpoints for pulldown pressure and rotary speed were stored in a file that could be updated by the mine. During a regular automated drilling session, the controller read the setpoints from the file, and subsequently generated the corresponding voltages at the input of the respective actuators for pulldown pressure and rotation speed.

In a similar approach to the manual operation, the control logic reduces the setpoints in the event of drilling difficulties. The pulldown pressure is reduced from its initial programmed setpoint, whenever the limits for rotary torque are exceeded, in order to confine the rotation torque within the nominal operating ranges specified by the manufacturers. The rotary speed setpoint is reduced from its programmed setpoint, whenever limits for vibration are exceeded.

It is important to note that the implemented logic for pulldown pressure control did not follow the design recommended by the author, in his Master's Thesis work. However, the logic for reducing drilling vibration implemented the design specified in this thesis. It is the main objective of this thesis to design a vibration control strategy compatible with the author's recommended pulldown pressure control, as well as other control algorithms deemed to be valid.

### 8.2.4 Field Test Results

Several weeks were spent at the site for the installation of the instrumentation and hardware equipment. Once the field installation was completed, the automatic drill system was tested, and the control loops fine tuned. Drilling data was logged, enabling the analysis of the automatic control performance.

Figure 8.2 shows the vibration signals, as well as pulldown pressure, rotary speed and rotary current (torque) for a typical blasthole, drilled by the automatic drill system. The pulldown pressure and rotary speed setpoints were set to 800 psi and 45 rpm when drilling the collaring depth of 0.5 m, and 2000 psi and 80 rpm when drilling beyond the collaring depth. The head axial vibration signal experienced cabling problems, and could not be repaired during the test period, as special equipment (i.e. a bucket truck) was needed for the repair. Therefore, the head axial vibration signal is not shown in Fig.8.2.

The graphs show that the pulldown pressure is reduced by the controller at several instances, in order to keep the rotary current from exceeding the maximum preset threshold of 200 Amps. The spikes in rotary current are the result of the controller response time, since the controller turned active whenever the rotary current exceeded 200 Amperes.

The vibration signals remained within normal operating ranges. The vibration controller was active between depths 0 to 2 m, and 10 to 14 m, which can be noticed from the reduction of rotary speed at several instances.

In general, drilling the holes automatically resulted in a smooth operation, where no severe vibration effects could be felt by persons sitting in the operator's cab.

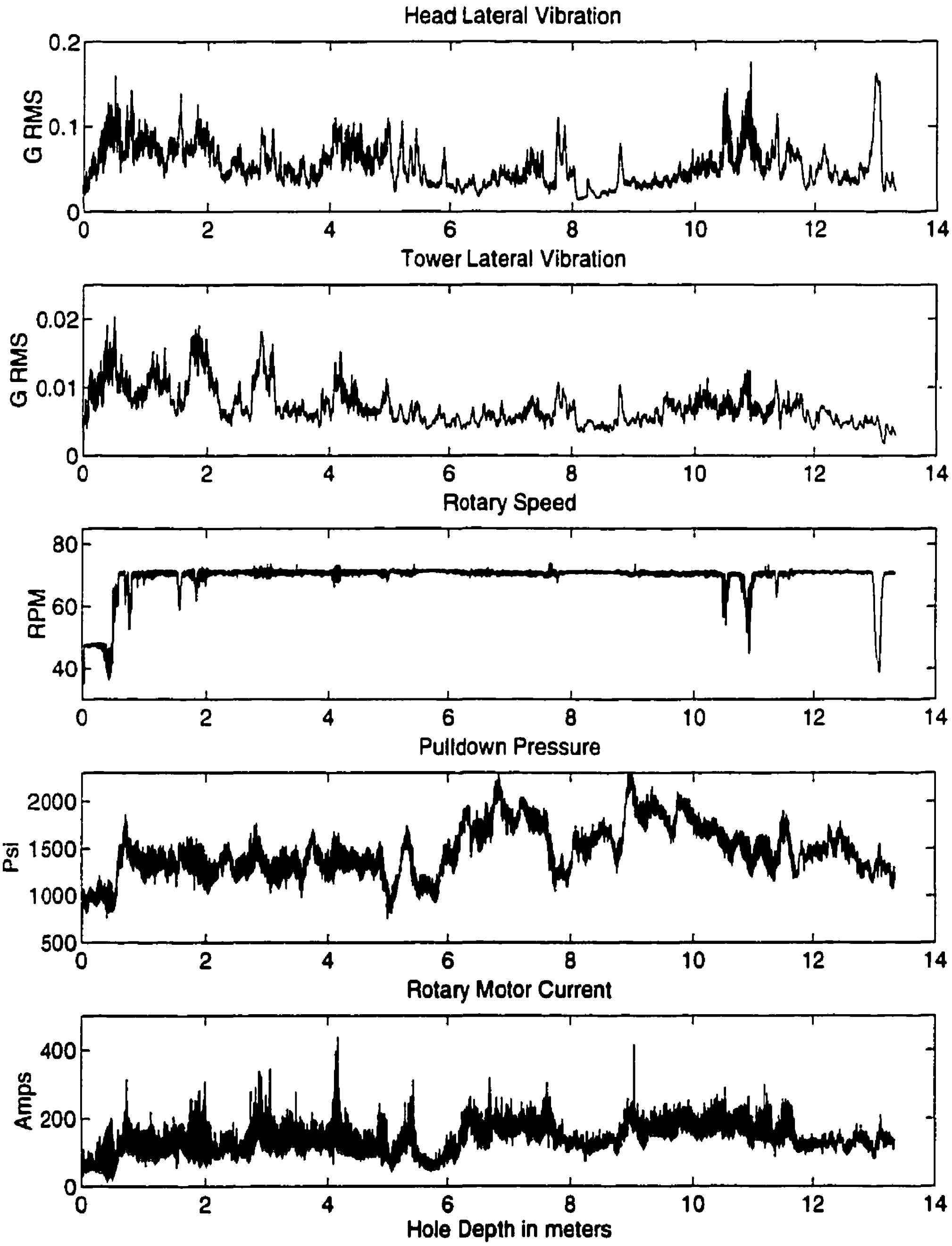


**Figure 8.2:** Data collected from drilling a borehole, at the Quintette Operating Corporation

Figure 8.3 shows a section of the borehole displayed in Fig. 8.2, which displays in greater detail the reaction of the controller to rising vibration levels. The section shown represents 1.4 m of drilled depth.

The rotary speed was set to 70 rpm for normal drilling. The vibration thresholds that triggered the controller to react were set to 0.1 G rms and 0.02 G rms for the head and tower lateral vibration respectively.

In the section shown, the controller was triggered at 3 instances, near 10.5, 10.8 and 11.4 meters. In all three situations, the vibration controller was triggered by vibration levels exceeding the head lateral vibration threshold while the tower vibrations remained well below the preset threshold level of 0.02 G rms. As the vibration controller reduced rotary speed, the vibration levels did not significantly increase, but remained controlled, in the neighborhood of 0.1 G rms, at the head level. The vibration controller proved to be effective and stable, since rotary speed converged back to its normal drilling setpoint of 70 rpm, shortly after the vibration started to build up.

Figure 8.3 also shows the behaviour of the pulldown pressure and rotary current during the same drilled interval. The pulldown pressure varies between 1200 and 1800 psi, as it attempts to maintain the rotary current at a nominal value of 200 Amps. The graph showing the rotary current indicates that the pulldown pressure controller was successful in meeting its designed objective.

Finally, the displayed variables indicate that the overall drilling control system remained stable, for the duration of the displayed signal.

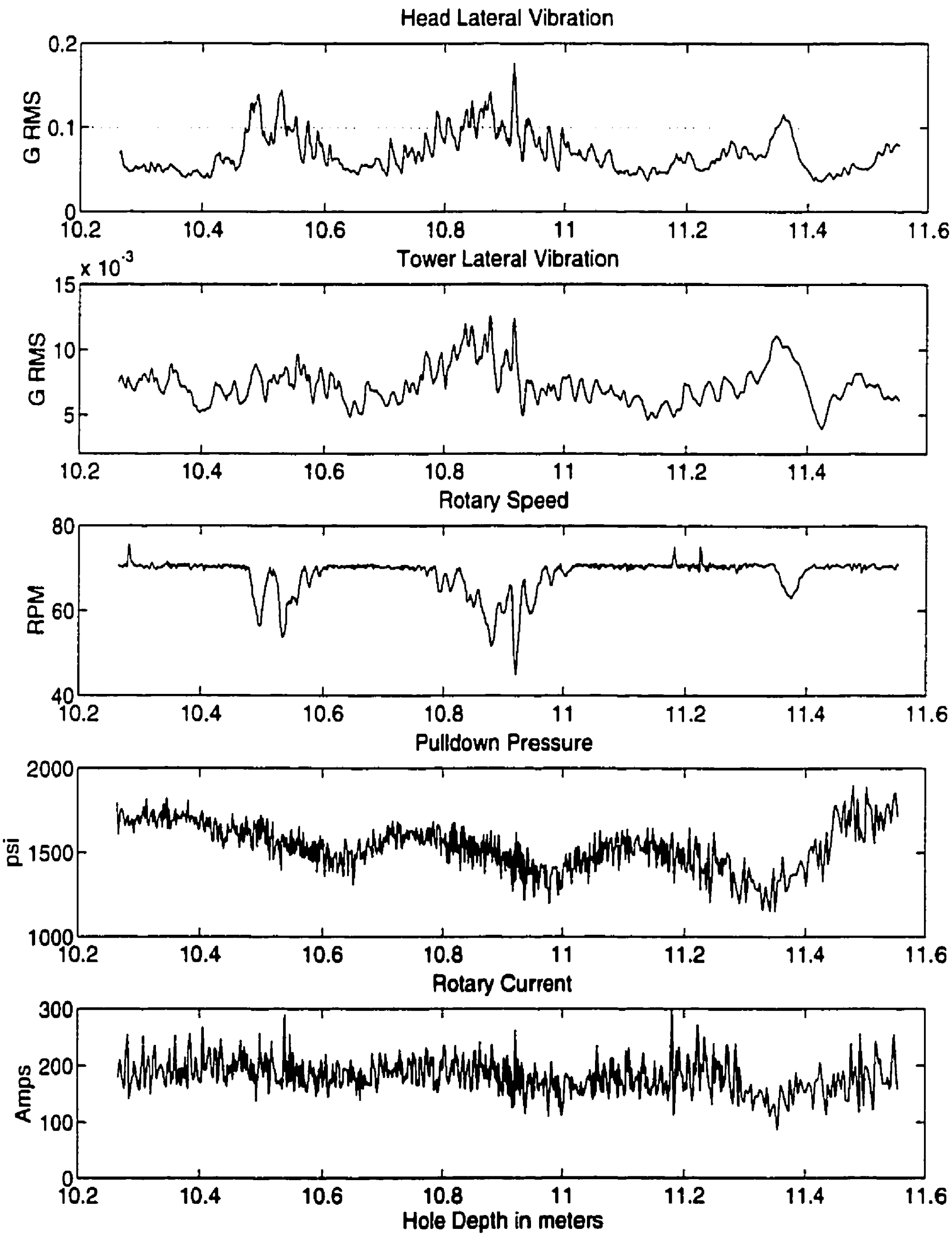


**Figure 8.3:** Section of borehole drilled at Quintette, November 1994

Figure 8.4 shows another example of the controller reaction to vibration. The drill was initially collaring the hole at a rotary speed of 45 rpm, then increased its rpm level to reach 80 rpm, once the collaring depth of 0.6 meter had been drilled.

While rotary speed was rising to 80 rpm, the drill experienced rising vibration, triggering the controller to occasionally reduce rotary speed, resulting in the "jagged" response observed on the rotary speed signal. The vibration thresholds that triggered the controller to react remained set at 0.1 G rms and 0.02 G rms for the head and tower lateral vibration respectively.

At a depth near 1 m, the vibration level rose again, triggering the controller to react by reducing rotary speed.

At depths of 1.3, 1.6 and 2.4 meters, the drill experienced severe vibration, where both the head lateral and tower lateral vibration exceeded their preset thresholds. Thus, the controller was triggered by both vibration signals, where two feedback control loops were active at the same time. In all vibration cases, the rotary speed converged back to its nominal setpoint of 80 rpm, after the vibration was successfully dampened.

The severity of the vibration can be observed in the rotary current signal, which exhibits amplitude spikes during the severe vibration periods. It appears as if the bit was experiencing difficulties in breaking the rock, and occasionally stalling, an indication of a weak coupling between the bit and the rock at the bit rock interface. The pulldown pressure was continuously adjusted by its feedback loop controller to prevent the rotary current from exceeding 200 Amps.

In all severe vibration cases, both the vibration and pulldown pressure controllers performed well in reducing vibration and protecting the rotary motor from overloading, without stopping the drilling operation. Both controllers remained stable as well.

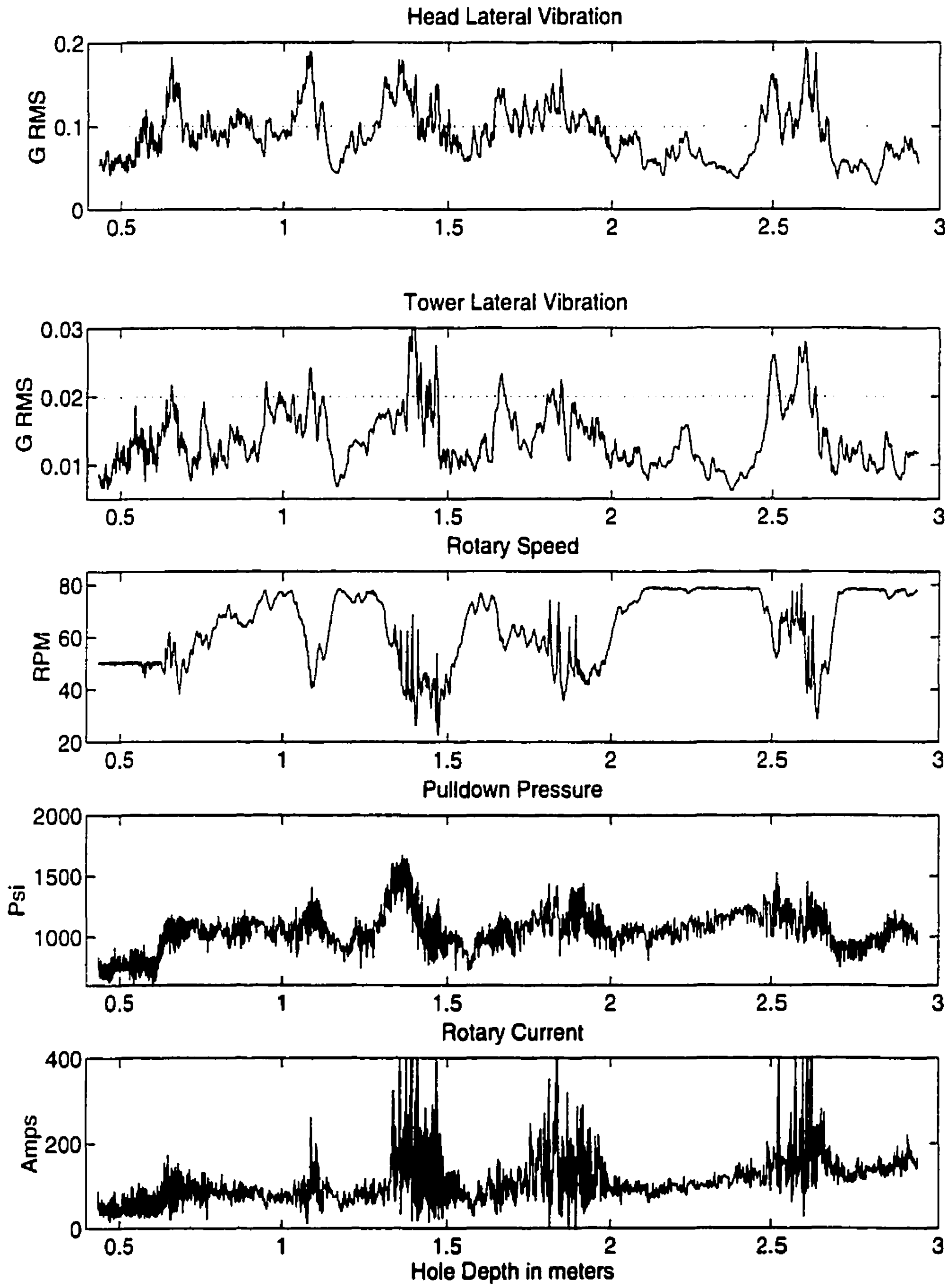


**Figure 8.4:** Section of borehole drilled at Quintette, November 1994

## 8.3 Bullmoose Operating Corporation

### 8.3.1 Drill Type: Ingersoll-Rand DM-H

The drill used for this study at the Bullmoose Operating Corporation was an Ingersoll-Rand DM-H drill, rated to provide 100,000 lbs of weight-on-bit. The DM-H was equipped with hydraulic motors for pulldown motion and rotation.

#### Feed mechanism

The weight-on-bit mechanism consisted of a hydrostatic transmission, where the motor and pump were respectively of fixed and variable displacement. The weight-on-bit was controlled by a proportional actuator that stroked the pump accordingly, in order to regulate the pressure at the desired setpoint reference. A set of switch contacts controlled the hydraulic flow direction, through an electrically controlled directional valve.

#### Rotation Mechanism

The rotation mechanism also consisted of a hydrostatic transmission, where the two rotary motors and pumps were respectively of fixed and variable displacement. Rotation speed was controlled by a proportional actuator that stroked the pump to control the hydraulic flow. Consequently, the motors' rotation speed was proportional to the hydraulic flow. Similar to the weight-on-bit mechanism, a set of switch contacts controlled the hydraulic flow direction, through an electrically controlled directional valve.

#### Computer Control of Rotary Speed and Pulldown Pressure

In order to provide computer control over pulldown pressure and rotary speed, the operator's pulldown pressure and rotary speed reference voltage were substituted with a computer generated analog reference, when the automatic drilling mode was engaged. Appropriate amplifiers were selected to fulfill the interfacing requirement.

### 8.3.2 DM-H Drill Instrumentation

The DM-H drill at this site was instrumented in a similar manner to the GD-120 drill discussed in the previous section. The hydraulic pressures in the feed and rotation circuits were measured using pressure transducers, while rotary speed was measured using a magnetic pick-up that generated pulses proportional to the rotary sped of the bit. The vibration was measured using piezoresistive transducers in a manner similar to the GD-120 drill. An optical encoder was used to measure the head position from which the bit penetration rate was calculated.

Table 8.2 summarizes the various sensors used to instrument the drill.

| Measurement Description | DM-H Drill Instrumentation |
|---|---|
| Pulldown Pressure | Pressure Transducer |
| Air Pressure | Pressure Transducer |
| Rotary Speed | Magnetic Pick up |
| Rotary Torque | Pressure Transducer |
| Depth and Penetration Rate | Optical Encoder |
| Head Axial, Head Lateral and Tower Lateral Vibration | Piezoresistive Accelerometer in every measured direction |

**Table 8.2:** Description of DM-H instrumentation

**Controller Implementation**

The controller implementation followed the same architecture as the controller implemented at the Quintette mine. A rugged industrial computer with display provided the user interface and display, while an Allen-Bradley PLC model PLC5/11 provided the drill Input/Output interface.

The control logic implemented the same algorithms as the GD-120, discussed in section 8.4.1.

### 8.3.3 Field Test Results

Figure 8.5a shows a segment of data from a blasthole drilled at the Bullmoose Operating Corporation, using the instrumented Ingersoll-Rand DM-H hydraulic drill. The section shown represents 5 m of drilled depth.

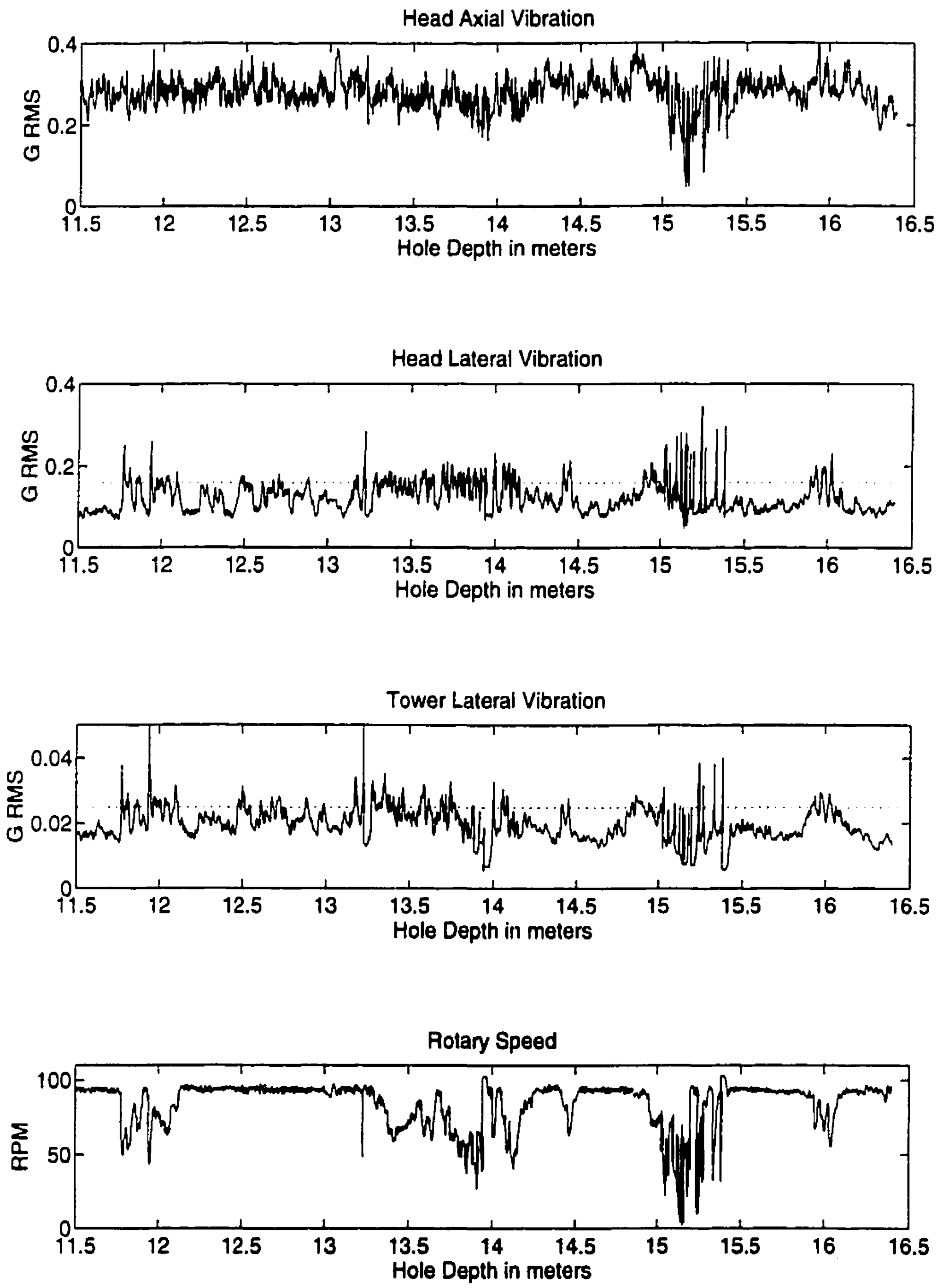


**Figure 8.5a:** Section of borehole drilled at Bullmoose, November 1994; DM-H drill

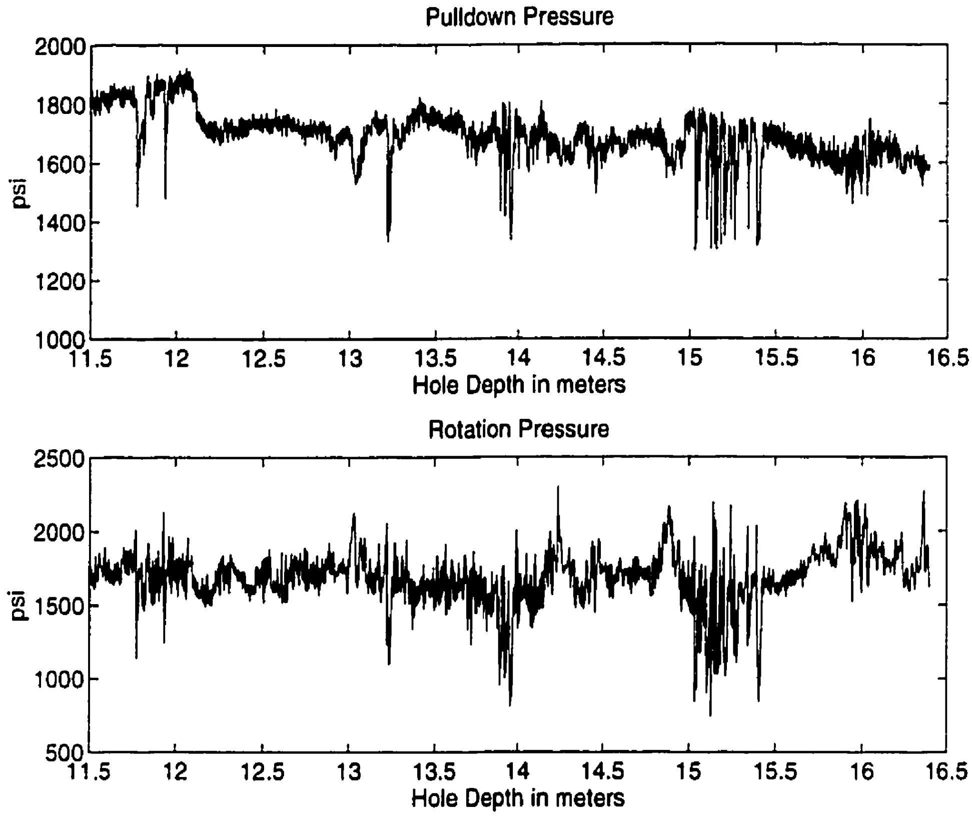


**Figure 8.5b:** Section of borehole drilled at Bullmoose, November 1994; DM-H drill

The rotary speed was set to 85 rpm, during normal drilling. However, the graphs show that the controller reduced rotary speed at several instances, while preventing the vibration signals, in all three measured locations, from exceeding the preset thresholds of 0.4, 0.16 and 0.025 G rms for the head axial, lateral and tower lateral vibration respectively. The head axial vibration levels are usually higher than the lateral vibration signals during a normal drilling operation, which justifies the selection of a higher threshold for the axial vibration signal.

Compared to the Gardner-Denver GD-120 drill at the Quintette Operating Corporation, it was observed that the DM-H drill vibration levels were generally higher during normal drilling operation. Consequently, the vibration thresholds selected for the DM-H were also higher than the corresponding ones selected for the GD-120 drill. The difference in vibration levels between the two drills is mainly due to the different structural design and weight of the drill.

The vibration controller was driven by the head and tower vibration signals, while the head axial vibration remained below its preset threshold. In all rotary speed reduction instances shown, both the head and tower lateral vibration thresholds were exceeded. However, the vibration controller was successful in regulating the vibration levels near the preset thresholds.

The section between 15 and 15.5 m depth shows a segment of difficult drilling where the vibration signals exhibit several spikes, resulting in an aggressive controller reaction that nearly dropped rotary speed to zero. The fluctuations of pulldown and rotation pressures shown in Fig. 8.5b also confirm the difficult coupling between the bit and rock. Nevertheless, the vibration controller remained stable, and rotary speed converged back to 85 rpm near 15.5 m.

Figure 8.6 shows the effect of tuning the controller with gains large enough to induce a "limit cycle" effect where rotary speed is aggressively reduced to reach zero, resulting in a sudden reduction in vibration, which prompts the controller to restore rotary speed back to the nominal setpoint, then back down to zero due to renewed vibration build up, and so forth.

It is therefore necessary to carefully choose controller gains that would result in a damped response, rather than entering limit cycles that may have damaging effects to the drill and the bit. Conversely, an excessively damped controller response could result in long response time that can also be damaging to the drill.

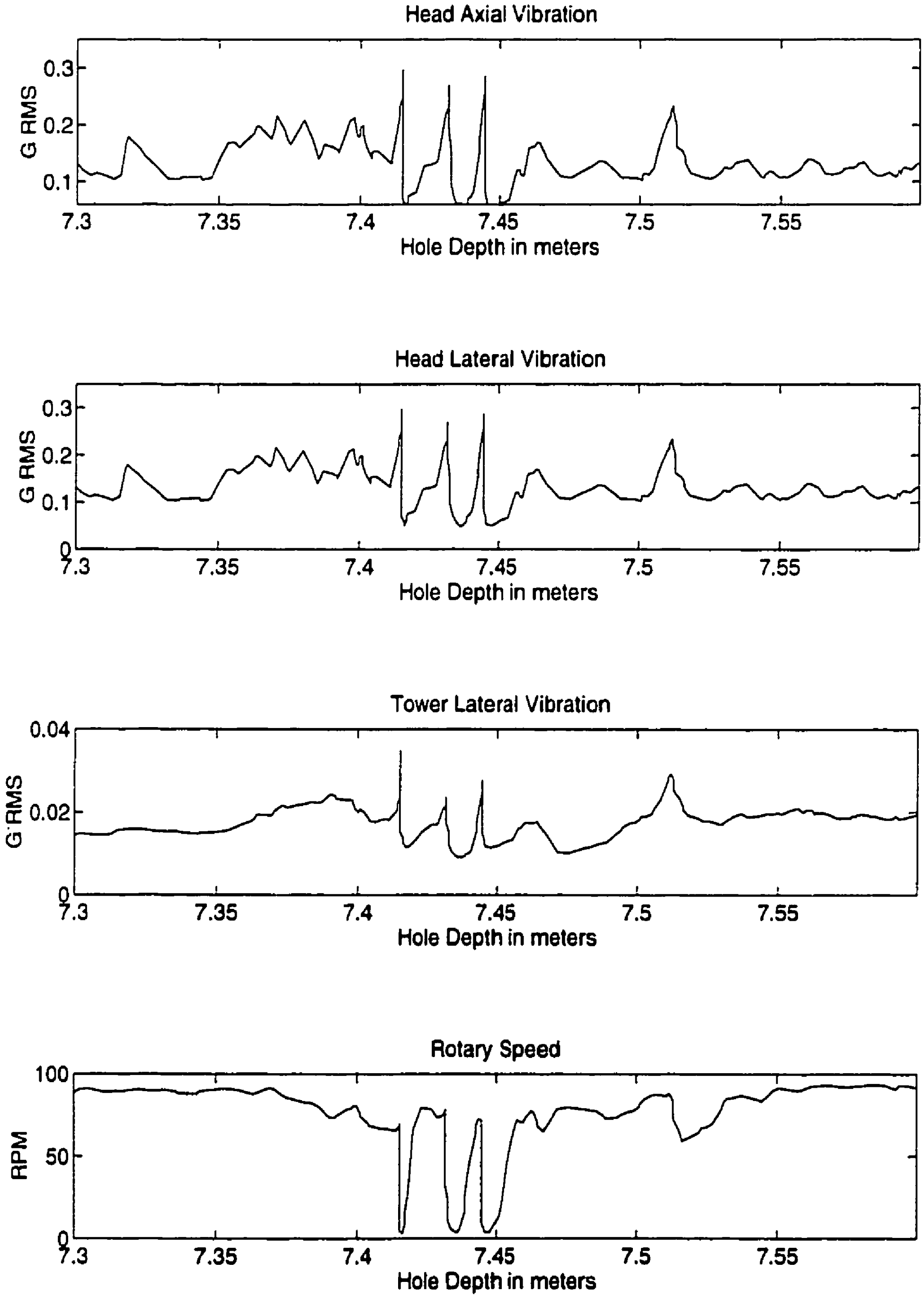


**Figure 8.6:** Section of borehole drilled atBullmoose, November 1994; DM-H drill

## 8.4 Practical Benefits of Automatic Drilling

The implementation of the automatic drilling systems on the drills at both sites was faced with the additional challenge of obtaining the drill operators' acceptance of such technology, generally viewed as a threat to their present employment.

### 8.4.1 Quintette Operating Corporation

The Quintette Operating Corporation configured the machine to drill only in automatic mode. The decision allowed them to collect reliable statistical information about the benefits of drill automation, although the decision was not positively welcomed by the drill operators.

It was found that, on average, the drill's availability increased from 77% to 85% due to lower maintenance problems and failures, with maintenance costs down by 35% and that the bit life per drilled distance had improved. However, the mine found that a skilled operator could outperform the automatic system. The automation benefits are relevant when all variables are considered, such as variation in operators skill, moments of distraction or fatigue, and failures due to operator errors or mishandling of the equipment. By the end of 1995, Quintette had automated a second drill.

At the present time, the Aquila Mining Systems Ltd. of Montreal is commercializing the automatic drilling control system, labeled DM-3. Quintette has ordered four DM-3 systems, aimed at automating their remaining drill fleet by the end of 1997.

The two current installations are still operational to date at the mine.

### 8.4.2 Bullmoose Operating Corporation

The Bullmoose Operating Corporation did not force the operators to drill in automatic mode exclusively. As a result, Bullmoose was unable to correlate their drill statistics with the benefits provided by the automatic control system, since the drill was operated in automatic mode, only at the operator's discretion.

The current installation is still operational to date at the mine.

## 8.5 Conclusion

The vibration controller designed in this work has been implemented and tested on two production drills equipped with different rotation mechanisms: one equipped with an electric motor, with speed controlled via a Ward-Leonard speed control system, while the other was equipped with a hydraulic rotation circuit.

Since the vibration controller presented in this work was designed to deal with a range of diverse drill rotation mechanisms, the two test platforms presented a good case study for testing the vibration controller, since they represented two different dynamic responses under actual production conditions.

The preliminary tests were conducted in two neighbouring coal mines, with each drill instrumented with three accelerometers to measure vibration: two at the rotary head measuring vibration in the axial and lateral directions, and one at the tower base measuring vibration in the lateral direction.

The field tests were successful, with results showing that the controller proposed in this thesis is viable when properly tuned. It reacted properly with rising levels of vibration, and remained stable under all drilling conditions encountered during testing.

Since the controller was successfully tested on two drills of different design and dynamics, then the tests showed that the controller is portable to different types of drills.

Finally, the field tests have shown that practical benefits can be expected from the implementation of such technology, such as reduced maintenance cost, higher drill availability and improved bit life.

# Chapter 9 CONCLUSIONS

## 9.1 Achievements

This thesis introduced a new approach for automatic rotary blasthole drilling control, based on closed loop feedback systems. The thesis described the formulation and development of a strategy for the automatic control of rotary speed, during drilling. This strategy is viable and compatible with a weight-on-bit control approach by the author, presented in his Masters degree work, and, also compatible with other weight-on-bit control strategies of similar functionality. The design criteria of this approach is to control rotary speed in order to dampen drilling vibrations as they occur (or, more practically, before they achieve significant levels) and return to the highest achievable productivity as soon as possible, once the vibrations have been attenuated.

The stated objectives were fulfilled by accomplishing several diverse tasks, listed below:

1. Past work and achievements in drilling control, both in the mining and oil drilling industry have been reviewed. It was found that the main result of earlier work was to establish a range of operating rotary speeds that would not excite the drill string into resonance.

2. The possibility of controlling the drill string vibration by manipulating rotary speed to avoid exciting the drill string into resonance was investigated. An analytical analysis of drill string natural modes and frequencies of vibration has been conducted, and supported by experimental testing, at the Ingersoll-Rand Rotary Drill Division, Texas,

U.S.A., testing facility (Nov. 1991 and May 1992). Based on these tests, it was concluded that several factors affected the accuracy of the prediction of natural frequencies, such as the rock type being drilled, the position of the rotary head along the length of the mast (e.g. position of the centralizer bushing with respect to rotary head) and non-linear effects due to backlash at the centralizer bushing and between the rotary head and mast (these effects increase with machine aging). Nevertheless, the estimated natural frequencies could be used as a basis to improve drill string and machine mechanical design.

3. A manually operated drill rig was instrumented and tested in a limestone quarry. The tests were aimed at refining physical models and relationships between the drilling variables. A better understanding of the drilling process, e.g. variable dependencies, power flow, vibration signals correlation as well as the drill operator's reaction to vibration was achieved, and feedback signals most directly related to vibration were also identified. The methodology and instrumentation which were used during field testing proved adequate.

4. A comprehensive suite of software tools was developed to assist in the complicated analysis of the test results, enabling the development of the proposed drilling model. The results were displayed in the form of strip chart plots, power spectra of vibration signals, as well as steady state plots of penetration rate, rotation pressure and vibration versus the manipulable variables of feed pressure and rotary speed. These plots provided a better understanding of the interaction between the drill rig and the rock in tricone bit drilling.

5. The machine dynamics for rotary speed and pulldown actuators were identified using system identification techniques, based on field data.

6. A software simulator of the drilling process was implemented, based on the drilling model equations derived from field testing. The computer drilling simulator provided a

flexible and powerful tool for interfacing control algorithms, which enabled their testing and fine tuning.

7. A strategy for automatic rotary speed control has been devised, based on field results and observations. The control system was interfaced to the drilling simulator and tested with different controller sampling times. The simulation results have shown that the controller achieves the desired specifications.

8. The vibration controller designed in this work has been implemented and tested on two drills equipped with different rotation mechanisms: one equipped with an electric motor, while the other was equipped with a hydraulic rotation circuit. The two test platforms presented a good case study for testing the vibration controller, since they represented two different dynamic responses under actual production condition. The field tests were successful, with results showing that the controller proposed in this thesis is viable when properly tuned. It reacted properly with rising levels of vibration, and remained stable under all drilling conditions encountered during testing.

## 9.2 Primary Research Contribution

Several studies on drilling vibration as well as empirical models relating the variables of penetration rate and rotary torque to weight-on-bit and rotary speed have been proposed in the past, however, the majority were developed in the area of oil well drilling for the petroleum industry. The empirical models presented in the area of mining blasthole drilling were mainly derived from tests performed on homogeneous rock test slabs in the laboratory. This thesis has extended their analyses to include blasthole drills string vibration, as well as new empirical models relating the drilling variables, derived from field data, where real drilling conditions were encountered.

Although automatic drilling control systems are offered by some drill manufacturers for a limited number of drill models, a new approach for rotary speed control, that can be applied in conjunction with a control approach for weight-on-bit, has been introduced and simulated. The simulation and subsequent field tests have proven the viability of the proposed control strategy for the design criteria of controlling vibration. It has the merit of reducing machine wear and tear while attempting to maintain rotary speed at the nominal desired rotary speed.

## 9.3 Industrial Relevance

The results of this work have been adopted by the Aquila Mining Systems Ltd. of Montreal who is presently offering an automatic drilling control system, as part of its product line.

Also, several rotary drill manufacturers have shown increasing interest in the work presented in this thesis. The presented control strategy may be adopted for their future drills, or equally serve as a basis for devising their own control strategies.

The empirical models of the drilling process and the details of building a simulator can be used by the drill manufacturers to construct their own on their computing facilities. This would enable them to test their current or future control strategies. Alternatively, they can use the simulator to test the functionality of each control system they implement on a new machine.

The analysis of drill string vibration and the excitation mechanisms encountered while drilling may also prove useful to the drill manufacturers, who can use such information to improve the structural design of their drills.

### 9.3.1 Merits of the Proposed Control Algorithm

The proposed control algorithm offers the following features:

1. Since the controller was successfully tested on two drills of different design and dynamics, then the tests showed that the controller is portable to different types of drills.

2. The control strategy is modular in the sense that it can be expanded to include as many feedback signals as necessary or desired.

3. Fast response time, as soon as one or more feedback signals exceed their preset limit, i.e. as soon as vibrations start building up, before they reach critical levels. The

controller reduces rotary speed until a satisfactory level of vibration is reached, without driving the drill to a full stop.

4. The controller automatically restores rotary speed to the level at which it was operating prior to the onset of excessive vibration.

5. The behaviour of the controller does not require a prior knowledge of geology.

6. The sensitivity of this control loop with respect to variations in feed pressure initiated by the drill operator is negligible. However, this does not necessarily mean that it would not interact in an undesirable manner with another feedback loop which varied feed pressure while controlling penetration per revolution.

In addition, the controller offers the following technical advantages:

1. It is simple to implement, easy to tune and valid for different machine types and sizes.

2. It can be enhanced, in future revisions, by building additional levels of complexity, without modifying its current structure, such as adding supervisory loops, adaptive control and self tuning algorithms.

## 9.4 Recommendations for Future Work

The data acquired during field testing provided a valuable analysis of drilling performance in a limestone quarry and development of empirical models of the drilling process. However, the results were based upon a particular set of controlled field conditions, namely the drill rig, the bit type and characterized rock unit.

Future work for expanding the database would focus on further field testing and analysis of the relationships between other types of rocks and bits. Also, the drilling variables could be correlated to the actual physical wear of the bit in terms of changes to insert shape/size, bearings and cone shell condition. The structural vibration of the drill rig and the drill string could be modeled as well. These additional results would be integrated into the drilling simulator.

Further testing of the controller on different drill rigs, as well as different ground environments should be undertaken. The aging of the drill and its effect on the vibration thresholds upon which the controller reacts will have to be further investigated.

The synthesis of the use of "optimal" control strategies for feed pressure and rotary speed control with respect to drilling economics can also be investigated.

# References

**[Aboujaoude 1991]** Aboujaoude. C. E.: "Modeling, Simulation and Control of Rotary Blasthole Drills", Masters Thesis, Department of Electrical Engineering, McGill University, Dec. 1991

**[Allen 1987]** Allen, M. B., "BHA Lateral Vibrations: Case Studies and Evaluation of Important Parameters" SPE/IADC 16110 paper presented at the Drilling Conference, New Orleans, March 15-18 1987

**[Astrom 1984]** Astrom, K.J.: *Computer Controlled Systems* Prentice Hall 1984

**[Bailey 1960]** Bailey, J.J., Finnie I.: " An Analytical Study of Drill-String Vibration". *Journal of Engineering for Industry,* Trans. ASME, Vol 82, Series B, No.2, May 1960

**[Beardsley 1991]** Beardsley, F. Personal communication.

**[Besaisow 1986]** Besaisow, A.A., Payne, M.L.: "A study of Excitation Mechanisms and Resonance Inducing BHA Vibrations". *Proc. SPE* , Paper No. 15560, New Orleans, Oct. 1986

**[Bradley 1975]** Bradley, W. B., "Factors Affecting the Control of Borehole Angle in Straight and Directional Wells" *Journal of Petroleum technology,* June 1975, p. 679

**[Clausing 1959]** Clausing, D. P.: "Comparison of Griffith's Theory with Mohr's failure criteria", Paper presented at Third Symp. on Rock Mech., Colorado School of Mines (1959).

**[Currier 1972]** Currier, R. G.: "Status Report on Automated Drills", Presented at the O.P.M.A., Electrical Division, Annual Meeting. June 1972.

**[Cheatham 1981]** Cheatham, J. B., Ho, C. Y. : " A Theoretical Model for Directional Drilling Tendency of a Drill Bit in Anisotropic Rock " SPE unsolicited paper 10642, Sept. 1981.

**[Dareing 1968]** Dareing, D. W., Livesay, B.,J.: "Longitudinal and Angular Drill String Vibrations With Damping". *Journal of Engineering for Industry*, Trans. ASME. Vol. 90, November 1968, pp. 671-679

**[Dareing 1983]** Dareing, D. W., Livesay, B.,J.: " Guidelines for controlling drill string vibrations", ASME paper presented at sixth Annual Energy-Sources Technology Conference, Houston, Texas, February 1983

**[Deily 1968]** Deily, F. H., Dareing, D. W., Paff, G. F., Ortloff, J. E., and Lynn, R. D.: "Downhole Measurements of Drill-String Forces and Motions". *Journal of Engineering for Industry*, Trans. ASME. Vol. 90, Series B, No.2, May 1968, pp. 217-226

**[Draper 1981]** Draper, N., Smith, H.: " Applied Regression Analysis, second edition" Wiley Interscience 1981.

**[Doveton 1986]** Doveton, J., H.: *Log Analysis of Subsurface Geology*. Wiley Interscience 1986.

**[Eitelberg 1987]** Eitelberg, E. :"A Regulating and Tracking PI(D) Controller". *Int. Jour. Control*. (1987 vol. 45 pp.91-95)

**[Fairhurst 1956]** Fairhurst, C. and Lacabanne, W. D.: "Some Principles and Developments in Hard Rock Drilling Techniques", Paper presented at Annual Drill. and Blast. Symp., U. of Minnesota (1956)

**[Hartman 1959]** Hartman, H. L.:"Basic Studies of Percussion Drilling", *Min. Eng*. (1959) **11**, No.1.

**[Hodgins 1992]** Hodgins, B. L.: "Developments to Enhance the Productivity and Cost-Effectiveness of Large Rotary Blasthole Drills", Third Large Open Pit Mining Conference, Australia. Sept. 1992.

**[Houpis 1985]** Houpis, C. H., Lamont, G. B.: *Digital Control Systems, Theory, Hardware, Software*, McGraw Hill 1985

**[Huang 1968]** Huang, T., Dareing, D. W.: "Buckling and Lateral Vibration of Drill Pipe", *Journal of Engineering for Industry,* Trans. ASME. Vol. 90, November 1968, pp. 613-619

**[Ingersoll-Rand 93]** Aboujaoude, C. E., Daneshmend, L. D., Peck, J. P. : "Final Report: Vibration Analysis and Control of an Ingersoll-Rand DM45 Hydraulic Rotary Blasthole" , Submitted to the Ingersoll-Rand Co. February 10th 1993

**[James 1989]** James, M.L., Smith, G.M., Wolford J.C., Whaley P.W.: *Vibration of Mechanical and Structural Systems,* Harper and Row 1989

**[Jogi 1986]** Jogi, P. N., Burgess, T.M., and Bowling, J.P. "Three Dimensional Bottom-Hole Assembly Model Improves Directional Drilling" IADC/SPE 14768 paper presented in Dallas, Tx, Feb 9-12, 1986

**[Kuo 1991]** Kuo, B.C. *Automatic Control Systems*, sixth edition, Prentice Hall, 1991. Chapter 9.

**[Li 1974]** Li, T.M.: "Rotary Drilling With Automated Controls - new force in open-pit blast hole production". *Coal Age Operating Handbook of Coal Surface Mining and Reclamation*, vol. 2 (1974) Chironis, N,P, ed., McGraw-Hill Inc., New York, pp. 212-219.

**[Ljung 1987]** Ljung, L.: *System Identification: Theory for the user.* Prentice Hall 1987

**[Matlab]** Simulink User's Manual.

**[Maurer 1959]** Maurer, W. C.: "Impact Crater Formation in Sandstone and Granite, " MS Thesis T-887, Colorado School of Mines (1959)

**[Maurer 1962]** Maurer, W.C.: "The Perfect Cleaning Theory of Rotary Drilling. *Jour. Pet. Tech.*, (November 1962, p.1270-1274).

**[Millheim 1981]** Millheim, K. K., Apostal, M. C. : " The Effects of Bottom-Hole Assembly Dynamics on the Trajectory of a Bit. " *Jour. Pet. Tech.* (December 1981, p.2323)

**[Oppenheim 1989]** Oppenheim, A. V., Schafer, R. W.: *Discrete-Time Signal Processing* Prentice-Hall 1989

**[Palm 1983]** Palm, J.W. *Modeling, Analysis and Control of Dynamic Systems* . John Willey & sons 1983.

**[Paslay 1963]** Paslay, P. R., Bogy, D.B.: "Drill String Vibrations Due to Intermittent Contact of Bit Teeth". *Journal of Engineering for Industry,* Trans. ASME. Vol 85, Series B, No.2, May 1963, pp. 187-194

**[Paslay 1964]** Paslay, P. R., "Onset on Dynamic Instability of Drillstrings Under Lateral Constraints," Transactions of the ASME, May 1964

**[Schivley 1987]** Schivley, G. P. : " Focus on Rotary Drill Rigs", *Compressed Air Magazine*, June 1987

**[Smith 1994]** Smith International Corp. 1994 Sales Brochure.

**[Simon 1959]** Simon, R.: "Discussion of a Laboratory Study of Rock Breakage by Rotary Drilling". *Jour. Pet. Tech.* (Dec. 1959) 78A-80

**[Tamrock 1989]** Naapuri, J. Surface Drilling and Bblasting, Tamrock Company, 1987

**[Vandiver 1989]** Vandiver, J.K., Nicholson, J. W., Shyu, R. J.: "Case Studies of the Bending Vibration and Whirling Motion of Drill Collars.", IADC/SPE 18652, paper presented in New Orleans, Louisiana, Feb. 28 - Mar. 3, 1989

**[Watton 1991]** Watton, J.: *Fluid Power Systems* , Chapter 4, Prentice Hall 1989

**[Warren 1984]** Warren, T.M.: "Factors Affecting Torque for a Tricone Bit", *Jour. Pet. Tech.*, (Sept. 1984) p.1500-1508.

**[Williamson 1986]** Williamson, J. S. and Lubinski, A, "Predicting Bottom-Hole Assembly performance." IACD/SPE 14764 paper presented in Dallas, TX, Feb. 9-12, 1986

# APPENDIX A

## Charts of Drill String Natural Frequencies

**LATERAL VIBRATIONS (Fixed frame - Free bit)**

**1 Drill Pipe**

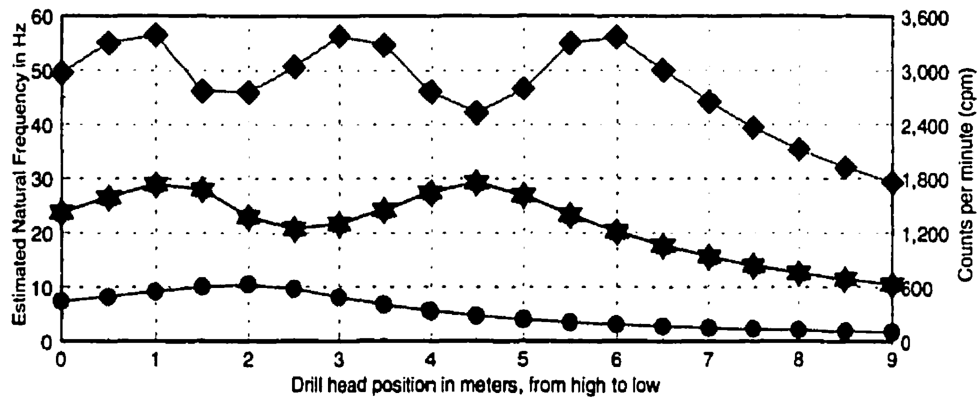


**2 Drill Pipes**

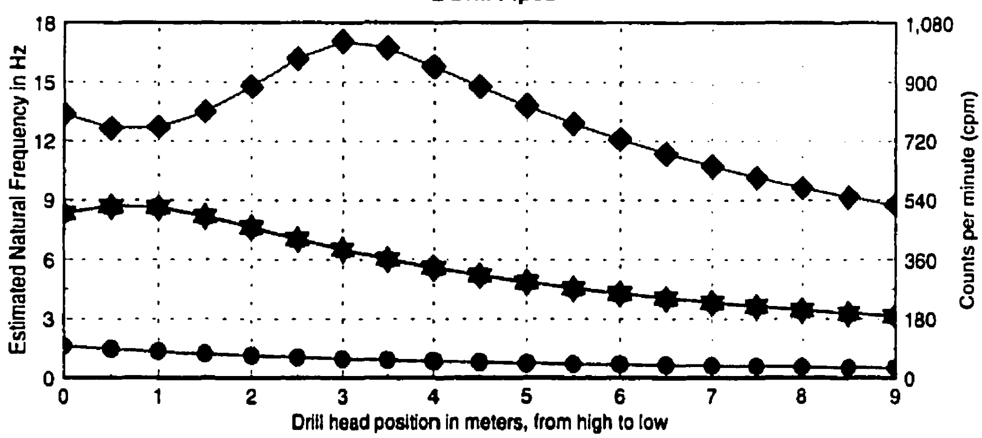


**3 Drill Pipes**

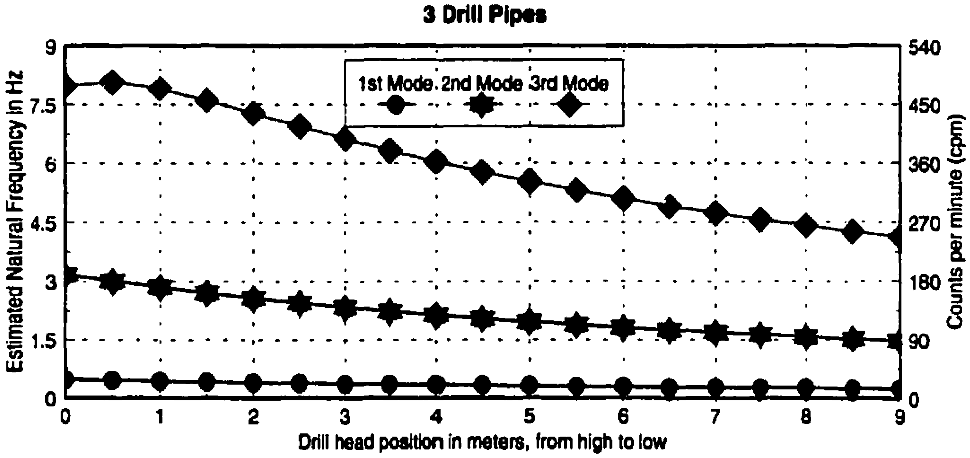

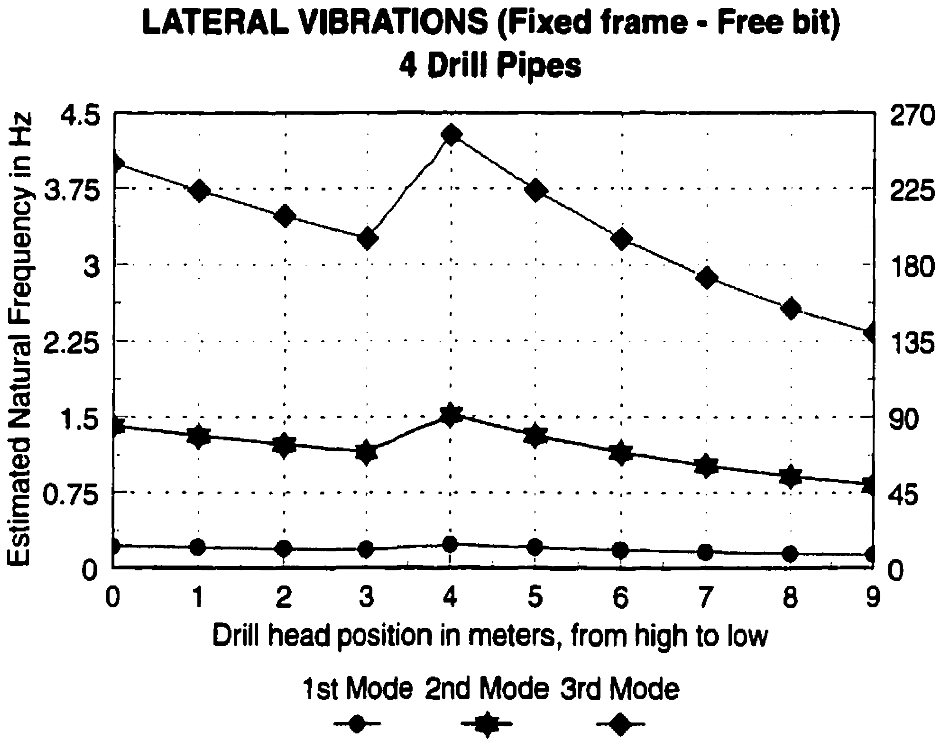
LATERAL VIBRATIONS (Fixed frame - Free bit)
4 Drill Pipes
Estimated Natural Frequency in Hz
4.5
3.75
3
2.25
1.5
0.75
0
270
225
180
135
90
45
0
Counts per minute (cpm)
0 1 2 3 4 5 6 7 8 9
Drill head position in meters, from high to low
1st Mode 2nd Mode 3rd Mode

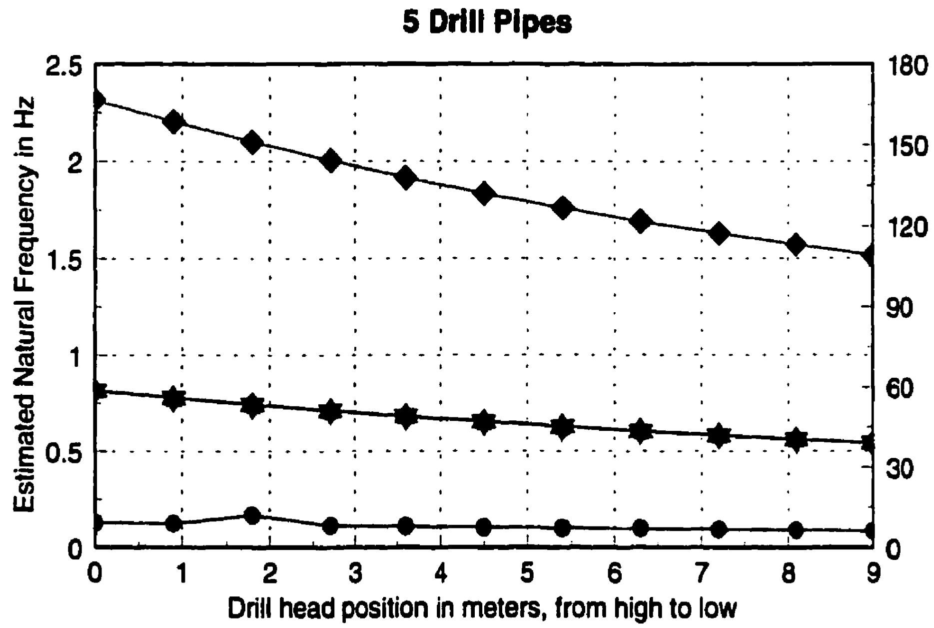
5 Drill Pipes
Estimated Natural Frequency in Hz
2.5
2
1.5
1
0.5
0
180
150
120
90
60
30
0
Counts per minute (cpm)
0 1 2 3 4 5 6 7 8 9
Drill head position in meters, from high to low

## LATERAL VIBRATIONS (Fixed frame - Pinned bit)

### 1 Drill Pipe

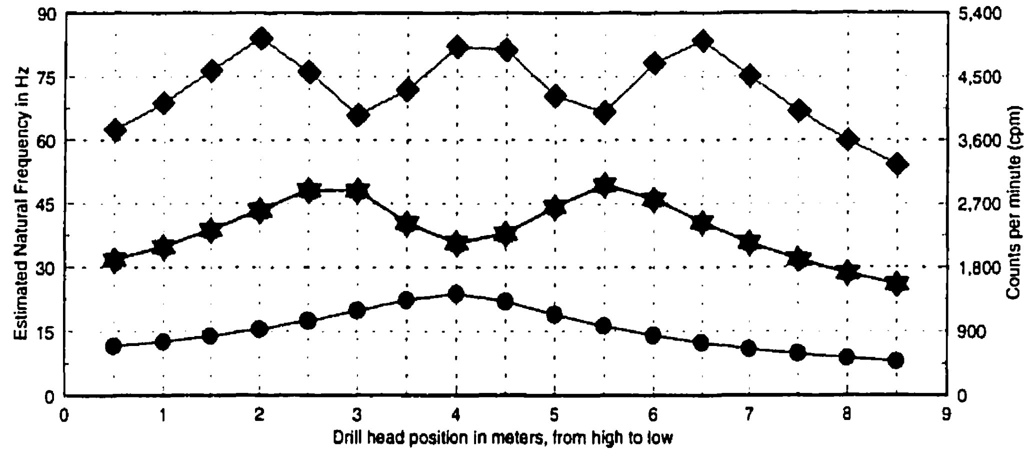


### 2 Drill Pipes

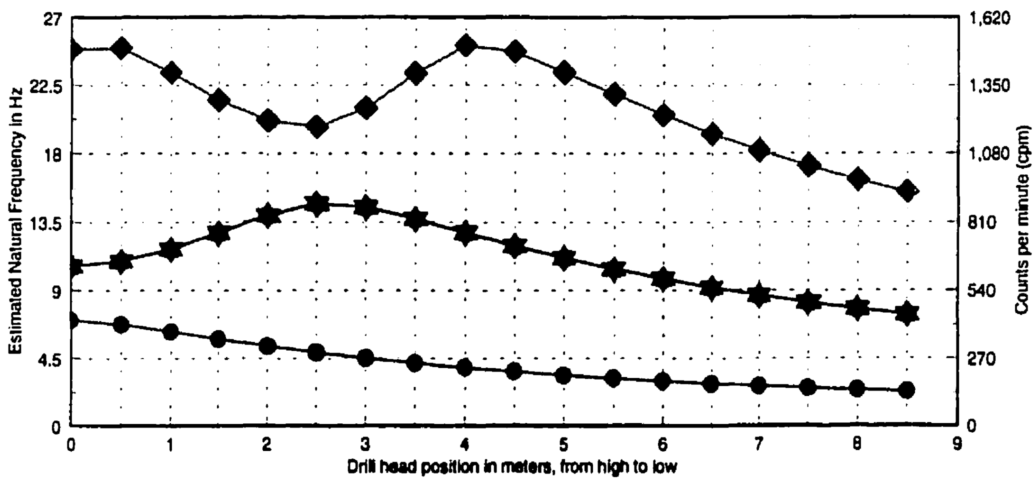


### 3 Drill Pipes

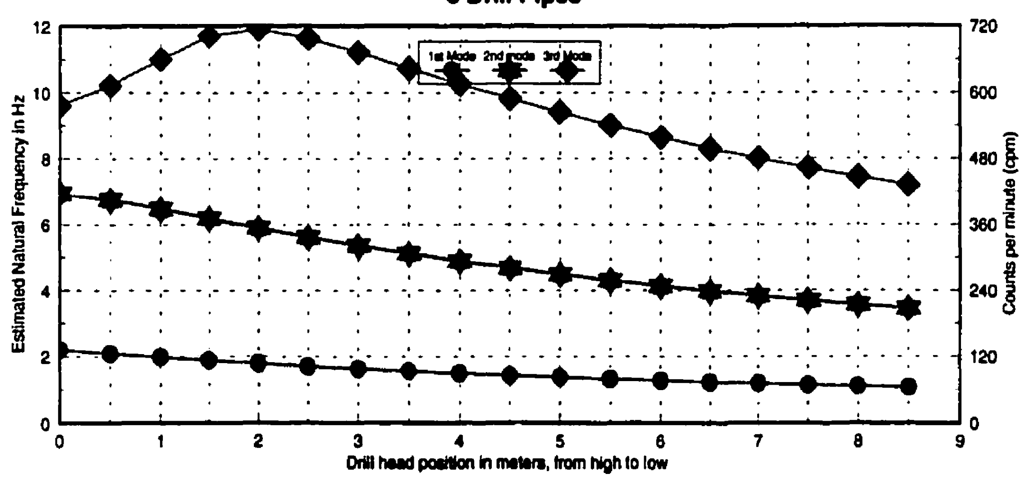

## LATERAL VIBRATIONS (Fixed frame - Pinned bit)

### 4 Drill Pipes

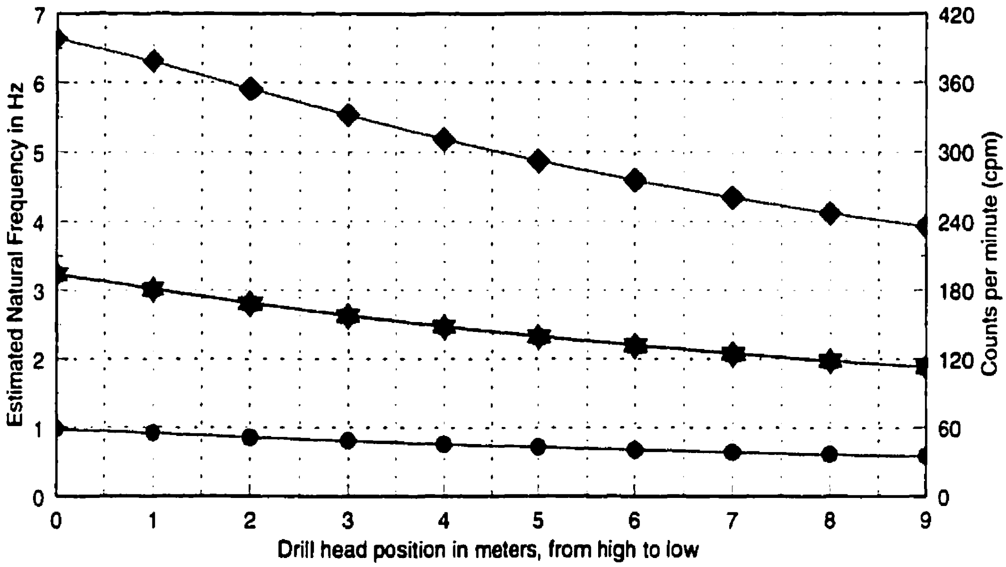


### 5 Drill Pipes

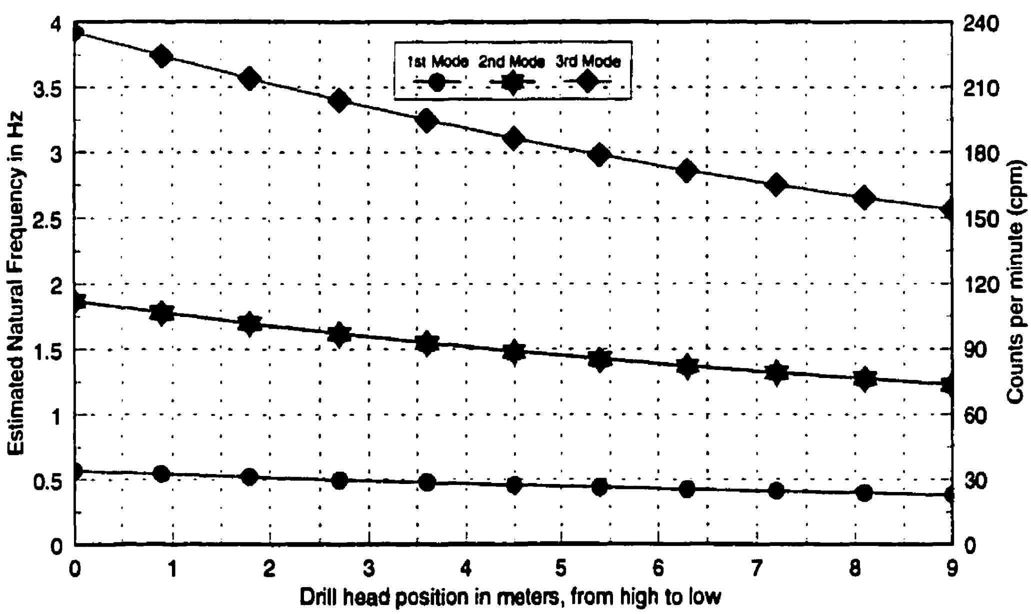

**LATERAL VIBRATIONS (Fixed frame - Fixed bit)**

**1 Drill Pipe**

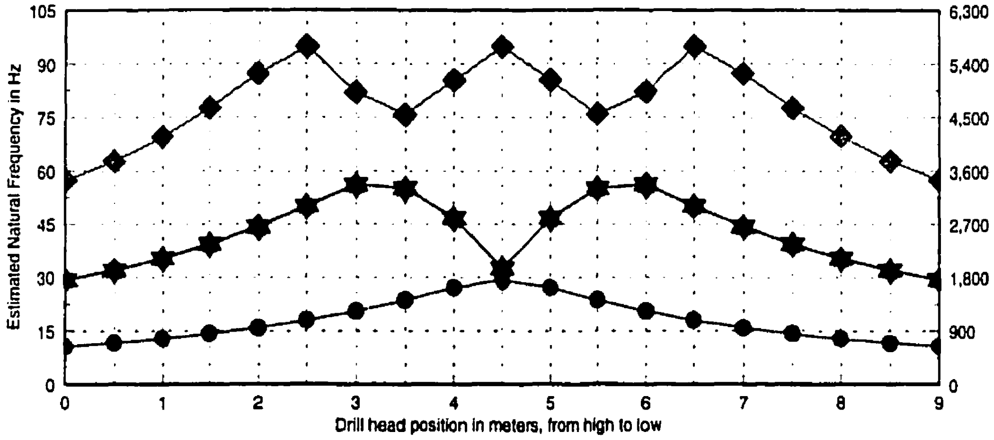


**2 Drill Pipes**

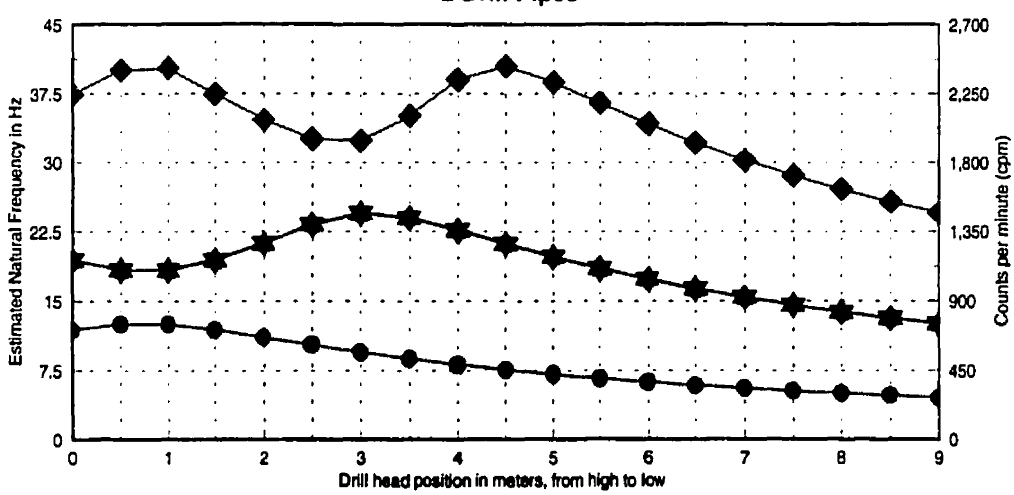


**3 Drill Pipes**

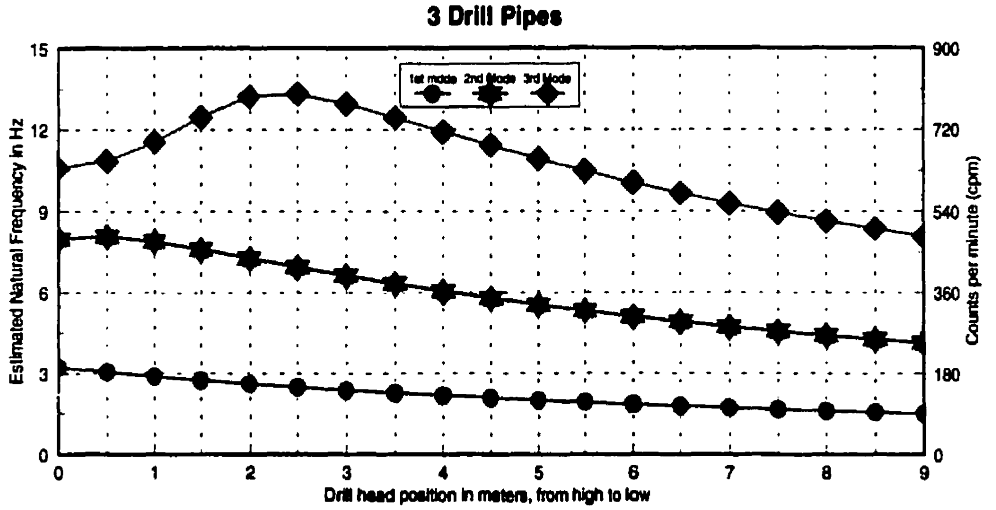

## LATERAL VIBRATIONS (Fixed frame - Fixed bit)

### 4 Drill Pipes

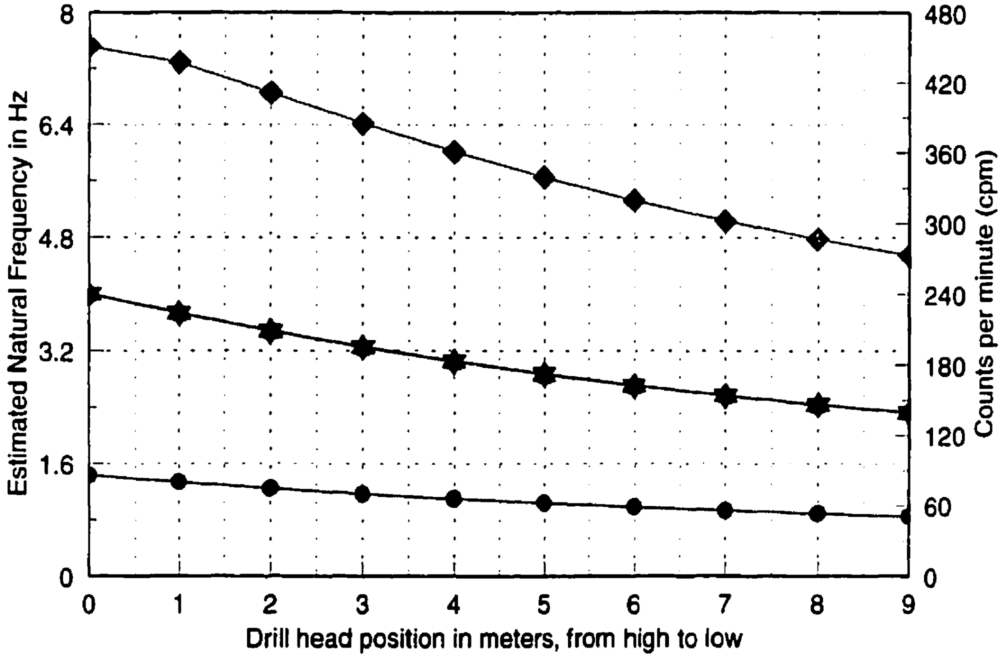


### 5 Drill Rods

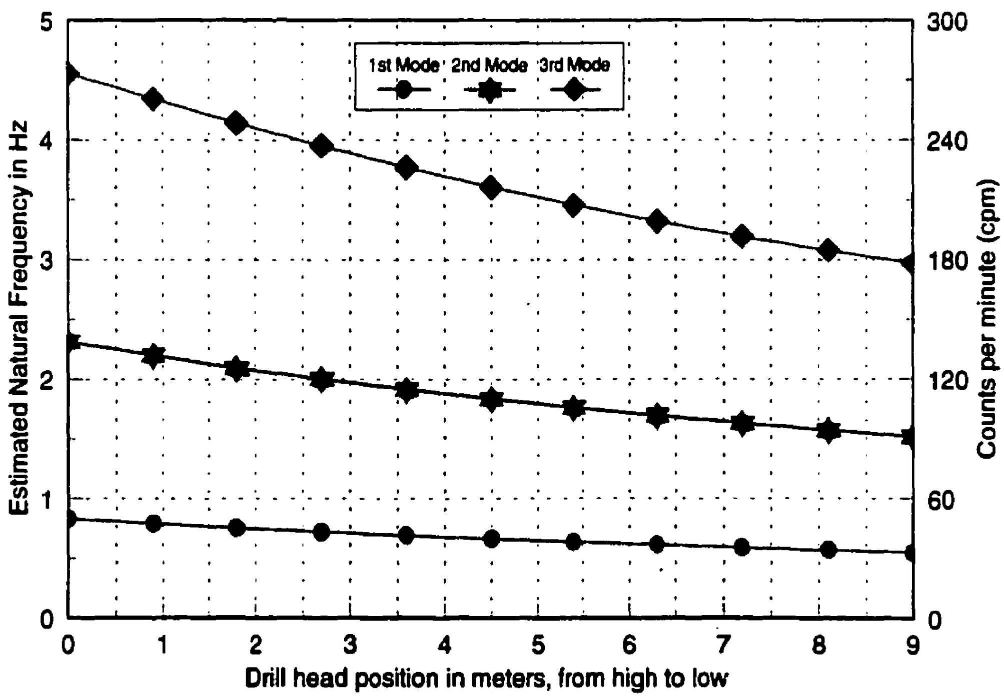

# APPENDIX B

## Strip Chart Records of Boreholes Drilled at the Lafarge Quarry

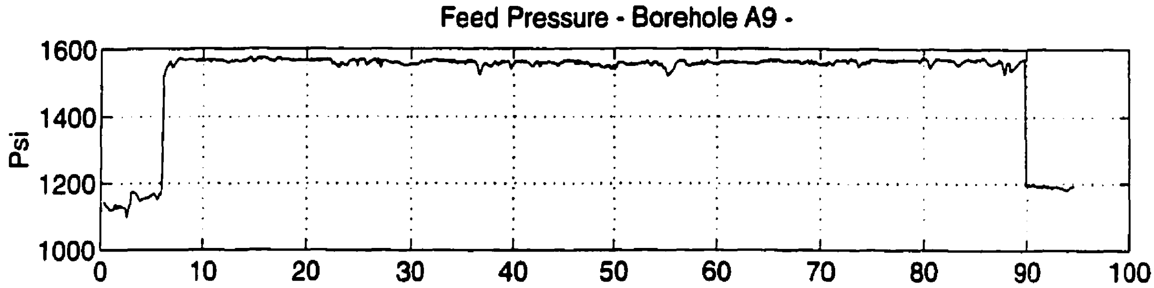
Feed Pressure - Borehole A9 -
Psi
1600
1400
1200
1000
0 10 20 30 40 50 60 70 80 90 100

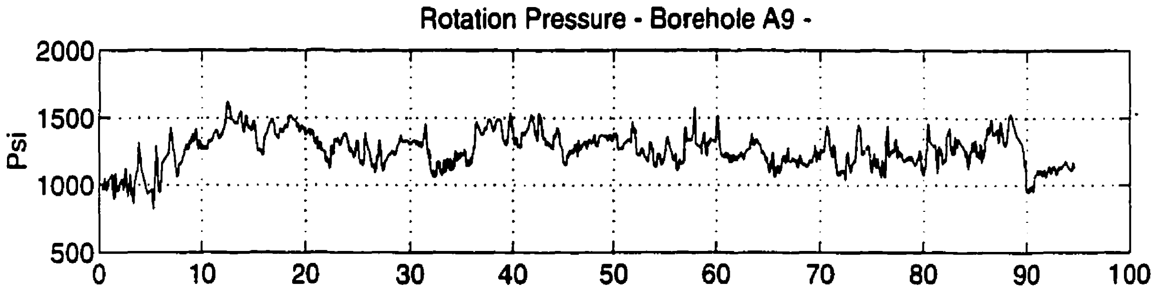
Rotation Pressure - Borehole A9 -
Psi
2000
1500
1000
500
0 10 20 30 40 50 60 70 80 90 100

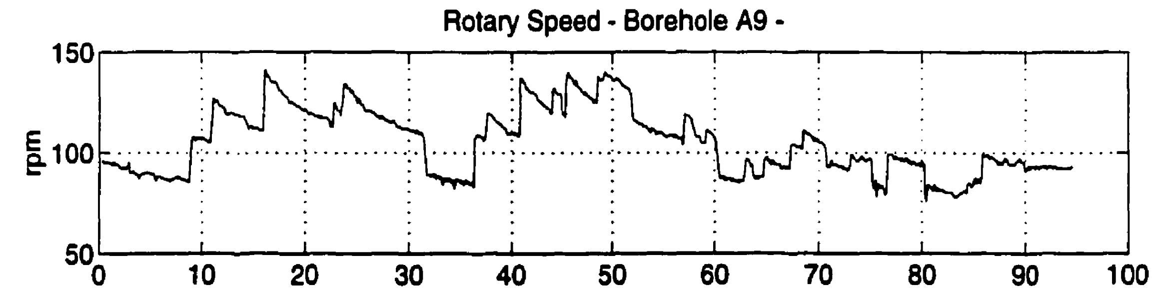
Rotary Speed - Borehole A9 -
rpm
150
100
50
0 10 20 30 40 50 60 70 80 90 100

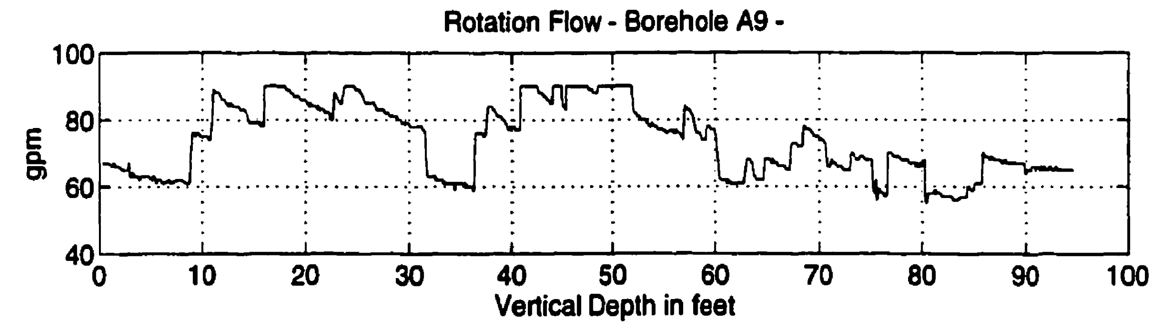
Rotation Flow - Borehole A9 -
gpm
100
80
60
40
0 10 20 30 40 50 60 70 80 90 100
Vertical Depth in feet

Head axial vibration - Borehole A9 -

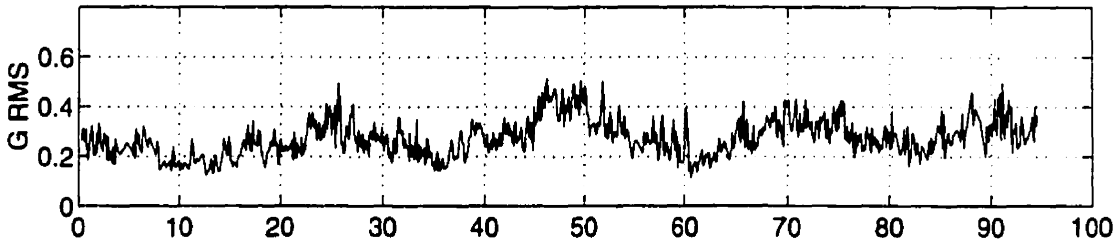


Head lateral vibration - Borehole A9 -

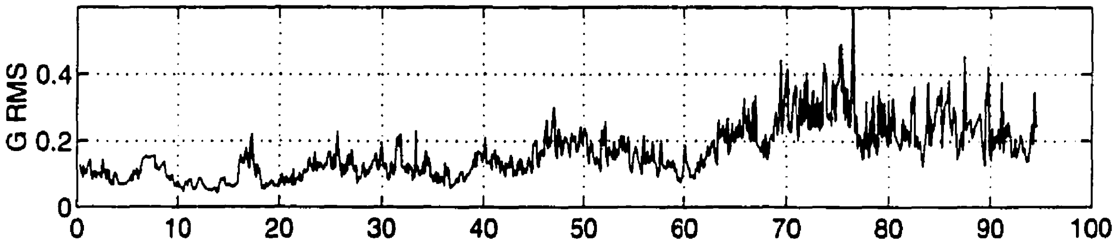


Head transversal vibration - Borehole A9 -

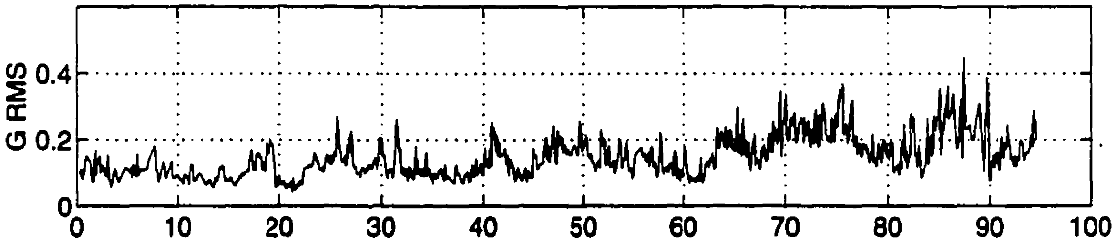


Tower Lateral vibration - Borehole A9 -

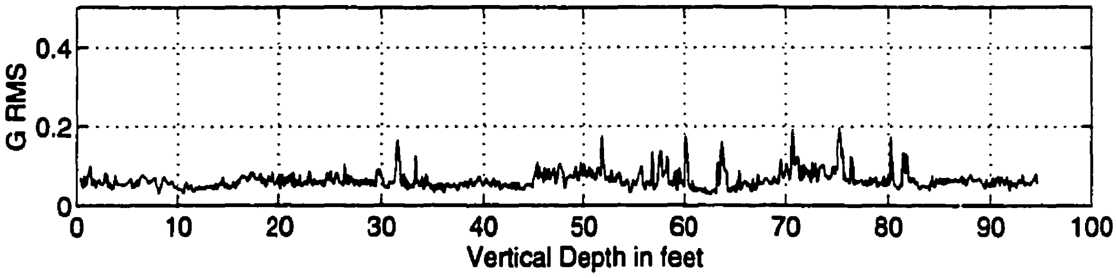

Penetration rate - Borehole A9 -

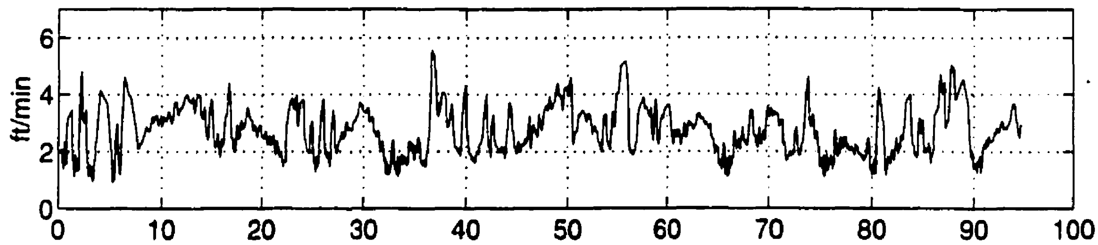


Penetration per Revolution - Borehole A9 -

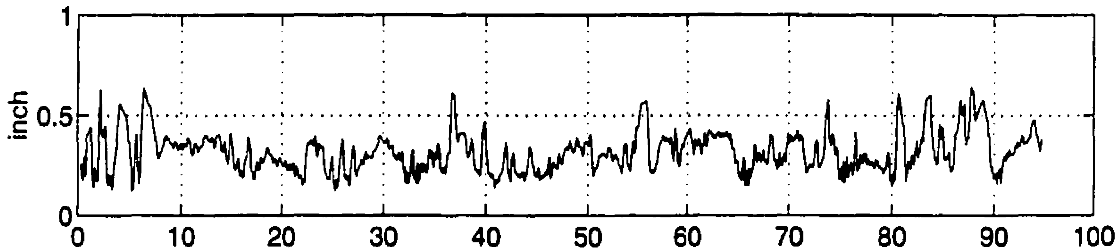


Bailing Air Pressure - Borehole A9 -

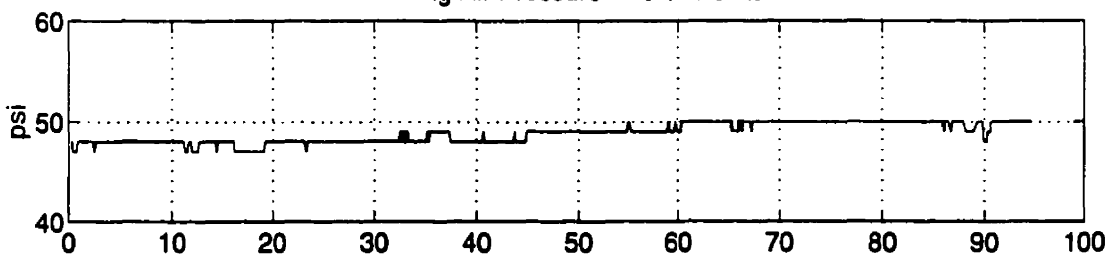


Rock Young Modulus - Borehole A9 -

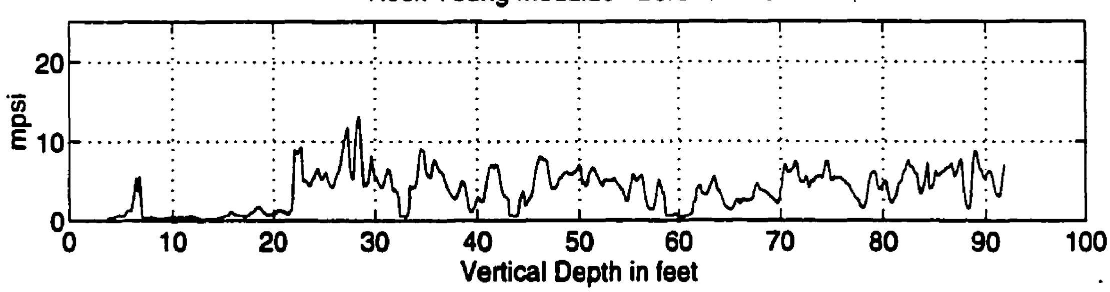

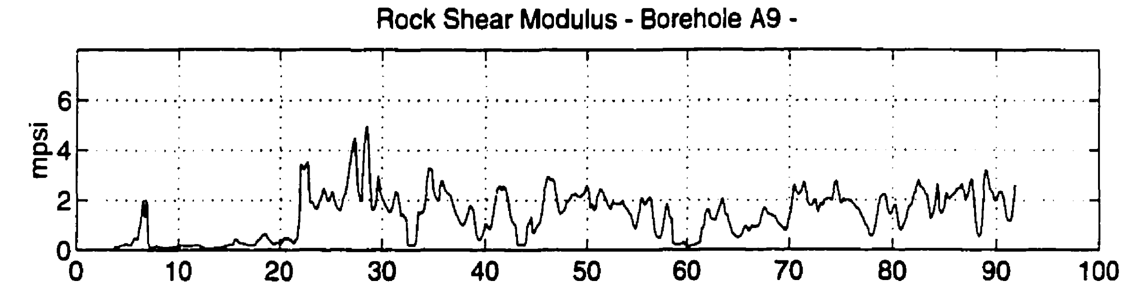
Rock Shear Modulus - Borehole A9 -
mpsi
0
2
4
6
0
10
20
30
40
50
60
70
80
90
100

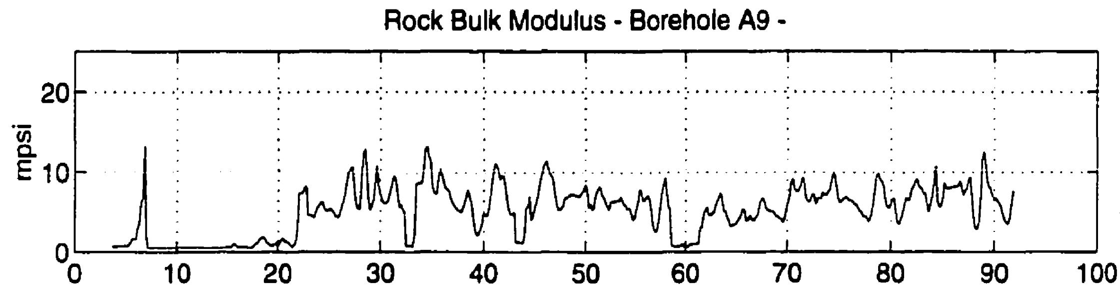
Rock Bulk Modulus - Borehole A9 -
mpsi
0
10
20
0
10
20
30
40
50
60
70
80
90
100

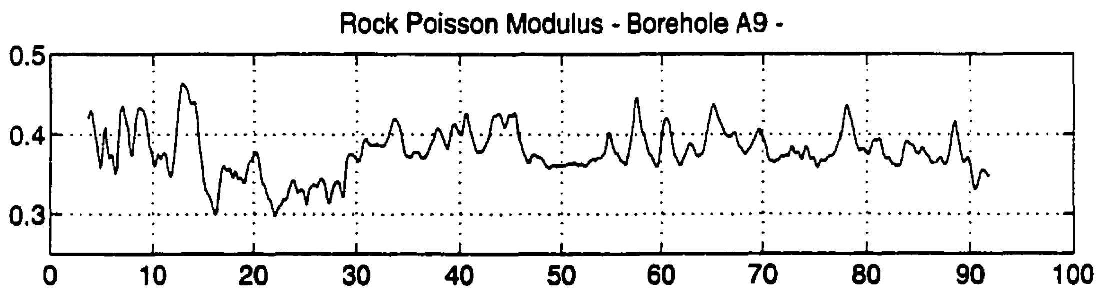
Rock Poisson Modulus - Borehole A9 -
0.3
0.4
0.5
0
10
20
30
40
50
60
70
80
90
100

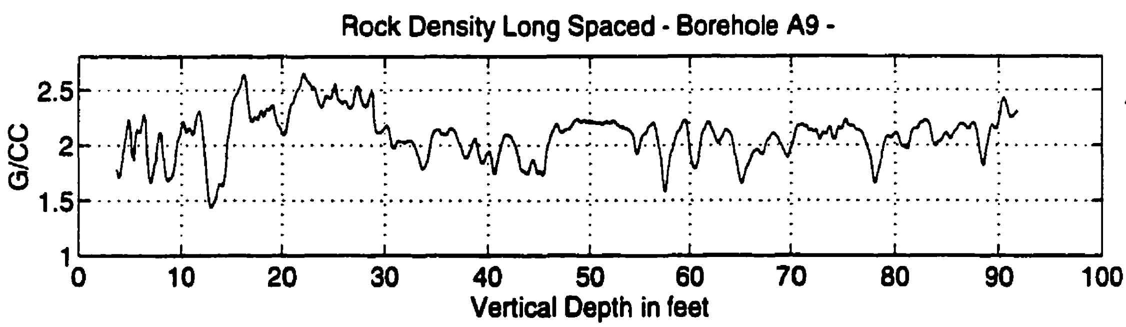
Rock Density Long Spaced - Borehole A9 -
G/CC
1
1.5
2
2.5
0
10
20
30
40
50
60
70
80
90
100
Vertical Depth in feet

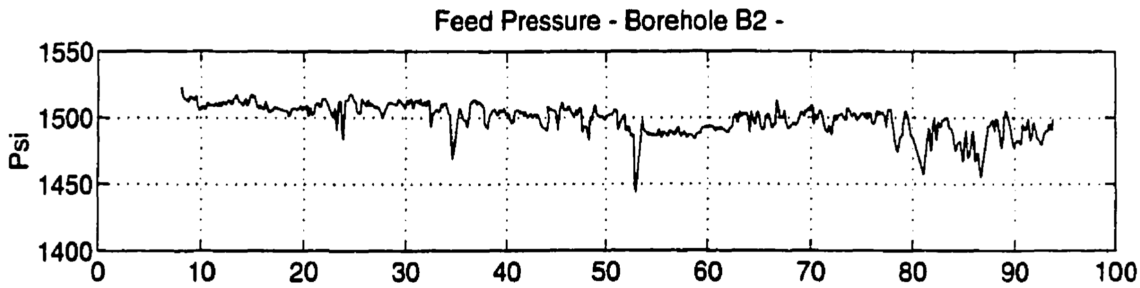
Feed Pressure - Borehole B2 -
Psi
1550
1500
1450
1400
0
10
20
30
40
50
60
70
80
90
100

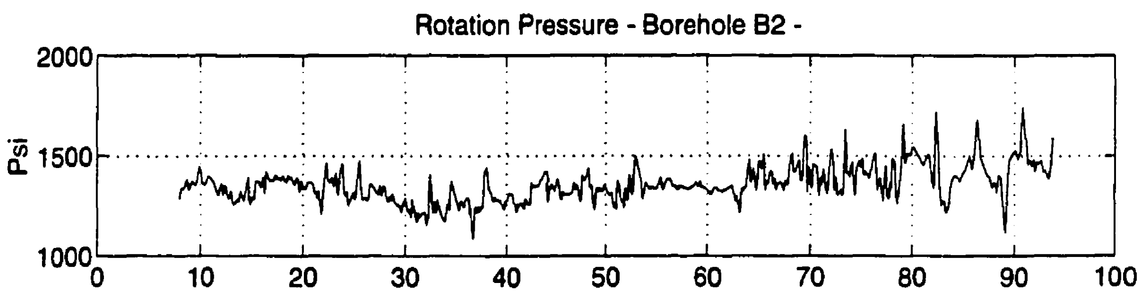
Rotation Pressure - Borehole B2 -
Psi
2000
1500
1000
0
10
20
30
40
50
60
70
80
90
100

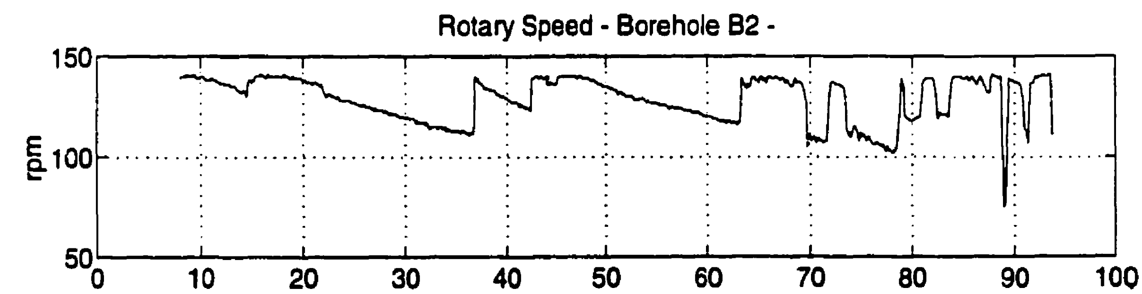
Rotary Speed - Borehole B2 -
rpm
150
100
50
0
10
20
30
40
50
60
70
80
90
100

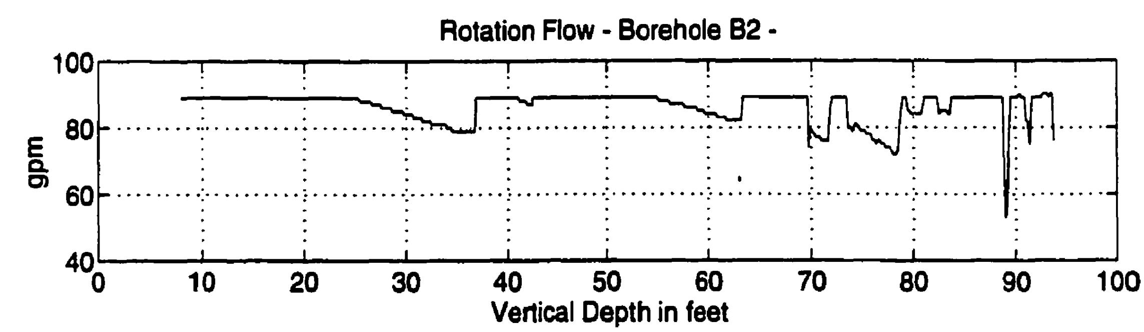
Rotation Flow - Borehole B2 -
gpm
100
80
60
40
0
10
20
30
40
50
60
70
80
90
100
Vertical Depth in feet

Head axial vibration - Borehole B2 -

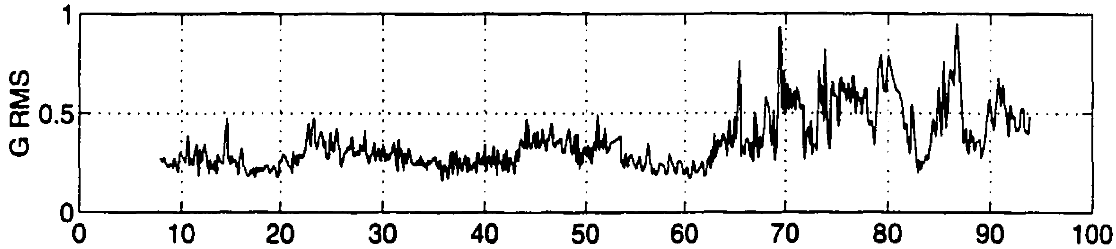


Head lateral vibration - Borehole B2 -

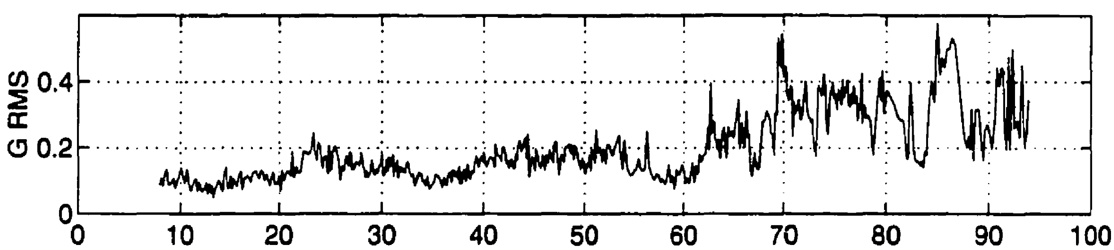


Head transversal vibration - Borehole B2 -

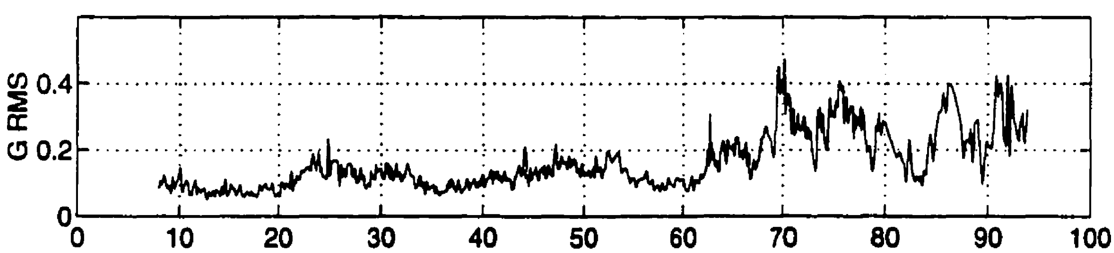


Tower Lateral vibration - Borehole B2 -

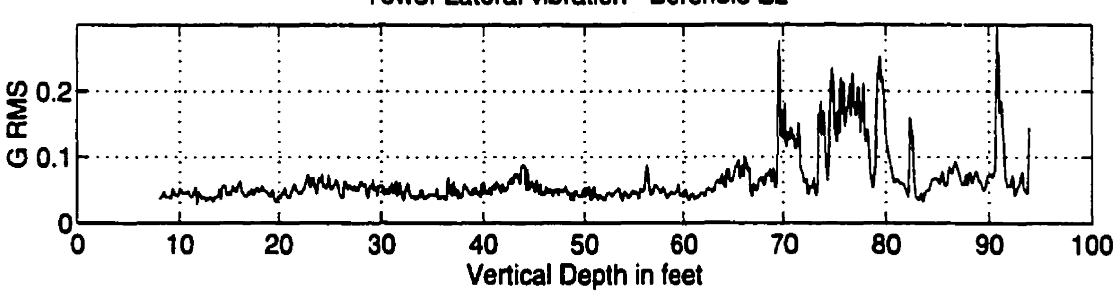

Penetration rate - Borehole B2 -

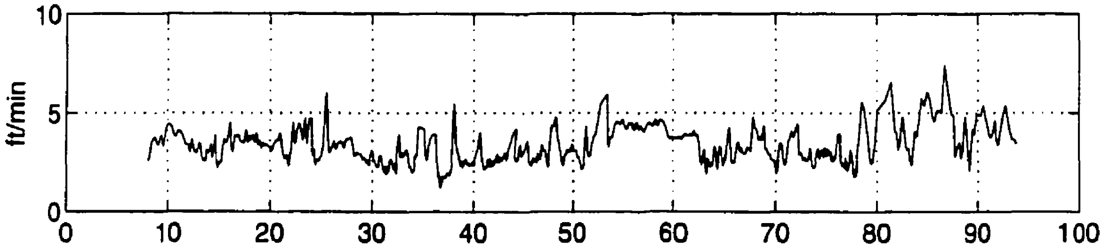


Penetration per Revolution - Borehole B2 -

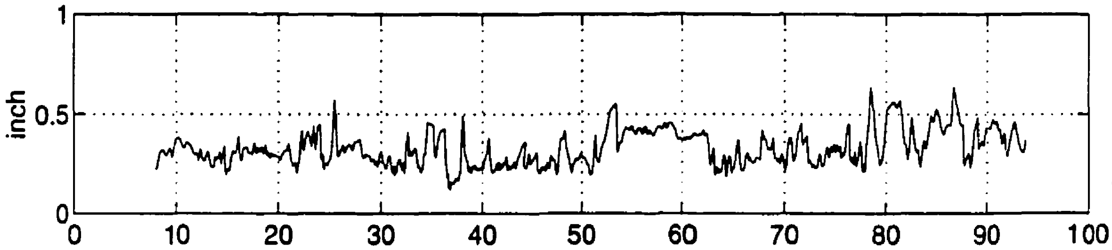


Bailing Air Pressure - Borehole B2 -

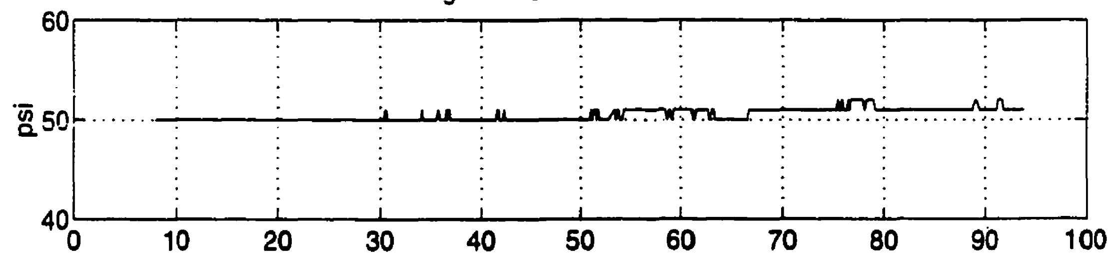


Rock Young Modulus - Borehole B2 -

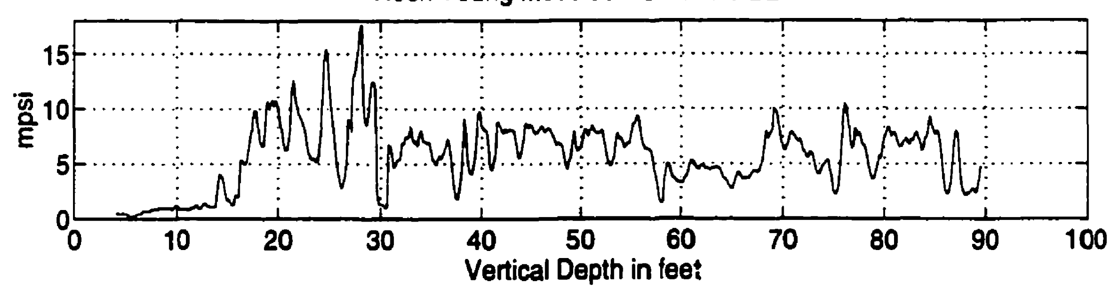

Rock Shear Modulus - Borehole B2 -

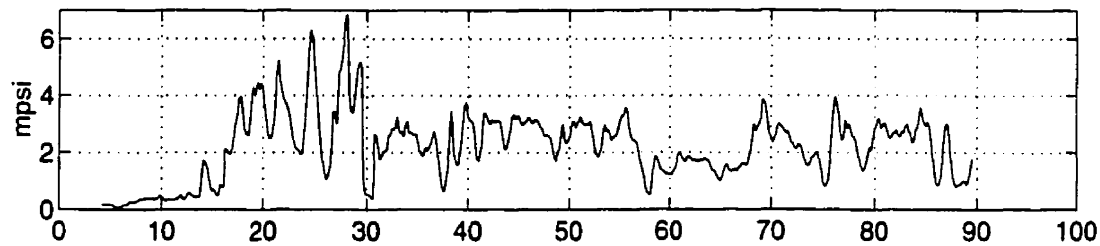


Rock Bulk Modulus - Borehole B2 -

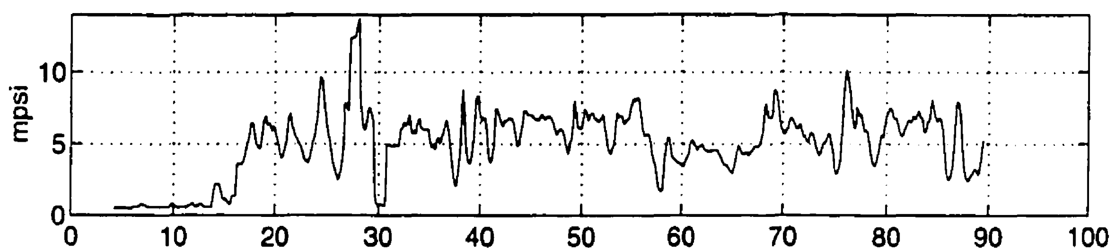


Rock Poisson Modulus - Borehole B2 -

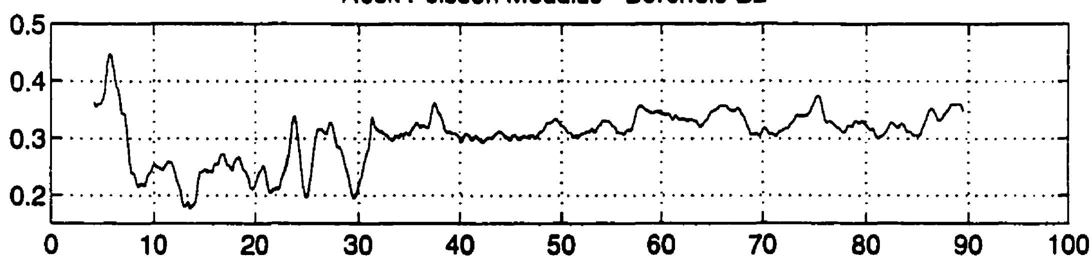


Rock Density Long Spaced - Borehole B2 -

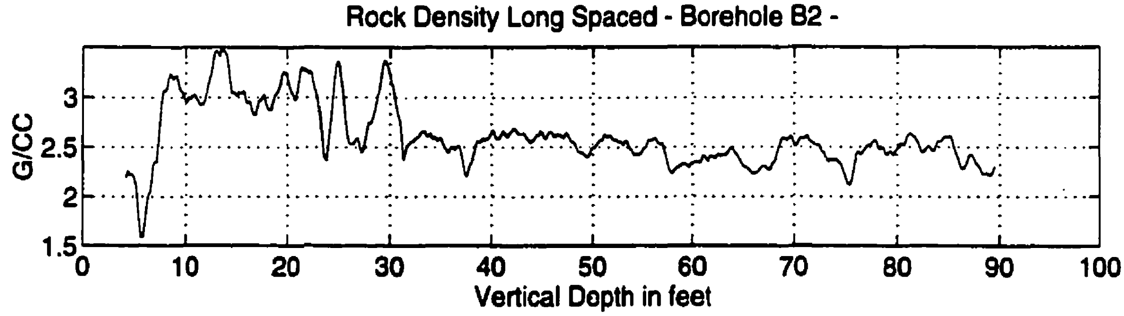

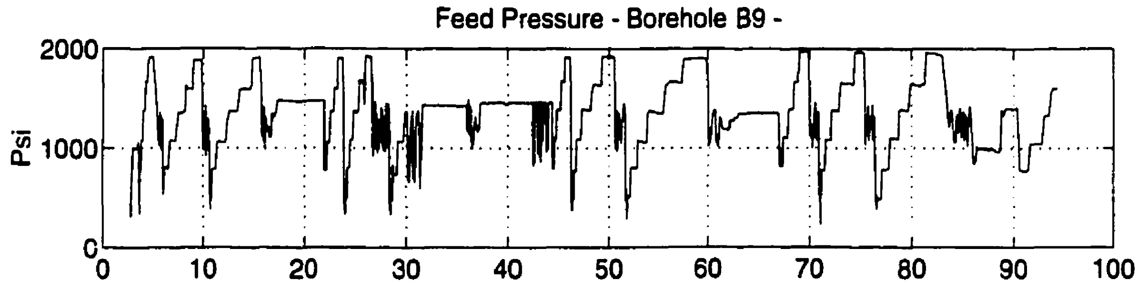
Feed Pressure - Borehole B9 -
Psi
2000
1000
0
0 10 20 30 40 50 60 70 80 90 100

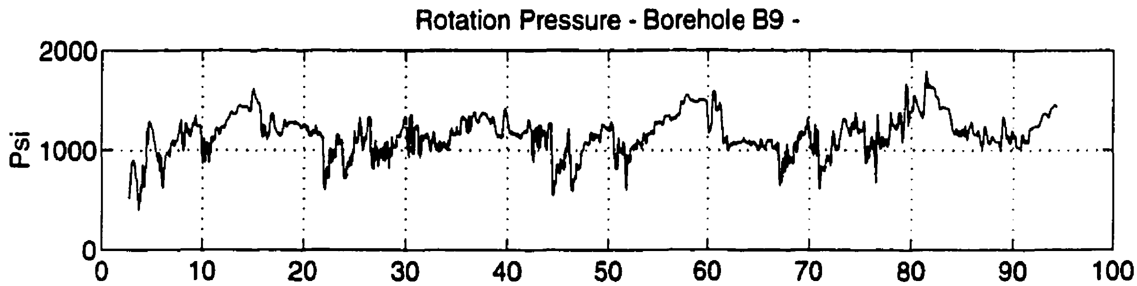
Rotation Pressure - Borehole B9 -
Psi
2000
1000
0
0 10 20 30 40 50 60 70 80 90 100

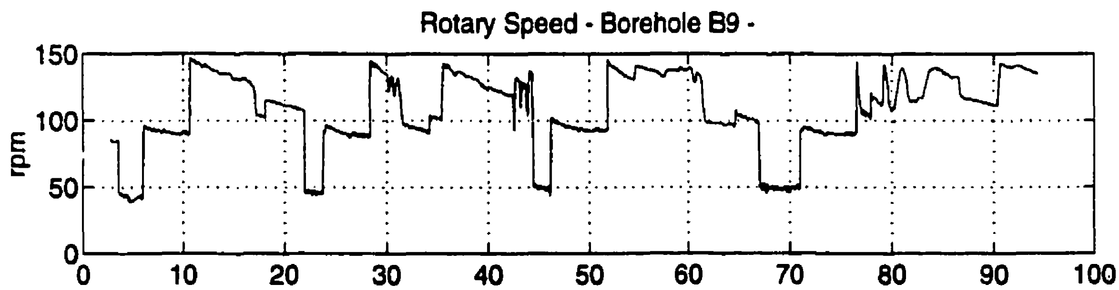
Rotary Speed - Borehole B9 -
rpm
150
100
50
0
0 10 20 30 40 50 60 70 80 90 100

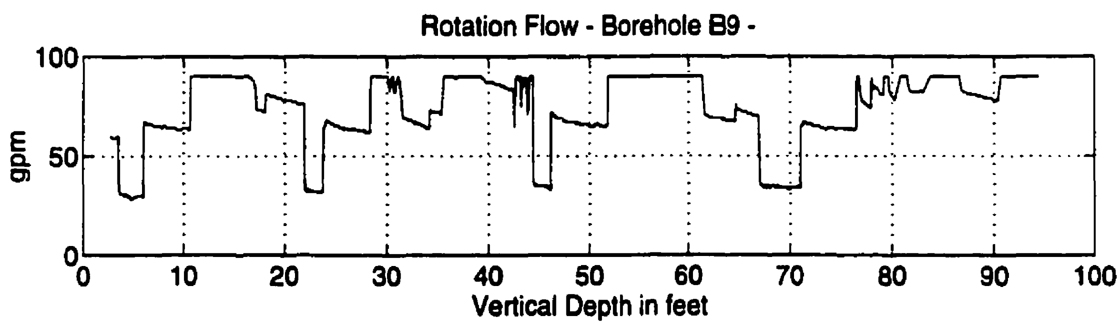
Rotation Flow - Borehole B9 -
gpm
100
50
0
0 10 20 30 40 50 60 70 80 90 100
Vertical Depth in feet

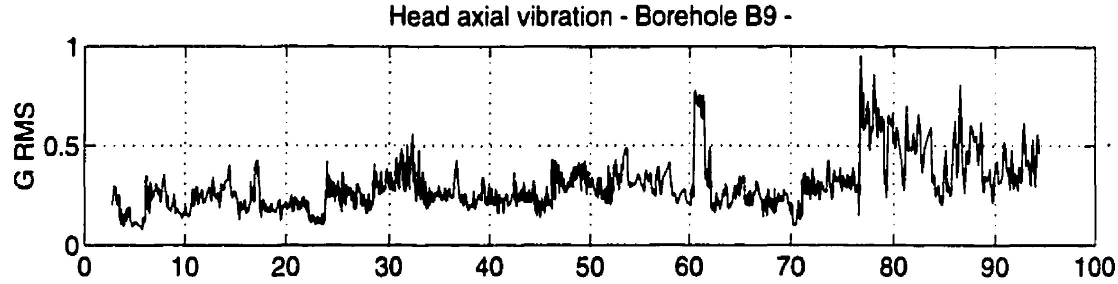
Head axial vibration - Borehole B9 -
G RMS
1
0.5
0
0 10 20 30 40 50 60 70 80 90 100

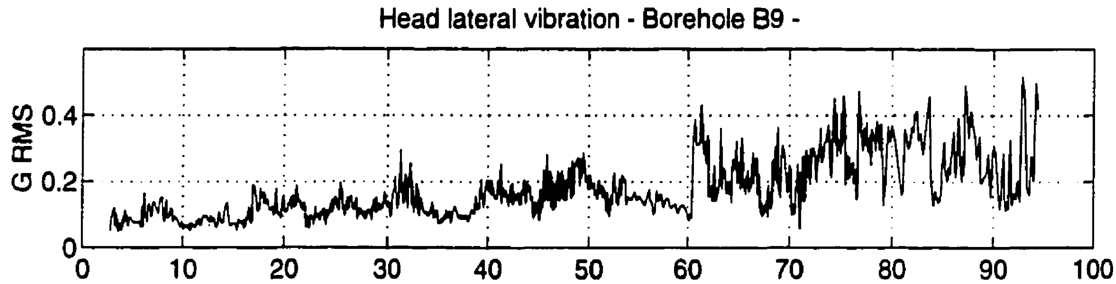
Head lateral vibration - Borehole B9 -
G RMS
0.4
0.2
0
0 10 20 30 40 50 60 70 80 90 100

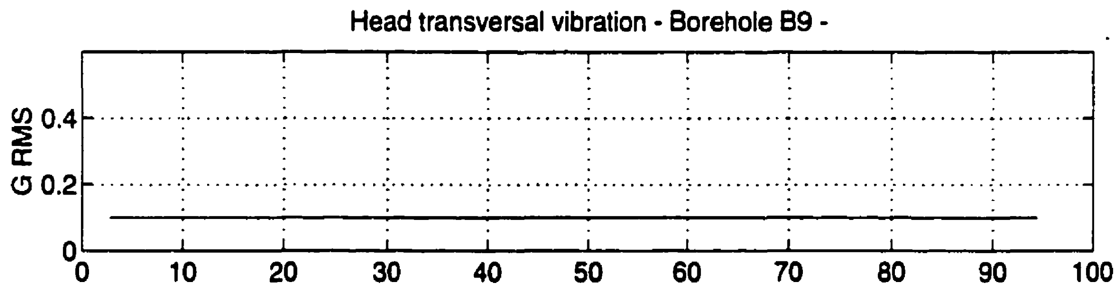
Head transversal vibration - Borehole B9 -
G RMS
0.4
0.2
0
0 10 20 30 40 50 60 70 80 90 100

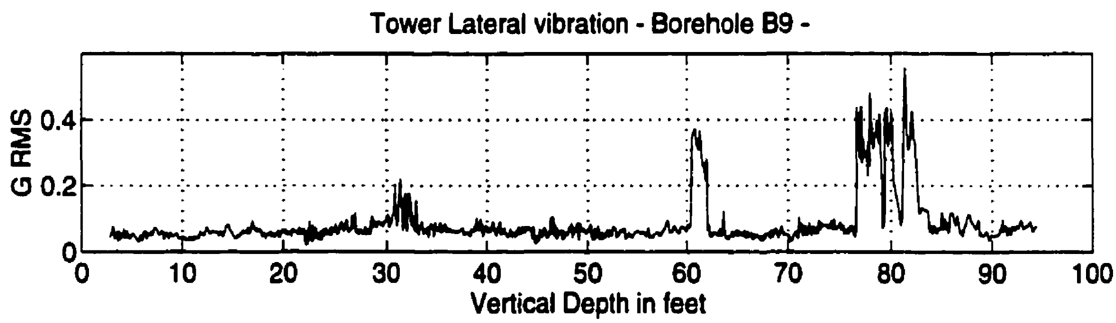
Tower Lateral vibration - Borehole B9 -
G RMS
0.4
0.2
0
0 10 20 30 40 50 60 70 80 90 100
Vertical Depth in feet

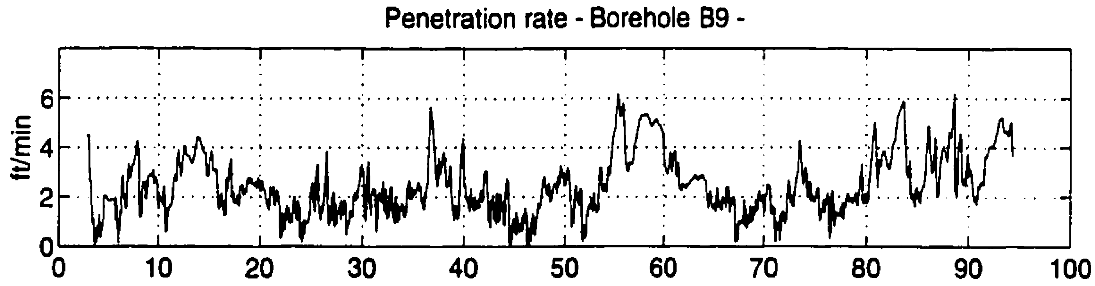
Penetration rate - Borehole B9 -
ft/min
0
2
4
6
0
10
20
30
40
50
60
70
80
90
100

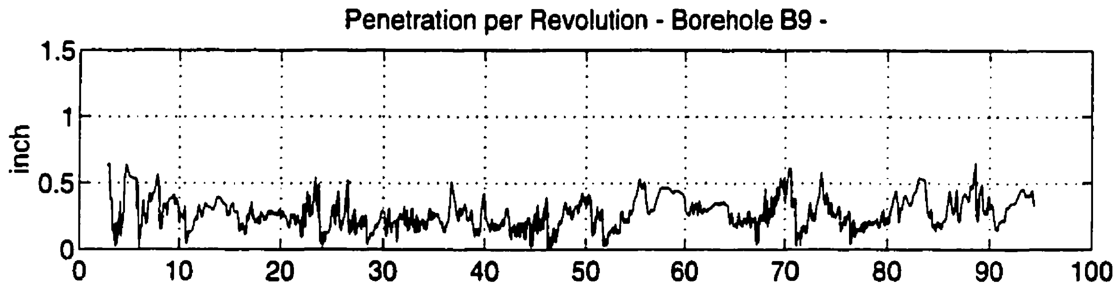
Penetration per Revolution - Borehole B9 -
inch
0
0.5
1
1.5
0
10
20
30
40
50
60
70
80
90
100

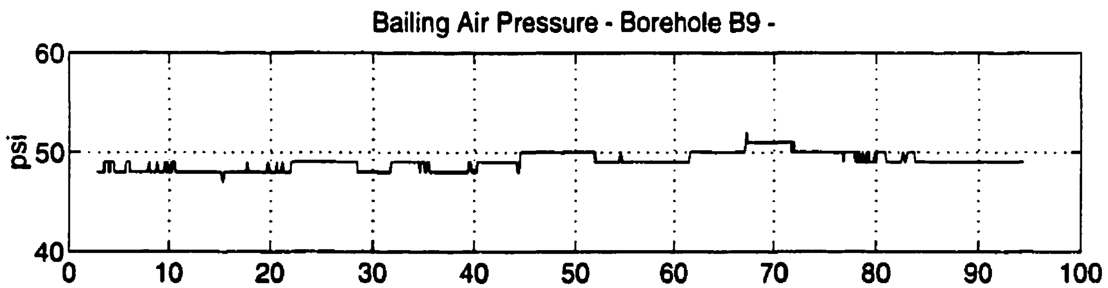
Bailing Air Pressure - Borehole B9 -
psi
40
50
60
0
10
20
30
40
50
60
70
80
90
100

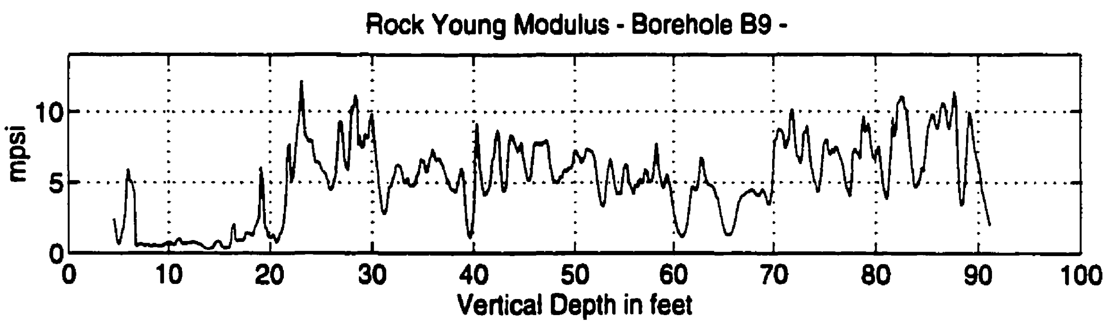
Rock Young Modulus - Borehole B9 -
mpsi
0
5
10
0
10
20
30
40
50
60
70
80
90
100
Vertical Depth in feet

Rock Shear Modulus - Borehole B9 -

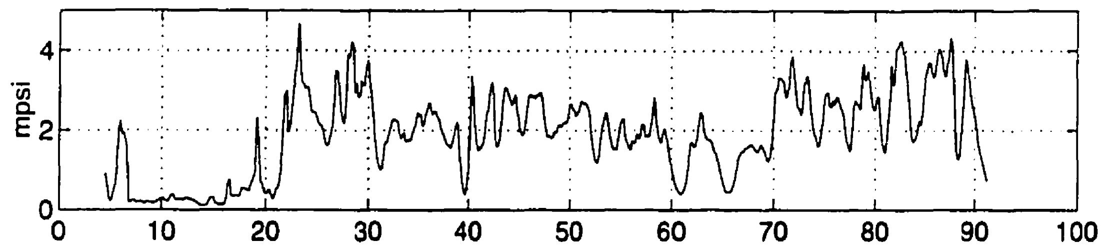


Rock Bulk Modulus - Borehole B9 -

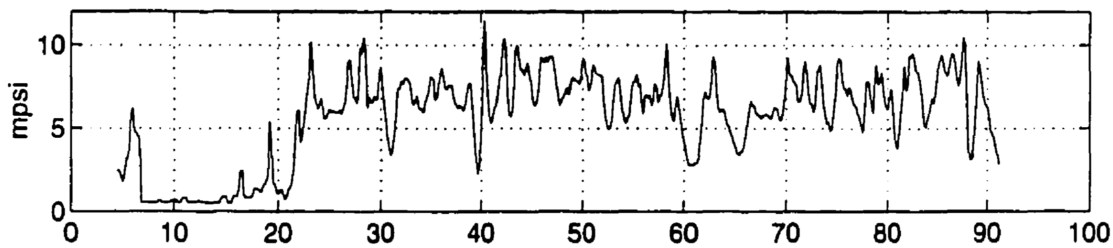


Rock Poisson Modulus - Borehole B9 -

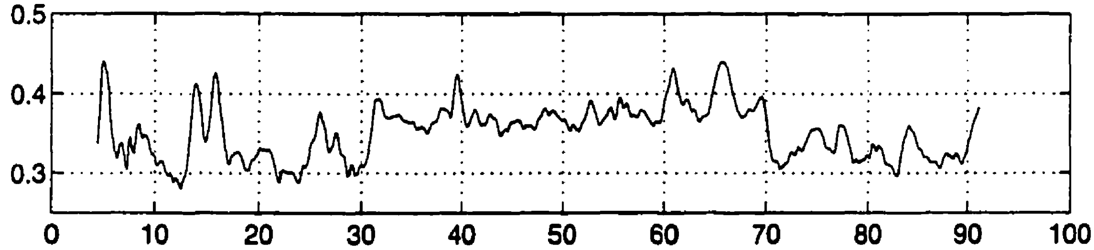


Rock Density Long Spaced - Borehole B9 -

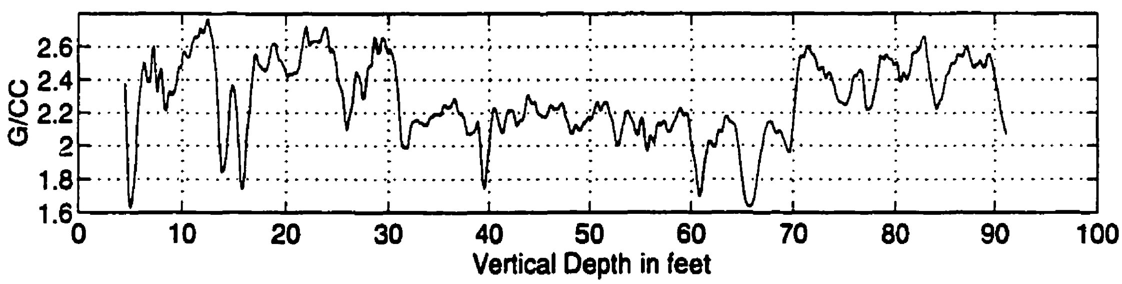

Feed Pressure - Borehole A1A -

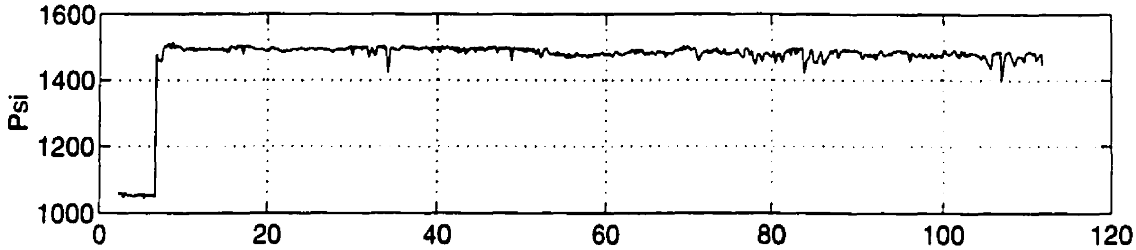


Rotation Pressure - Borehole A1A -

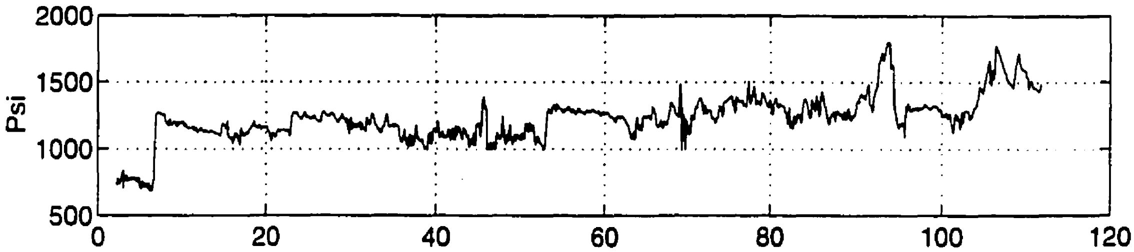


Rotary Speed - Borehole A1A -

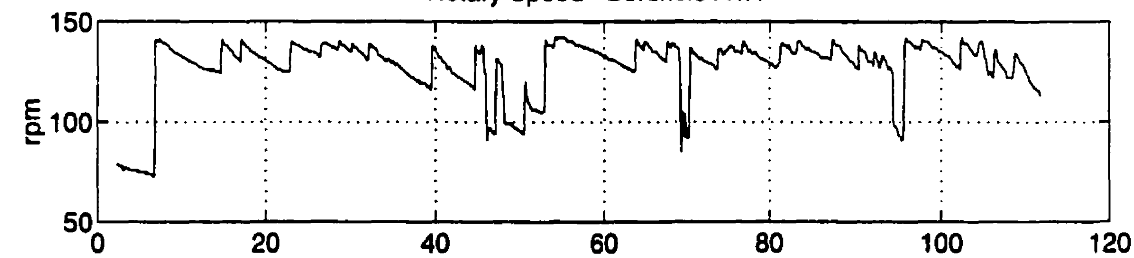


Rotation Flow - Borehole A1A -

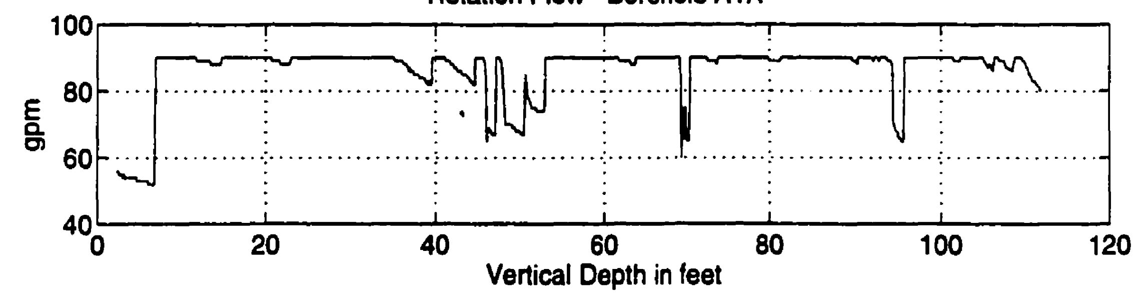

Head axial vibration - Borehole A1A -

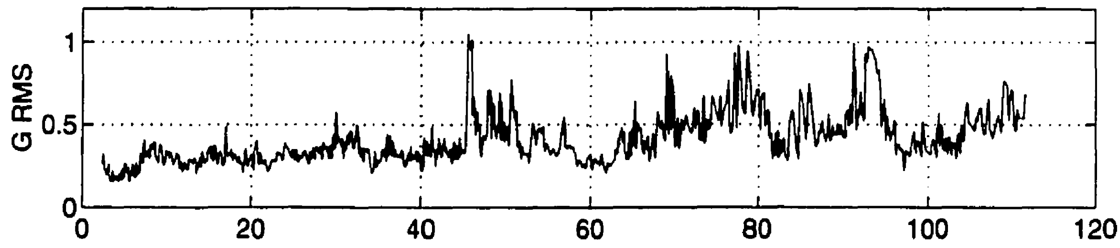


Head lateral vibration - Borehole A1A -

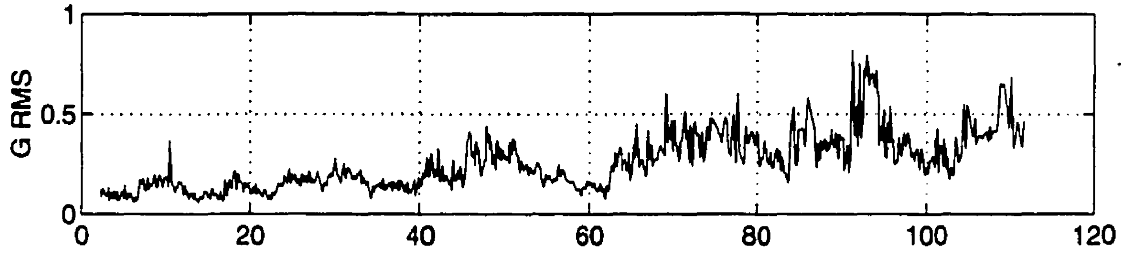


Head transversal vibration - Borehole A1A -

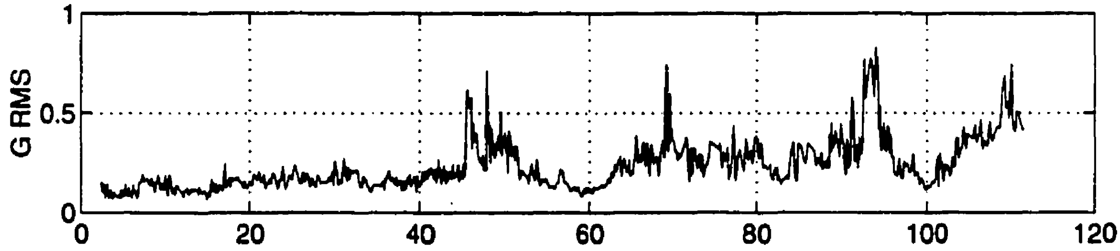


Tower Lateral vibration - Borehole A1A -

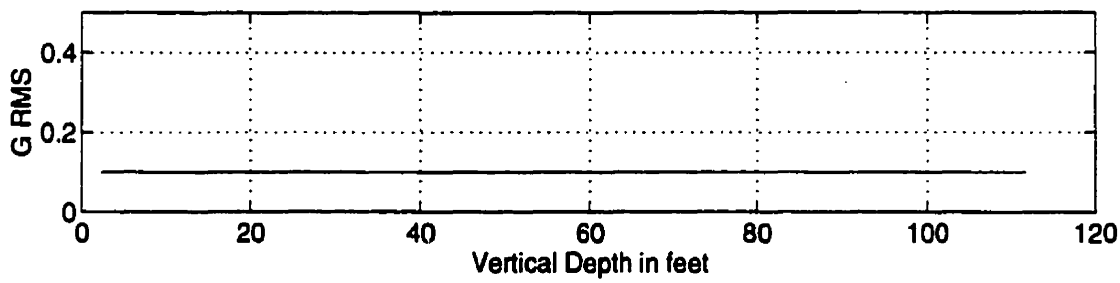

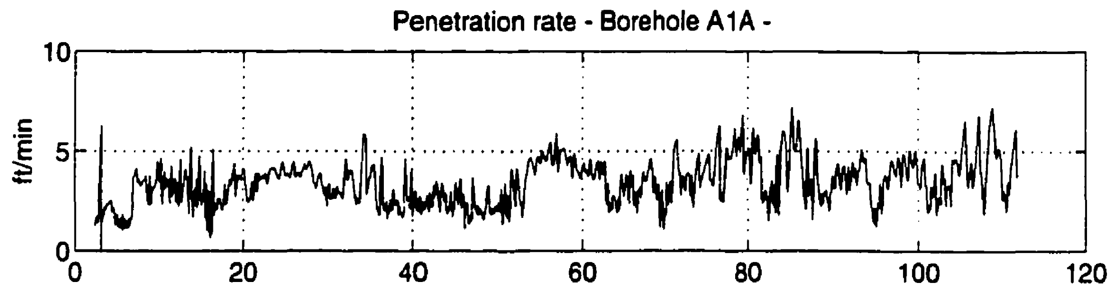
Penetration rate - Borehole A1A -
ft/min
10
5
0
0
20
40
60
80
100
120

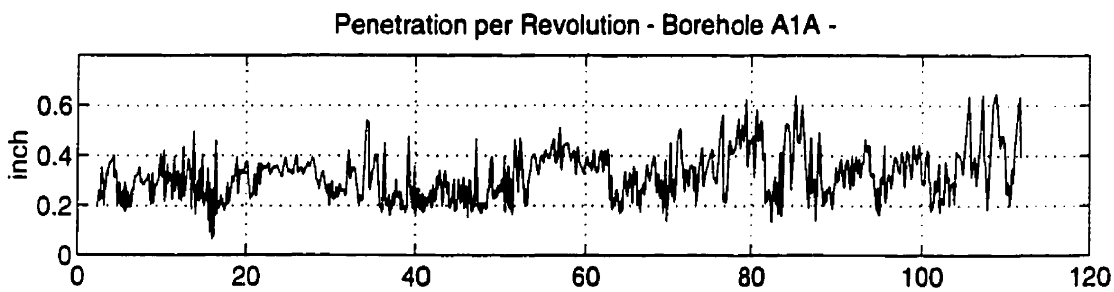
Penetration per Revolution - Borehole A1A -
inch
0.6
0.4
0.2
0
0
20
40
60
80
100
120

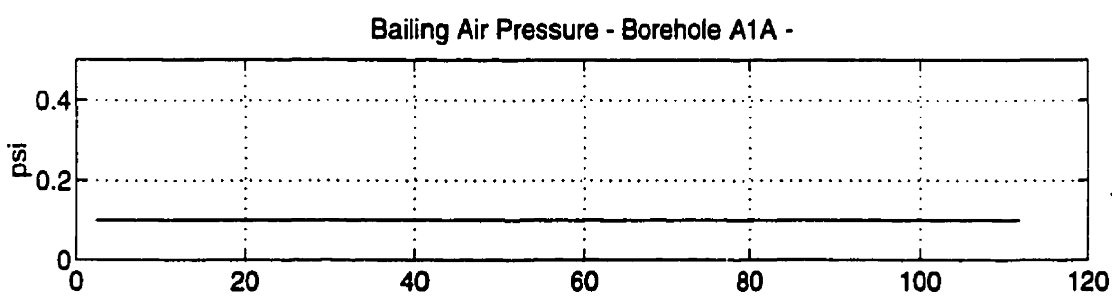
Bailing Air Pressure - Borehole A1A -
psi
0.4
0.2
0
0
20
40
60
80
100
120

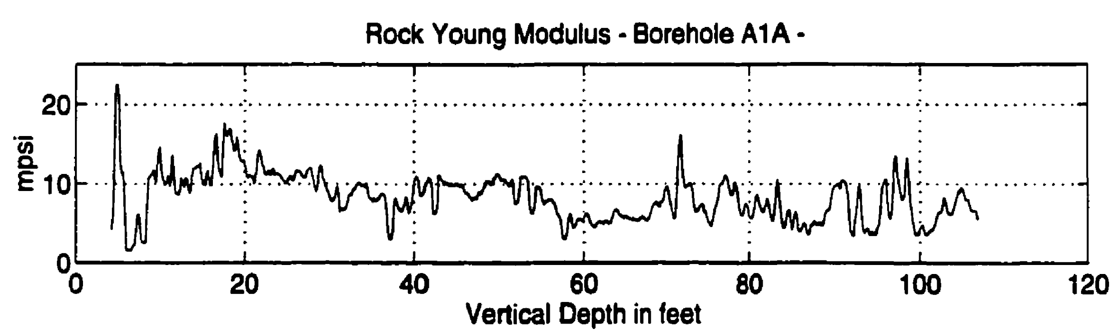
Rock Young Modulus - Borehole A1A -
mpsi
20
10
0
0
20
40
60
80
100
120
Vertical Depth in feet

Rock Shear Modulus - Borehole A1A -

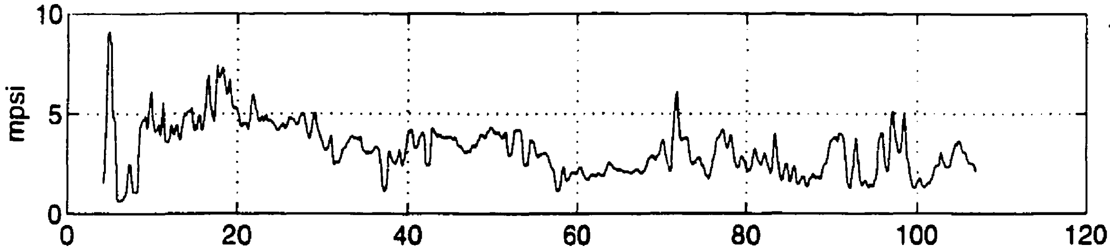


Rock Bulk Modulus - Borehole A1A -

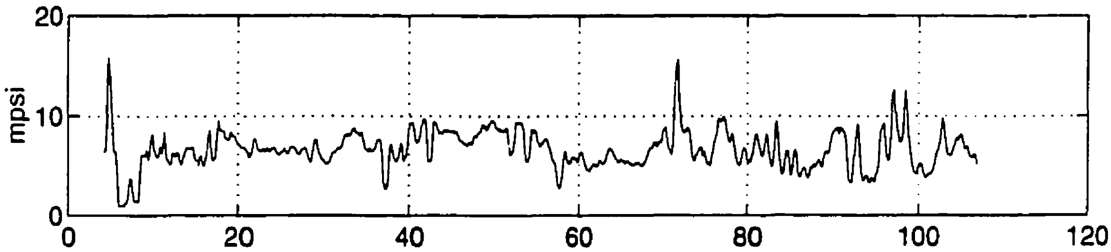


Rock Poisson Modulus - Borehole A1A -


Rock Density Long Spaced - Borehole A1A -

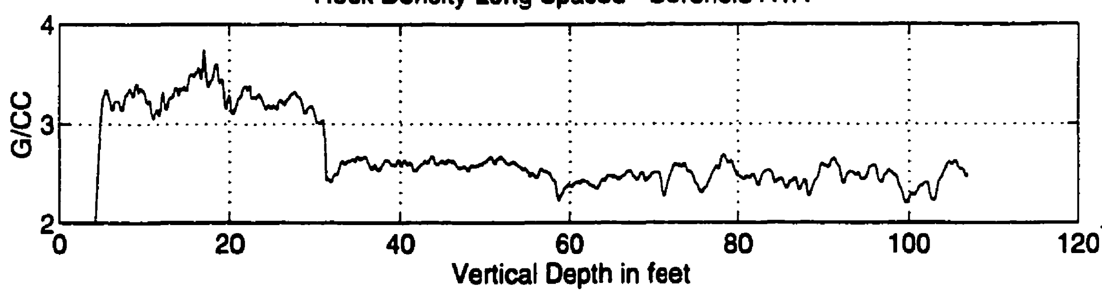

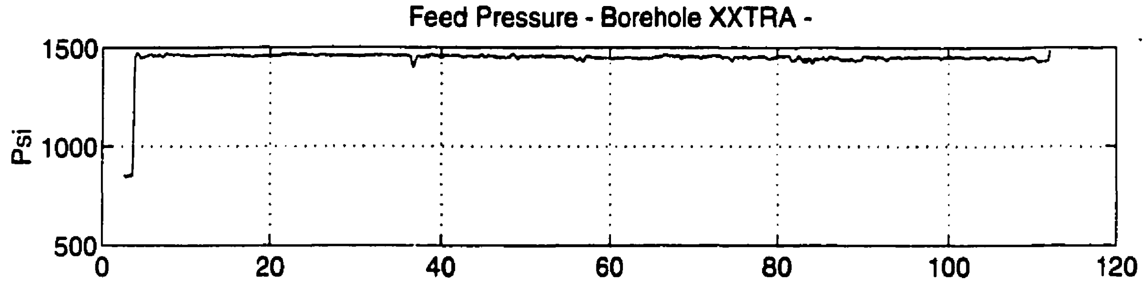
Feed Pressure - Borehole XXTRA -
1500
1000
500
Psi
0
20
40
60
80
100
120

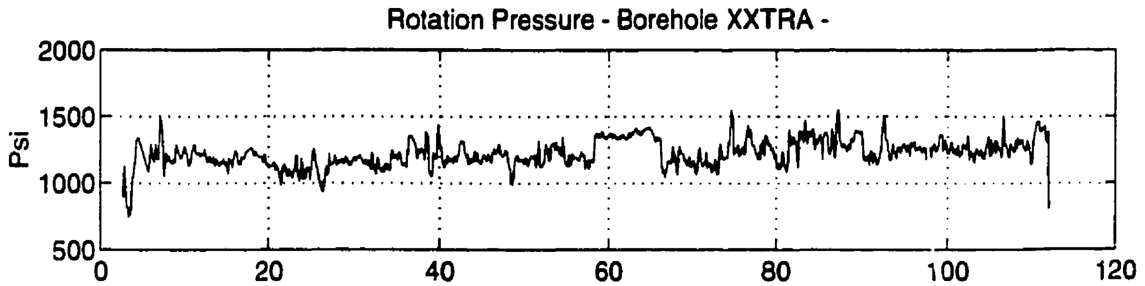
Rotation Pressure - Borehole XXTRA -
2000
1500
1000
500
Psi
0
20
40
60
80
100
120

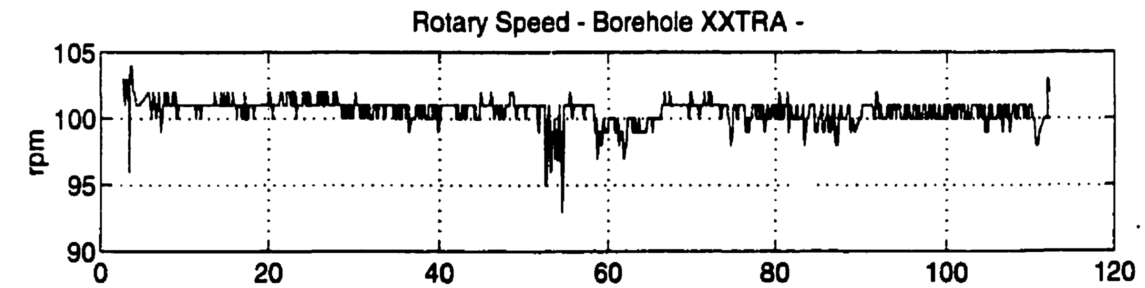
Rotary Speed - Borehole XXTRA -
105
100
95
90
rpm
0
20
40
60
80
100
120

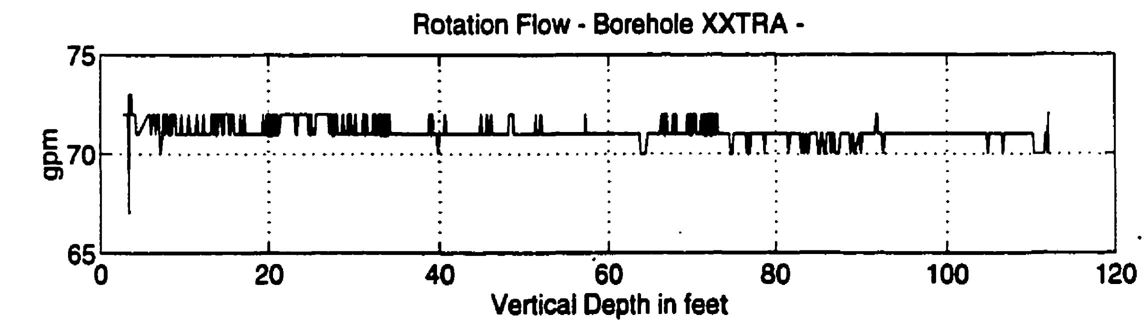
Rotation Flow - Borehole XXTRA -
75
70
65
gpm
0
20
40
60
80
100
120
Vertical Depth in feet

Head axial vibration - Borehole XXTRA -

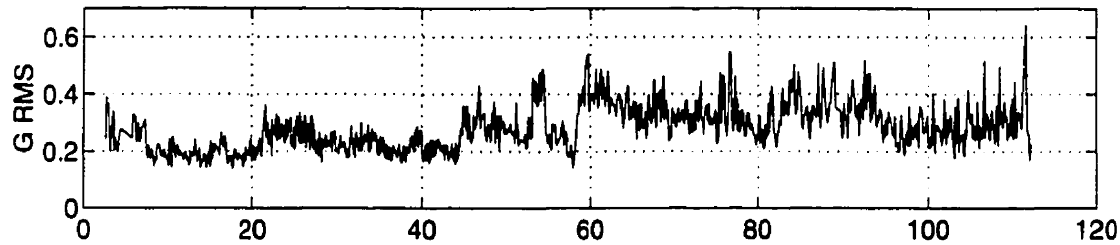


Head lateral vibration - Borehole XXTRA -

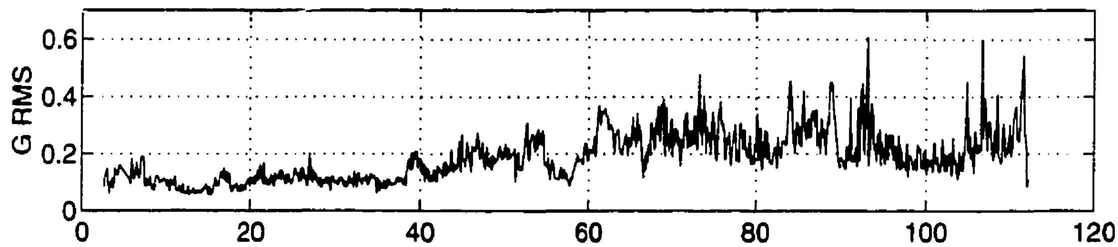


Head transversal vibration - Borehole XXTRA -

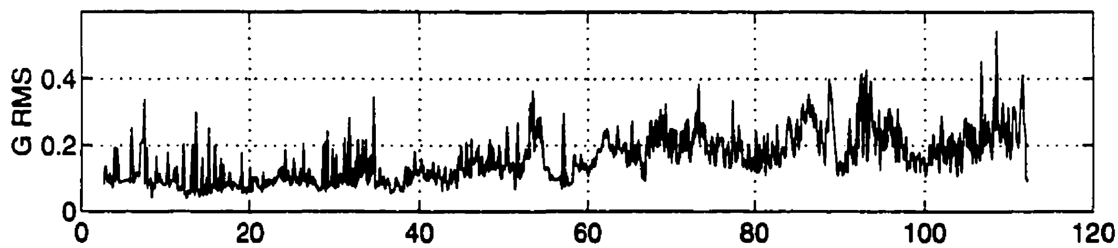


Tower Lateral vibration - Borehole XXTRA -

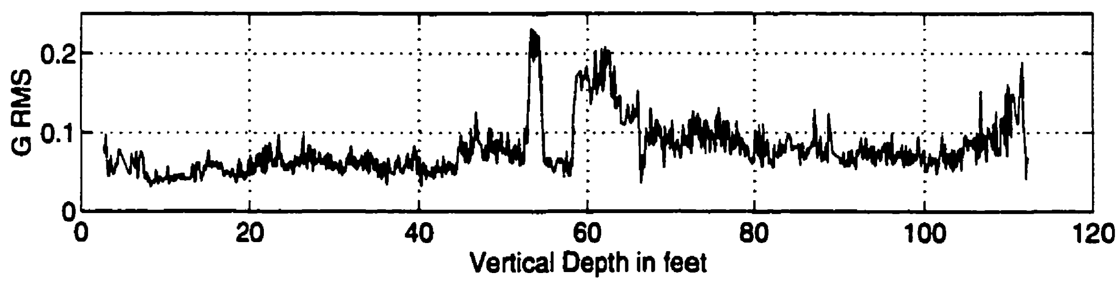

Penetration rate - Borehole XXTRA -

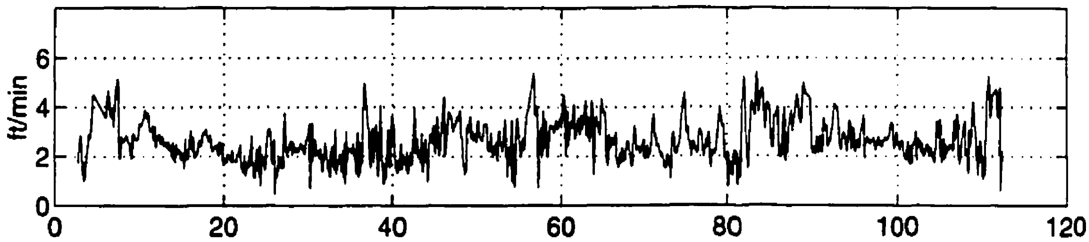


Penetration per Revolution - Borehole XXTRA -

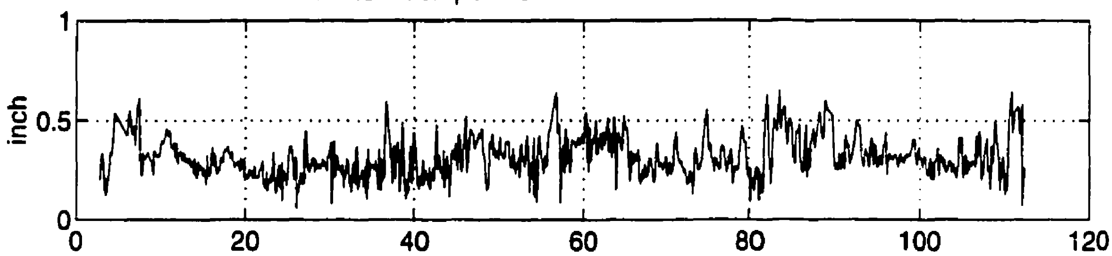


Bailing Air Pressure - Borehole XXTRA -

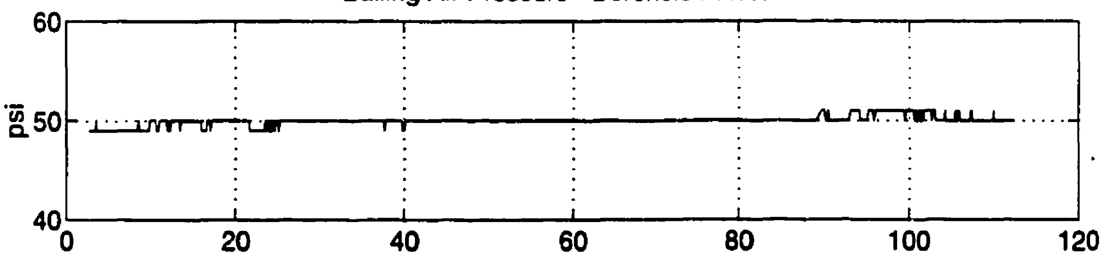


Rock Young Modulus - Borehole XXTRA -

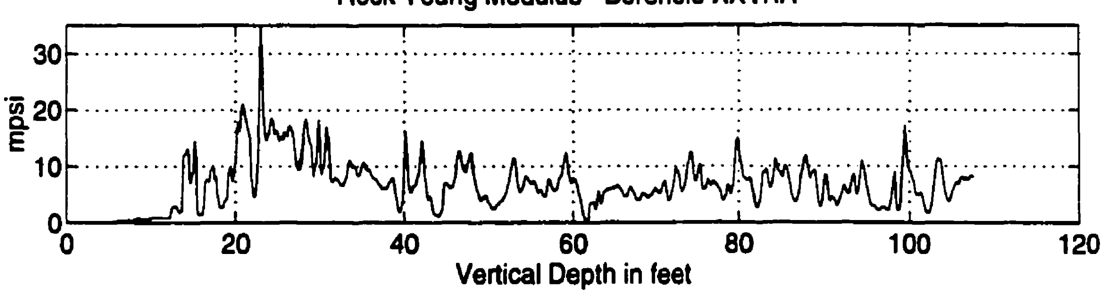

Rock Shear Modulus - Borehole XXTRA -

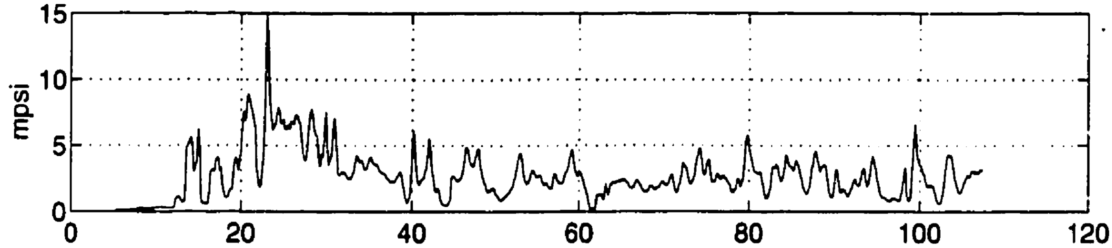


Rock Bulk Modulus - Borehole XXTRA -

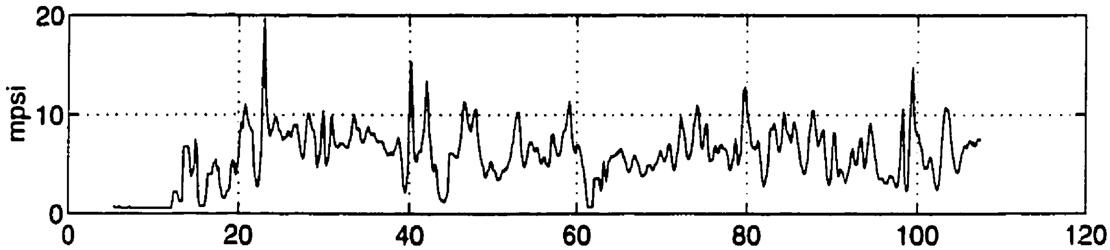


Rock Poisson Modulus - Borehole XXTRA -

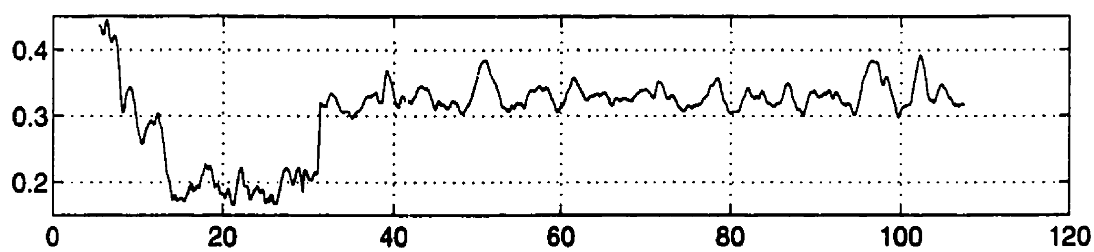


Rock Density Long Spaced - Borehole XXTRA -

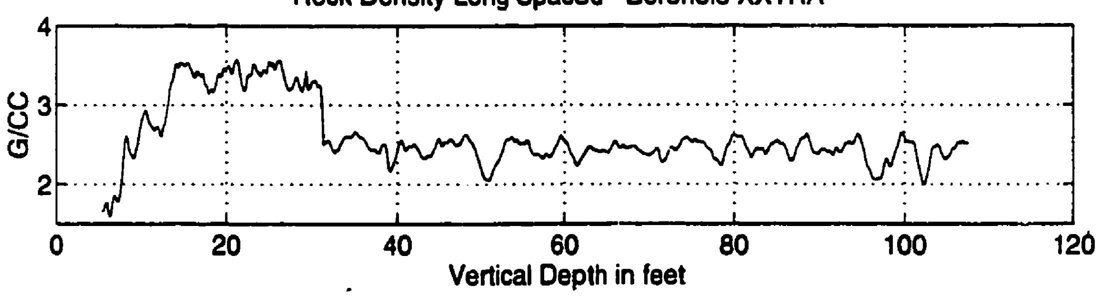

# APPENDIX C

## Simulink Block Models

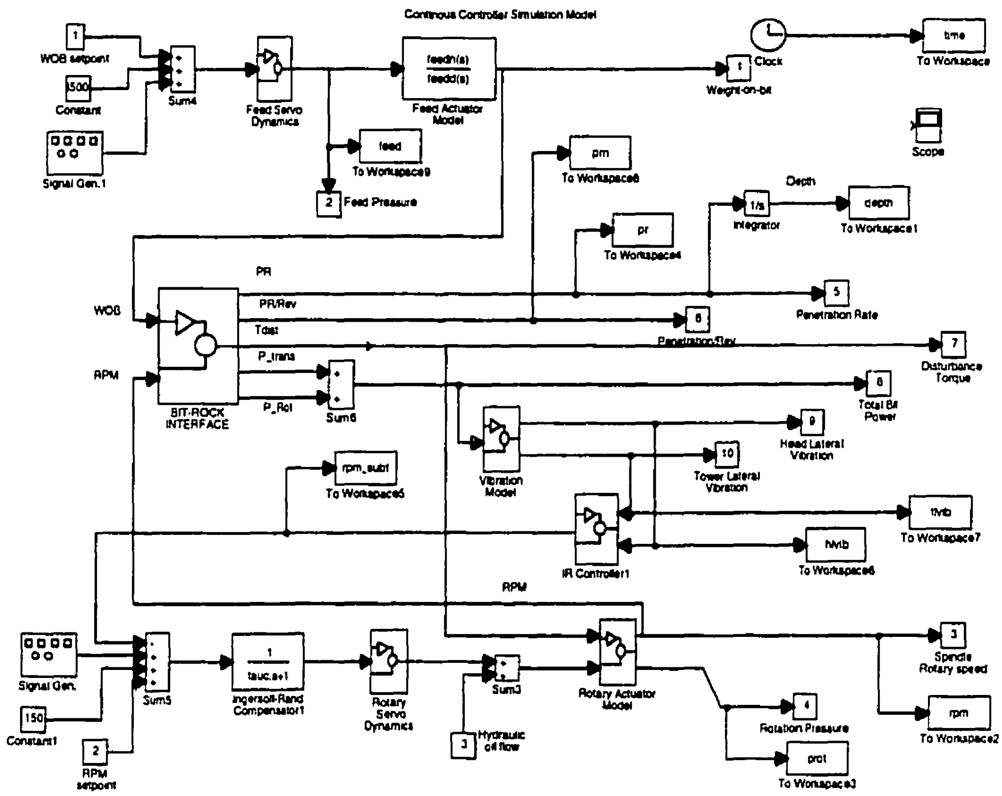
Continuous Controller Simulation Model
1
WOB setpoint
1500
Constant
Signal Gen.1
Sum4
Feed Servo Dynamics
feedn(s)
feedd(s)
Feed Actuator Model
feed
To Workspace9
2
Feed Pressure
1
Weight-on-bit
Clock
time
To Workspace
Scope
pm
To Workspace8
pr
To Workspace4
Depth
1/s
Integrator
depth
To Workspace1
PR
PR/Rev
Tdist
P_trans
P_Rot
WOB
RPM
BIT-ROCK INTERFACE
Sum6
5
Penetration Rate
6
Penetration/Rev
7
Disturbance Torque
8
Total Bit Power
9
Head Lateral Vibration
10
Tower Lateral Vibration
Vibration Model
rpm_subt
To Workspace5
IR Controller1
tlvib
To Workspace7
hlvib
To Workspace6
RPM
Signal Gen.
150
Constant1
2
RPM setpoint
Sum5
1
tauc.s+1
Ingersoll-Rand Compensator1
Rotary Servo Dynamics
Sum3
3
Hydraulic oil flow
Rotary Actuator Model
3
Spindle Rotary speed
rpm
To Workspace2
4
Rotation Pressure
prot
To Workspace3

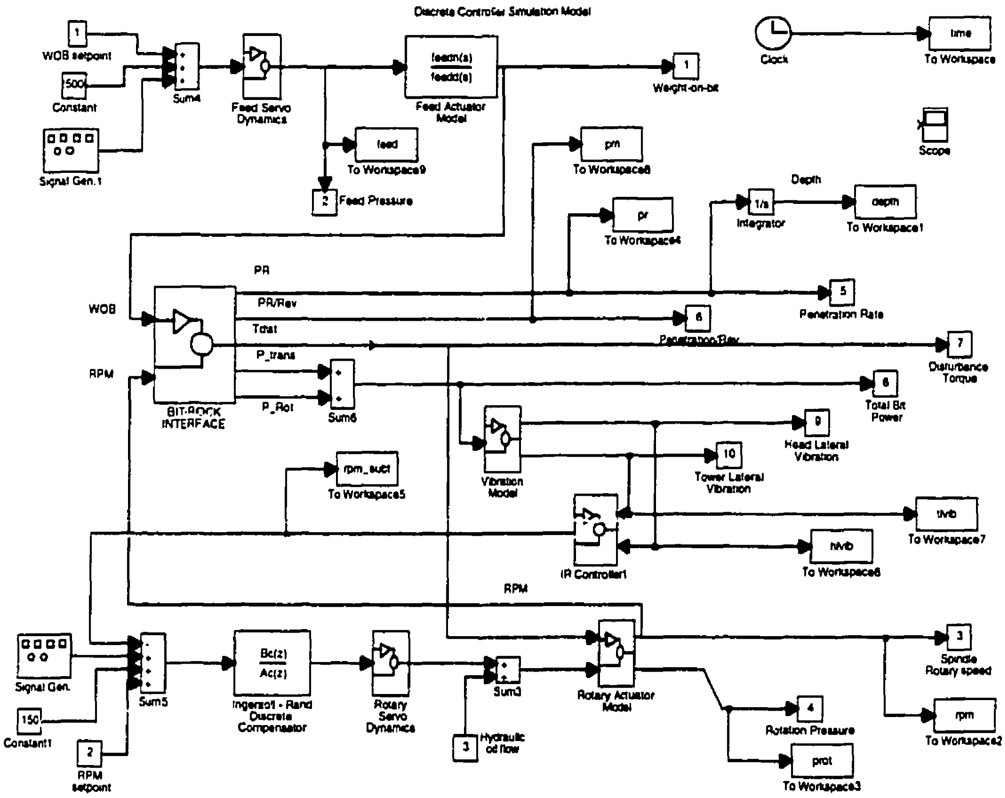
Discrete Controller Simulation Model
1
WOB setpoint
500
Constant
Signal Gen.1
Sum4
Feed Servo Dynamics
feedn(s)
feedd(s)
Feed Actuator Model
feed
To Workspace9
2 Feed Pressure
1
Weight-on-bit
Clock
time
To Workspace
Scope
pm
To Workspace8
pr
To Workspace4
Depth
1/s
Integrator
depth
To Workspace1
PR
PR/Rev
Tdist
P_trans
P_Rot
WOB
RPM
BIT-ROCK INTERFACE
Sum6
5
Penetration Rate
6
Penetration/Rev
7
Disturbance Torque
8
Total Bit Power
9
Head Lateral Vibration
10
Tower Lateral Vibration
Vibration Model
rpm_sub
To Workspace5
tlvib
To Workspace7
hlvib
To Workspace6
IR Controller1
RPM
Signal Gen.
150
Constant1
2
RPM setpoint
Sum5
Bc(z)
Ac(z)
Ingersoll - Rand Discrete Compensator
Rotary Servo Dynamics
Sum3
3
Hydraulic oil flow
Rotary Actuator Model
3
Spindle Rotary speed
rpm
To Workspace2
4
Rotation Pressure
prot
To Workspace3

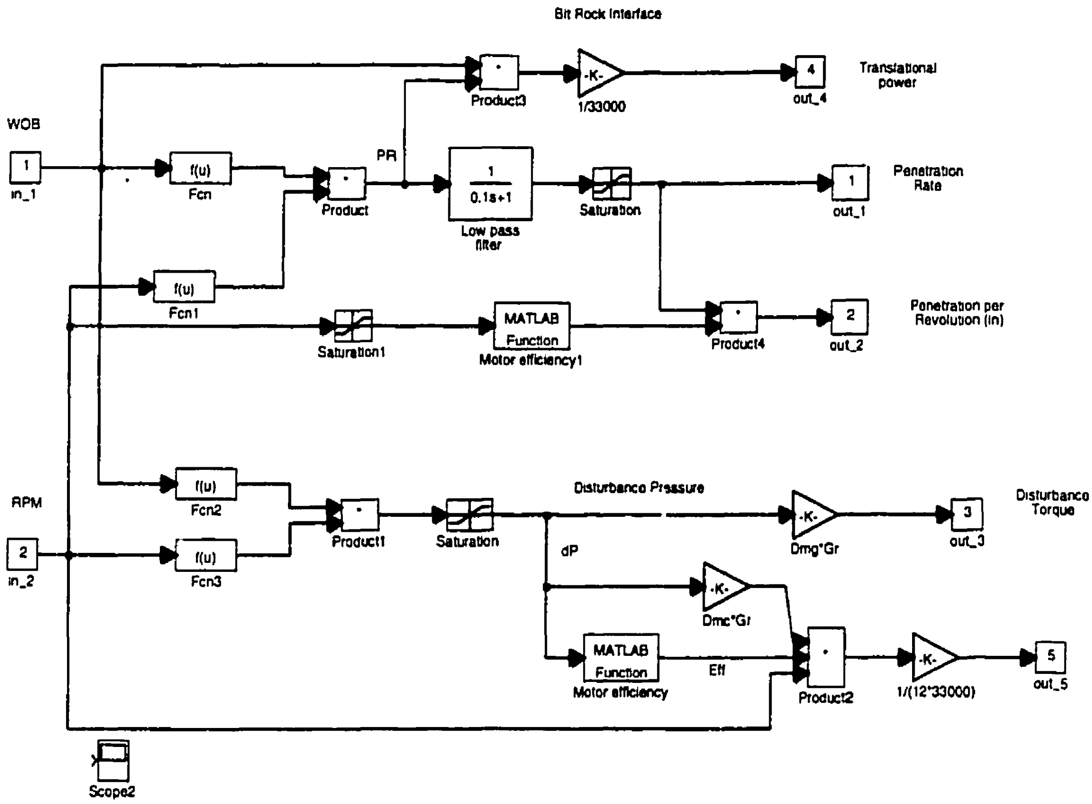
Bit Rock Interface
WOB
1
in_1
f(u)
Fcn
Product
PR
1
0.1s+1
Low pass filter
Saturation
1
out_1
Penetration Rate
Product3
-K-
1/33000
4
out_4
Translational power
f(u)
Fcn1
Saturation1
MATLAB Function
Motor efficiency1
Product4
2
out_2
Penetration per Revolution (in)
RPM
2
in_2
f(u)
Fcn2
f(u)
Fcn3
Product1
Saturation
Disturbance Pressure
-K-
Dmg*Gr
3
out_3
Disturbance Torque
dP
-K-
Dmc*Gr
MATLAB Function
Motor efficiency
Eff
Product2
-K-
1/(12*33000)
5
out_5
Rotational Power
Scope2

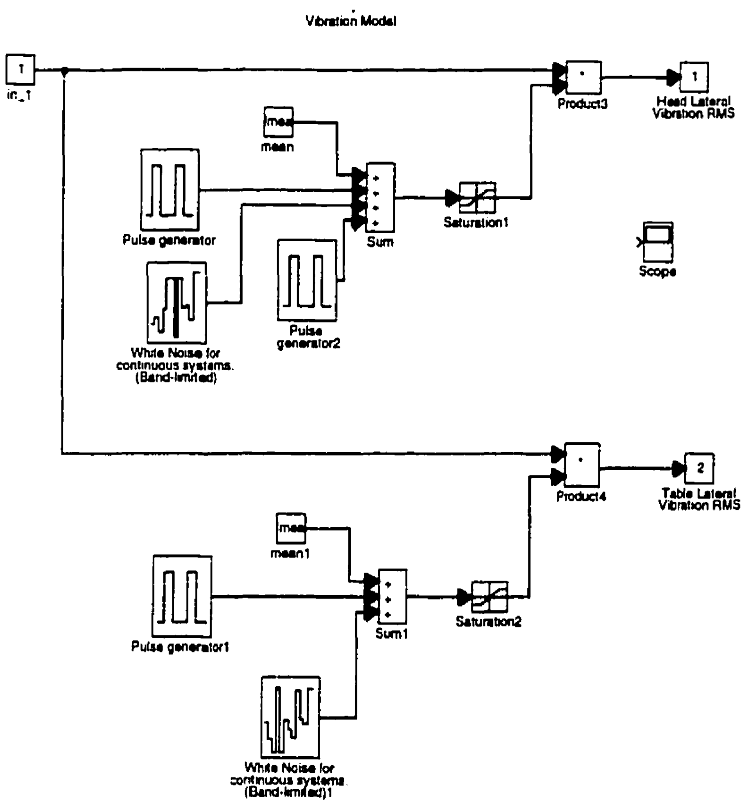
Vibration Model
in_1
mean
mean1
Pulse generator
Pulse generator1
Pulse generator2
White Noise for continuous systems. (Band-limited)
White Noise for continuous systems. (Band-limited)1
Sum
Sum1
Saturation1
Saturation2
Product3
Product4
Head Lateral Vibration RMS
Table Lateral Vibration RMS
Scope

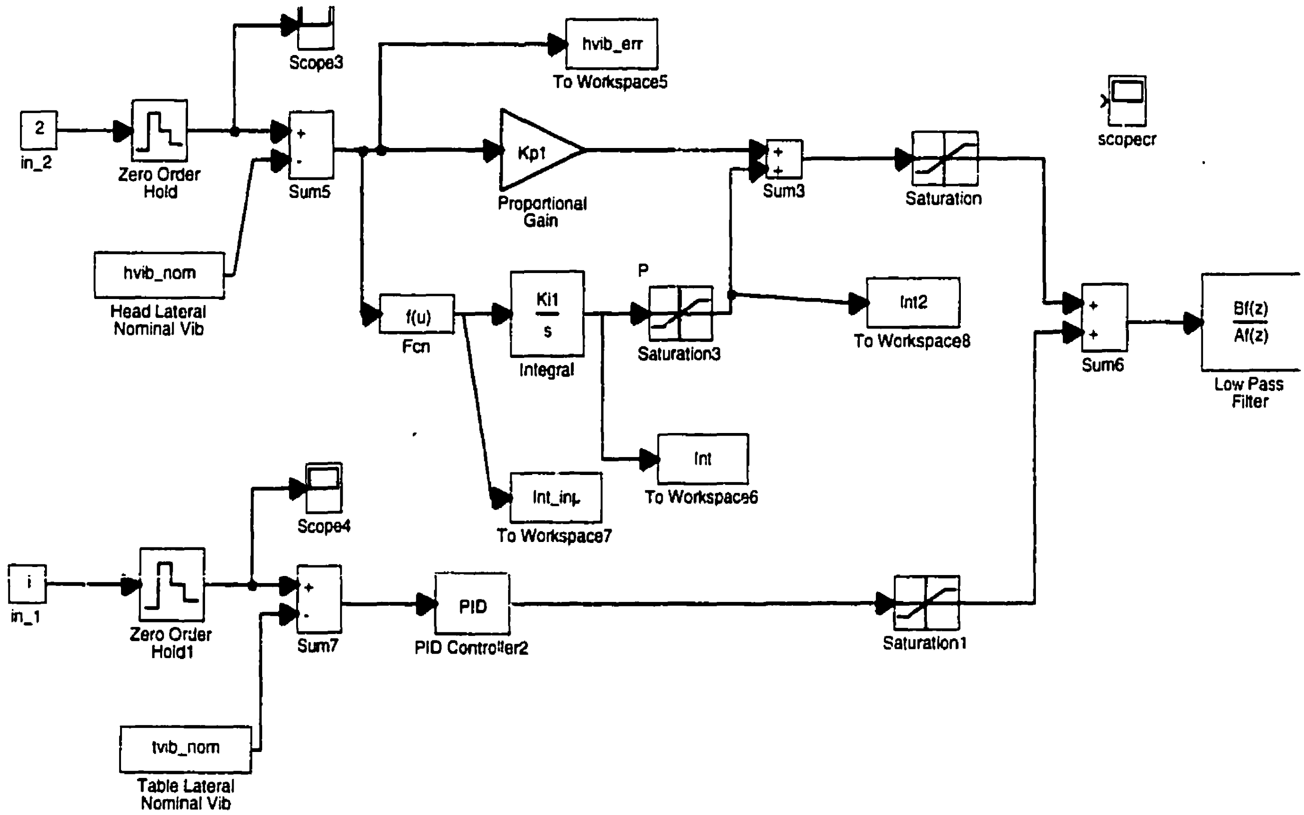

Scope3
hvib_err
To Workspace5
scopecr
2
in_2
Zero Order Hold
Sum5
Kp1
Proportional Gain
Sum3
Saturation
hvib_nom
Head Lateral Nominal Vib
f(u)
Fcn
Ki1
s
Integral
P
Saturation3
Int2
To Workspace8
Sum6
Bf(z)
Af(z)
Low Pass Filter
Int
To Workspace6
Int_inp
To Workspace7
Scope4
i
in_1
Zero Order Hold1
Sum7
PID
PID Controller2
Saturation1
tvib_nom
Table Lateral Nominal Vib